National Library of Canada
Acquisitions and Bibliographic Services Branch
395 Wellington Street
Ottawa, Ontario
K1A 0N4

Bibliothèque nationale du Canada
Direction des acquisitions et des services bibliographiques
395, rue Wellington
Ottawa (Ontario)
K1A 0N4

Your file Votre référence

Our file Notre référence

NOTICE

The quality of this microform is heavily dependent upon the quality of the original thesis submitted for microfilming. Every effort has been made to ensure the highest quality of reproduction possible.

If pages are missing, contact the university which granted the degree.

Some pages may have indistinct print especially if the original pages were typed with a poor typewriter ribbon or if the university sent us an inferior photocopy.

AVIS

La qualité de cette microforme dépend grandement de la qualité de la thèse soumise au microfilmage. Nous avons tout fait pour assurer une qualité supérieure de reproduction.

S'il manque des pages, veuillez communiquer avec l'université qui a conféré le grade.

La qualité d'impression de certaines pages peut laisser à désirer, surtout si les pages originales ont été dactylographiées à l'aide d'un ruban usé ou si l'université nous a fait parvenir une photocopie de qualité inférieure.

Canada

ANALYSIS OF TALL BUILDING TUBULAR STRUCTURES BY FINITE STORY METHOD

Li Lin

A Thesis
in
The Faculty of Engineering

Presented in Partial Fulfilment of the Requirements
for the Degree of Doctor of Philosophy at
Concordia University
Montreal, Quebec, Canada

March 1995

ISBN 0-612-01275-1

Canada

ABSTRACT

ANALYSIS OF TALL BUILDING TUBULAR STRUCTURES BY FINITE STORY METHOD

Li Lin, Ph.D.
Concordia University, 1995

This research concerns the three-dimensional approximate analysis of tall building tubular structures subjected to lateral loads. The complexity in the structural response of unsymmetrical tall buildings always necessitates three-dimensional analysis. Efficient and reliable approximate methods are therefore needed for the early design stages.

A unified approach, termed the finite story method, is presented for displacements and dynamic properties of either symmetrical or unsymmetrical framed tube, core tube and tube-in-tube structures. The method is based on the assumption that nodal vertical displacements and rotations about the horizontal axes of the framed tube structure are linear combinations of nodal displacement fields representing nodal displacement patterns due to overall structural shear, bending and torsional deformations. Nodal displacements are obtained by interpolating the components of overall deformations which are described by floor rigid body displacements. Thus, the principal unknowns in the overall analysis of framed tube structures are reduced to five per floor. A unique condensed overall stiffness matrix corresponding to floor horizontal motions and rotations about the vertical axis is obtained, which ensures good solutions for both displacements and dynamic properties.

The core tube is modeled as a thin-walled beam represented by its extended stiffness matrix. Reliable solutions for core tube torsional deformations, bimoments and

warping stresses are obtained. The efficiency and accuracy of the method is demonstrated in static and dynamic examples by comparing the results with standard three-dimensional finite element analysis and other methods.

By linking the core walls, floor slab out-of-plane stiffness contributes to the lateral load resistance of core tube structures. The additional effect of floor slabs in coupling the core tube and the peripheral framed tube in tube-in-tube structures is studied by first examining a one-story model. The present finite story method is then applied to analyze tube-in-tube structures accounting for floor slab out-of-plane stiffness.

ACKNOWLEDGMENT

The author is profoundly grateful to her supervisors Dr. O. A. Pekau and Dr. Z. A. Zielinski, for their guidance, patience, suggestions, and corrections. Their engineering judgment and conscientious supervision ensured the completion of the present work.

The author wishes to express her deep appreciation to Dr. H. K. Ha, for his fruitful discussions and help and; to Prof. B. Stafford Smith, for his encouragement and generous provision of research materials.

The author would like to thank the Department of Civil Engineering at Concordia University for the use of computer facilities.

Sincere thanks also go to the author's beloved ones, for their understanding and patience, especially to Qi, without whose support this work could not have been completed.

The financial support from the Quebec government's FONDS POUR LA FORMATION DE CHERCHEURS ET L'AIDE A LA RECHERCHE, under the Grant No. 20-F080, as well as from the Natural Sciences and Engineering Research Council of Canada, under the Grant No. A8258, are gratefully acknowledged.

CONTENTS

LIST OF FIGURES

LIST OF TABLES

LIST OF NOTATIONS

A	Area of member cross-sections
A_s	Shear area of column and beam element cross-sections
a, b	linear dimension of cross-sections of thin-walled beams or slabs
$B_{\bar{\omega}}$	bimoment
C	centroid of cross-section
$\{D_k\}$	generalized displacement coordinates at the kth floor
$\{D^f\}_k$	generalized displacement coordinates of framed tubes
$\{D\}$	overall generalized displacement coordinates
$\{\bar{d}_i\}$	local displacement vector of node i
$\{d_i\}$	global displacement vector of node i
E, E_x, E_y	Young's modulus
F_x, F_y, F_z	forces in the X, Y, and Z directions
G, G_{xy}	shear modulus
$[G]$	overall displacement transformation matrix
$[g_i]$	nodal displacement transformation matrix at node i
$[g_b]$, $[g_c]$	nodal displacement transformation matrices of beams and columns
I_p	tangent second moment of inertia
I_x, I_y, I_z	flexural moment of inertia
$I_{\bar{\omega}x}, I_{\bar{\omega}y}$	second moment of inertia of sectorial area coordinate
$I_{\bar{\omega}}$	principal sectorial moment of inertia
J_o, J_c, J	torsional constants of open, closed sections and core tube element
$[K]$	overall stiffness matrix of the 3-D FEM

$[k_b]$, $[k_c]$	stiffness matrices of beam and columns in the global coordinate system
$[k_w]$	stiffness matrix of core element
$[\bar{k}]$	element stiffness matrix in the local coordinate system
$[K^*]$	overall stiffness matrix corresponding to {D}
$[M^*]$	overall mass matrix corresponding to {D}
l	length of member
M_x, M_y, M_z	moments about the X, Y and Z axes
$[\bar{m}]$	mass matrix in element in the local coordinate system
m_c, m_b	numbers of columns and beams in the kth story
m_w	number of thin-walled beam elements in the kth story
$[m_b]$, $[m_c]$	consistent mass matrices of beam and columns in the global coordinate system
$[M^{f*}]_k$	mass matrix of the kth story corresponding to the $\{D^f\}_k$
n_c	number of nodes of core tubes at the kth floor level
O	origin of the global coordinate system
O_1	arbitrary pole in the cross-section of thin-walled beams
$\{P^*\}$	external lateral vector corresponding to {D}
r	perpendicular distance from O_1 to M where the sectorial coordinate is to be determined
[R]	rigid end transformation matrix
s	curvilinear coordinate of the middle surface measured from the origin
[S]	stiffness matrix of the two-story substructure
$[S^{f*}]_k$	stiffness matrix of the kth story corresponding to the $\{D^f\}_k$
$[S^c]_k$	stiffness matrix of the core tube in the kth story

$[S^{c*}]_k$	modified stiffness matrix of the core tube in the kth story
$[S^s]_k$	condensed kth floor substructure stiffness matrix
S_ω	first moment of inertia of sectorial area coordinate
t	thickness of walls and slabs
t_l	thickness of the equivalent laminas
[T]	coordinate transformation matrix
$[T_i]$	coordinate transformation matrix at node i
u, v, w	nodal displacements in the X, Y, and Z direction
$u_k, v_k, \theta_{zk}, \theta_{xk}, \theta_{zk}$	kth floor slab in-plane displacements
$w^c, \theta^c_{xk}, \theta^c_{yk}$	nodal displacements of core tube elements
X, Y, Z	Cartesians coordinate system (global)
x_i, y_i	coordinates of node i
x_S, y_S	location of the shear center O with respect to the centroid C
β'	warping function
$\beta_i^{(j)}, \alpha_{xi}^{(j)}, \alpha_{yi}^{(j)}$	displacement distribution coefficients of node i
$\theta_x, \theta_y, \theta_z$	nodal rotations about the X, Y, and Z axes
μ	warping characteristic parameter
$\sigma_{\bar{\omega}}$	normal warping stress
ν	Poisson's ratio
Ω	twice the area enclosed by the middle surface of wall cross-sections
ω	natural frequency of vibration
$\bar{\omega}$	sectorial coordinate
ΔD_k	increment of generalized displacement coordinate at the kth floor level

Chapter 1

Introduction

1.1 General

Tall buildings are distinguished from other buildings, within an engineering perspective, by the rules of structural design which are governed by the behavior under lateral loads where the building's slenderness becomes the dominate factor.

Various tall buildings are seen in cities around the world. Tubular structures have been employed, developed and have become increasingly more popular for tall buildings since the 1960's. The basic forms of tubular systems are the framed tube, core tube, tube-in-tube and bundled tube. The principle of design is to create a hollow cantilevered box beam above the ground; thus, the lateral loads are mainly or completely resisted by the facades of the cantilever. Compared with conventional frame or shear wall systems, tubular structures are more efficient in saving materials and providing large open spaces. Examples of well-known tubular structures are: the 110-story World Trade Center in New York, in which the core tube was not designed to resist lateral loads, thus resulting in the overall structural system acting as a framed tube; the 100-story John Hancock Center in Chicago which is a column diagonal trussed framed tube and; the world's tallest building, the 110-story Sears Tower in Chicago which is a bundled tube [1-4].†

† Numbers in square brackets [ ] refer to the references listed at the end of this thesis.

The structural analysis and design of such tall buildings demand a great deal of computational effort, since these involve a large number of elements and joints, load distributions among components and interactions between components. In addition, if a tall building does not possess coincident centers of stiffness and mass at each floor lying on a common vertical line throughout the total height, response to transverse dynamic loading becomes torsionally coupled. The resulting complexity necessitates three-dimensional (3-D) structural analysis. The standard finite element analysis with sophisticated theory and well-developed computer software is powerful in solving such 3-D problems. However, 3-D finite element analysis of tall building tubular structures requires large scale computers and is very time consuming. Thus, it is not feasible for the early design stages during which several design alternatives need to be studied and wherein structures are modified frequently. This poses problems in practical design calculations and has stimulated the search for simplified analysis procedures [5-8].

1.2 Existing approximate methods of tubular structural analysis

A tube-in-tube structure comprises the peripheral framed tube and the core tube interconnected by floor slabs. For each of these vertical components, various simplified approaches have been developed for the structural behavior under lateral loads. Floor systems acting as lintels in core tube structures have also been studied for the contribution to the overall lateral load resistance. The following provides a brief overview of existing approximate methods of analysis concerning tubular structural displacements and dynamic properties. These methods are examined in terms of the assumptions and simplifications in the structural modeling. Addressed in order are the analyses of framed tubes, core tubes, floor systems, and dynamic properties. The details of the more relevant of these methods concerning different kinds of tubular structures will be given in associated Chapters.

For symmetric framed tube structures, a method of hand calculation for the overall resistance and deflection has been proposed in [9]. In this method, based on the existence of the shear lag phenomenon, the overall lateral load resistance contributed by columns and beams lying in the middle zone of the flange frame panels is assumed to be negligible. The structure is thus approximated as a pair of equivalent channels for which the width of the flanges is chosen, according to design experience, to be no more than either half of the depth of the web frame panels or 10 per cent of the total height of the building. This method is useful for quick estimation of the overall lateral load resistance and initializing member sizes.

Another simplified approach for doubly symmetric framed tubes is the plane frame analogy [10-14]. The method is based on the assumption that the out-of-plane stiffness of frame panels is negligible, and the external lateral loads are considered to be resisted mainly by shear in web frames and axial forces in the flange frames. These primary reactions of the structure are modeled by an equivalent plane frame system in which the major interaction between the flange and the web frames in the framed tube, namely the vertical shear force, is simulated by fictitious members. This modeling enables framed tube structures subjected to either lateral loading or torsion to be analyzed by 2-D frame computer programs.

Similarly, simplified methods for framed tube analysis have been developed based on the orthotropic membrane analogy [15-22]. This analogy assumes that the points of contraflexure of beams and columns in uniform frame panels occur at the middle of these members. The elastic material properties of the equivalent membrane are then determined according to the principles of mechanics of materials [15, 16], with the influence of shear deformation in the finite-size joints included [17, 18]. The material properties of the orthotropic membrane have also been determined using the finite element method [19], in which the effects of stress concentration and non-linear distribution of stress could be included. The overall behavior of the equivalent cantilever box beam resulting from these

approaches has been analyzed by various methods, namely: a simplified method in which closed-form solutions for stresses were derived based on assumed stress distributions [15, 16, 22]; the finite strip method [20] and; the finite element method [21] in which the element stiffnesses are established based on the strains in a pure bending state.

An alternative approach for doubly symmetric framed tubes is the so-called extended rod method [23]. The governing differential equation is obtained according to Hamilton's principle in conjunction with assumed displacement functions. These displacement functions are given in terms of floor rigid body displacements, together with: (1) a parabolic function representing shear lag in the flange frames for structures under bending actions or; (2) the warping function adopted from Vlasov's thin-walled beam theory for structures under torsional actions. Closed-form solutions for the structure's displacement have been obtained following this method.

It is seen that most of the aforementioned methods are limited to framed tubes which are symmetric. Among these, the plane frame analogy [10-14], the finite strip method [20] and the strain-based finite element method [21] can also be used for tube-in-tube structural analysis. Besides these methods, tube-in-tube structures can also be approached by means of computer programs for space frame structures, in which the core walls are preliminarily replaced by equivalent sets of columns, rigid beams and braces, [6].

Core tubes as the second basic form of tubular structure have received similar extensive attention, particularly for structures subjected to torsion. Simplified approaches for the torsional behavior of core structures can be classified [28] as open section or closed section analysis. In the former the constraints provided by lintel beams or floor slabs are considered by either appropriately modifying the St. Venant torsional constant [24-28, 30] or by including the bimoments in the overall equilibrium equation [28, 31-35]. The latter assumes that the lintels at floor levels can be replaced by a uniform continuum with

equivalent flexibility, thus allowing the effects of circulatory shear stresses and the shift of the shear center due to the existence of the lintels to be included [28]. In addition, discrete approaches have become popular with the development of computer techniques in recent years. The general matrix method [36-39], the finite strip method [40] and various specially developed finite elements [41-44] have been applied to the analysis of core tube structures.

The third basic component of tube-in-tube structures, namely the horizontal floor system, acts as braces in the core tube and also couples the core with the peripheral framed tube, thus also contributing to the lateral load resistance [1, 6, 7]. The coupling effects of slabs in symmetric cross-wall systems have been investigated both theoretically and experimentally [46-49] and simplified calculations for the effective width of the slabs have been proposed. In these, the floor slabs are replaced by equivalent connecting beams, permitting the analysis of 3-D cross-wall systems to be simplified to the analysis of planar wall systems after considering symmetry conditions. Additionally, the warping stiffness contributed by floor slabs in core tube structures under torsion has been incorporated in the overall equilibrium conditions by determining the bimoments in floor slabs corresponding to a unit warping deformation [27], or by modifying the torsional constants of the core tubes [30], for which different edge conditions of the slabs have also been discussed [50].

The foregoing methods concern only static responses of tall buildings. On the other hand, assessing the dynamic properties of multi-story buildings has also been an important research topic. Stafford Smith and Crowe [55] have proposed a hand method of estimating the natural frequencies of symmetric systems of rigid frames, shear walls or combinations of these kinds of structures. The method is efficient and accurate in predicting the fundamental frequency of free vibration. Employing the aforementioned extended rod method [23] developed for static analysis of doubly symmetric framed tubes, Takabatake et al [56] extended the analysis to torsionally uncoupled free and forced

vibration of these structures. In this study, the natural frequencies of non-uniform symmetric framed tubes were obtained by the Galerkin method which yielded closed-form approximate solutions for these properties.

1.3 Scope and objectives

As seen from the preceding Section, most of the available analytical techniques are limited to only one form of tubular structure, either framed tube or core tube, although tube-in-tube structures consisting of a combination of these are common in design. Furthermore, the majority of the reported approximate approaches are confined to symmetric structural behavior only. Simplified analysis of unsymmetrical tube-in-tube structural behavior, particularly for torsionally coupled dynamic properties, has not been developed. Similarly, the bending and warping stiffnesses of floor slabs in connecting core walls have received extensive attention; however, in the case of tube-in-tube structures with floor slabs linking the foregoing vertical structural components and transmitting bending moments, little has been reported, although it has long been indicated [1] that the coupling effect between the inner core and the outer framed tube needs be considered.

Thus, this research concerns the approximate 3-D analysis of tall building tubular structures primarily under static lateral loading. The proposed method of analysis is equally applicable to structures such as space frames and frame-shear wall core structures, although attention is confined to framed tubes, core tubes and tube-in-tube structures. The structures studied herein are of rectangular cross-section, while members may be arranged unsymmetrically in framed tubes and the core tube may be located eccentrically within a framed tube. Thus, the overall structural system may be unsymmetrical, but remains in the linear elastic range. The structure is subjected to static loads applied at floor levels.

The objective is to present a consistent and unified approximate procedure for three-dimensional tall building tubular structural analysis which is effective in: (1) predicting static responses and dynamic properties of framed tube and tube-in-tube

structures which are either symmetric or unsymmetric and; (2) predicting structural behavior under torsional actions or combined loading conditions of core tube structures which are either open, closed or partially closed sections and; (3) estimating the contribution of floor slabs to the lateral load resistance in tube-in-tube structures.

1.4 Thesis organization

The work presented in this Thesis consists of four parts: (1) a simplified three-dimensional analysis procedure - termed finite story method based on nodal displacement fields - proposed and applied in predicting static responses and dynamic properties of framed tubes; (2) an extended element stiffness matrix for core tubes modeled as thin-walled cantilevers, obtained based on existing continuous approaches and modeling core tube torsion and warping behavior; (3) the extension of the proposed finite story method to analyze tube-in-tube structures and; (4) preliminary study of the coupling effect of floor slabs in tube-in-tube structures. A literature review regarding each part of the work is given separately in associated Chapters. The computations are made employing both a computer program developed based on the proposed FSM and the commercial finite element software NISA. As far as possible, results are also compared with other published methods.

In Chapter 2, following a review of three existing simplified methods of analysis, the finite story method (FSM) is proposed for framed tube structures. The theoretical basis of the method, the concept of nodal displacement fields, and the overall analysis procedure are presented. Numerical examples demonstrate the validity of the method. These involve either symmetric or unsymmetrical structural systems under bending and torsion actions, with natural frequencies and modes of vibration also determined.

Chapter 3 presents a simplified model for the core tube structures. This analytical model is intended for subsequent use in the extension of the above finite story method to

tube-in-tubes. The characteristics of a core tube structure and its structural behavior under torsion are described, and the existing research is briefly reviewed. To provide an understanding of the warping behavior of core tubes, the concept and basic formulation of thin-walled beam theory are described. The complete element stiffness matrix for core tube structures modeled as thin-walled beams is given, with numerical examples of symmetric and unsymmetric core tube structures subjected to concentrated torque at the top and uniformly distributed lateral load presented to confirm accuracy.

The finite story method presented in Chapter 2 is implemented by incorporating the above thin-walled beam modeling of core tubes and, applied to the analysis of tube-in-tube structures in Chapter 4. The floor slabs in this Chapter are assumed as in-plane rigid diaphragms. Examples of symmetric and unsymmetrical tube-in-tube structures under torsion and lateral loading, respectively, as well as dynamic properties of the unsymmetrical tube-in-tube are analyzed by both the finite story method and the finite element method. Finite element method is employed for the purpose of examining the accuracy and efficiency of the calculations by the present FSM.

Based on the formulations of the FSM for tube-in-tube structures in Chapter 4, Chapter 5 includes the modeling of out-of-plane stiffness of floor slabs in the analysis of these structures. Existing methods of estimating floor out-of-plane stiffness are reviewed. The coupling effects of floor slabs between the framed tube and the core tube are first examined by analyzing a single-story model by the finite element method. The structural modeling of floor systems in the finite story method is then presented. This is followed by the numerical example of a 30-story tube-in-tube structure with a waffle floor system subjected, separately, to lateral loading and torsion. The results are discussed with regard to the coupling effect of floor slabs in this tube-in-tube structure and, the accuracy of the present finite story method.

The conclusions obtained from this research, as well as suggestions for further work, are given in Chapter 6.

Chapter 2
Framed Tube Structures

2.1 Introduction

In this Chapter, framed tube structures under lateral loads and their dynamic properties are modelled. The structures and structural behavior under lateral loads are described, and existing simplified methods are briefly reviewed. The finite story method (FSM), an approximate method of structural analysis based on nodal displacement fields for three-dimensional problems, is presented. The effectiveness of the proposed method is corroborated by examples of space frame and framed tube structures subject to lateral loads and torques; also presented are the free vibration analyses of both symmetric and unsymmetrical structures. The calculations are carried out by both the developed FSM computer code and the finite element analysis software NISA.

2.1.1 Description of framed tube structures

A framed tube, Figure 2.1, is one of the basic structural forms of tubular systems. It consists of closely spaced columns placed on the periphery of a building and rigidly connected with deep spandrel beams at floor levels. This design creates a hollow tube with perforated openings that are compatible with windows. The essence of the structure is to make use of in-plane dimensions to reach the maximum flexural rigidity of the cross section. The resulting large clear space inside the building makes the structure efficient

and economical. The inherent advantages of the structure allow it to be widely used in the construction of buildings up to 100 stories.

Generally, the spacing between the peripheral column in the framed tubes varies from 1.5 m to a maximum of 4 m. The spandrel beams monolithically connected to the columns range from 600 mm to 1220 mm in depth, and 250 mm to 1000 mm in width [9]. In contrast to low rise building structures, the stiffness balance between the spandrel beams and the columns is controlled by lateral drift limitations, not by strength requirements. Khan [4, 9] has suggested that the column spacing and the proportioning of the spandrels and columns could be optimized, with regard to stiffness of the structure against lateral sway, by analyzing a substructure consisting of two columns cut at the mid-height of stories plus the spandrel beam between the columns.

Framed tubes under lateral loads act as cantilevered boxed beams in which bending moments are balanced by normal stresses in the cross-sections, with the overturning moments acting on the building from lateral loads being resisted by axial forces in the peripheral columns. However, their responses are more complex than that of a simple closed box beam. The mode of the overall deformation is a combination of frame racking shear and cantilever flexural bending. Which of these modes has greater presence depends on the opening ratio and on the proportions of the spandrels and the columns of the tube frame panels. Furthermore, the framed tube differs from a closed box beam in the existence of shear lag, which is a result of the shear flexibility of the spandrel beams. The latter in turn gives rise to column axial forces which are distributed nonlinearly over the cross section, as shown in Figure 2.1. Unlike a closed box beam in which normal stresses are distributed linearly in proportion to the distance to the neutral axis of the cross section, the column axial forces near the corners are increased, while the column axial forces in the central portions of frame panels are decreased.

2.1.2 Existing methods of analysis

Three basic methods exist for the analysis of framed tube structures - plane frame and orthotropic membrane analogies, and the displacement distribution factor method. The latter was not developed directly for framed tube analysis, since it was intended to be applied to the analysis of space frame and core-frame structures. Nevertheless, the finite story method proposed herein shares the displacement distribution concept of the displacement distribution factor method.

Plane frame analogy

Doubly symmetric rectangular framed tube structures under lateral loads, Figure 2.2a, can be analyzed by means of general two-dimensional (2-D) finite element programs [10-14]. This approach assumes that the out-of-plane stiffness of frames is negligible compared to their in-plane stiffness. Under symmetric lateral loads, a rectangular framed tube structure behaves in such a way that frame panels parallel to the lateral loads, the so-called web frames, mainly resist shear, while the flange frame panels perpendicular to the loads respond in axial deformation to balance the external overturning moments. The primary interaction between the web and flange frames is through the vertical shear at the corners. These characteristics can be modeled by an equivalent plane system as shown in Figure 2.2b.

In the substitute 2-D system of Figure 2.2b, the web frames and the flange frames are connected at floor levels by fictitious members or beams which only transfer vertical shears. Only one quarter of the original structure is analyzed because of symmetry. The external load is applied on the web frame (AB), while the flange (B'C) is under the action of vertical shear forces from the fictitious members. The vertical displacement at B and B' are made to be compatible. The behavior of symmetrical framed tube structures under pure torsional actions was also analyzed by an equivalent plane system [11, 13]. The floor rotations can be solved from equilibrium and compatibility conditions of the plane frame

system. This technique reduces substantially the computational work required in design and has been accepted by design engineers.

Orthotropic membrane analogy

In this method, frame panels of a framed tube structure with regular span and story height throughout are replaced by an equivalent orthotropic continuum membrane. The structural analysis is then based on the resulting orthotropic membrane tube [15-22].

It is assumed that the points of contraflexure of the beams and columns are at the middle of these members. Because the structure is uniform, only one segment between the contraflexural points around a joint, Figure 2.3, is analyzed to determine the elastic material properties of the equivalent orthotropic membrane [15,16]. These properties are so determined that a segment of the membrane which has the same thickness, width and height of the represented frame segment possesses the same axial and shear stiffnesses as the frame segment. Moselhi, Ha et al. [17, 18] refined the model presented by Coull et al. [15, 16] by including the constraint effect of the beam to the vertical deformation of the column, as well as shear deformation in the finite-size joint. Khan and Stafford Smith [19] have suggested analyzing the frame segment by the finite element method, so that stress concentration and non-linear distribution of stresses could be taken into account.

The elastic modulus E_x in the horizontal direction is considered infinite due to the high in-plane rigidity of floor slabs. To obtain the elastic modulus E_y in the vertical direction and the shear modulus G_{xy} of the membrane, vertical and horizontal forces are applied to the top of the column and the top of the membrane segment. By equivalent axial and shear flexibility, the required moduli can be determined [17, 18] from

$$\frac{Ph}{tBE_y} = \Delta_1 + \Delta_2 + \Delta_3$$

$$\frac{Qh}{G_{xy}tB} = \Delta_b + (\Delta_{vm} + \Delta_{vj})$$

where Δ_1, Δ_2 and Δ_3 are vertical deformations of column and beam segments; Δ_b = the deflection due to bending; Δ_{vm} = the member shear deformation; and Δ_{vj} = the deflection caused by shear deformation of the finite-size joint; t = the thickness of the equivalent wall panels; h = the story height; B = the center spacing of columns.

By this technique, a uniform rectangular framed tube structure is transformed into an equivalent orthotropic closed tube structure. The finite strip method and finite element method are applied to analyze the substitute system [20, 21]. Based on the equivalent closed tube and the principal behavior of a symmetric framed tube, Coull and Bose [15, 16] assumed that normal stress distributions can be approached by even parabolic functions of horizontal coordinates in flange frames and odd parabolic functions of horizontal coordinates in web frames. The governing differential equation was derived by virtue of the principle of least work, and closed-form solutions for stresses in the equivalent orthotropic membrane panels were obtained. Consequently, member forces in the original frame panels were obtained by integration of stresses. Design curves for three standard load cases - uniform, triangular and concentrated at the top - were provided for preliminary calculations. Kwan [22] assumed independent cubic functions representing normal stresses in web and parabolic functions representing normal stresses in flange frames; he also studied the effects of different parameters on the shear lag.

Distribution factor method

The distribution factor method simplifies structural analysis by reducing the number of displacement unknowns. The method is based on the fact that nodal displacements at floor levels are linear combinations of displacement patterns due to different forms of deformations of building structures. The concept of nodal displacement distribution factors was initially proposed by Leung in 1983 [57] for plane frame structural analysis, and further developed for three-dimensional analysis of space frames and applied to analysis of core frame systems [58-60]. The displacement distribution

factors represent nodal displacement patterns corresponding to unit floor slab in-plane rigid body displacements. In the method, vertical nodal displacements and nodal rotations about the two horizontal axes are obtained by interpolating the nodal displacement patterns. The principal unknowns in a structural analysis are the coefficients of the interpolation of these displacement patterns, the so-called mixing factors in [58] or generalized coordinates in [60], plus floor slab in-plane displacements, i.e., displacements in two horizontal directions and rotations about a vertical axis.

In the nodal displacement distribution factor method for plane frame structures [57], the nodal vertical displacements and in-plane rotations at the kth floor of an N-story frame are expressed as

$$v_i = \beta_i v_k$$

$$\theta_i = \alpha_i \theta_k \qquad (i = 1,2,...,m_c;\ k = 1,2,...,N)$$

where α_i and β_i denote distribution factors of node i at the kth floor; v_k and θ_k are termed the vertical and rotational displacement parameters at the kth floor; m_c is the total number of columns and; N represents the total number of stories in the building. The distribution factors are preliminarily determined by analyzing three-story segments isolated from the original plane frame, so that the displacement parameters are unknowns in the overall structural analysis. The method was subsequently extended to analyze space frame structures [58]. The nodal vertical displacements and rotations about the two horizontal axes in a space frame are defined as

$$w_i = \sum_{j=1}^{3} \beta_{ji} w_{jk}$$

$$\theta_{xi} = \sum_{j=1}^{3} \alpha_{xji} \theta_{xjk}$$

$$\theta_{yi} = \sum_{j=1}^{3} \alpha_{yji} \theta_{yjk}$$

where β_{ji}, α_{xji} and α_{yji} are displacement factors (j = 1,2,3) of node i at the kth floor and; w_{jk}, θ_{xjk} and θ_{yjk} are called mixing factors of the kth floor. Similai to the aforementioned plane frame analysis, the distribution factors were preliminarily determined by analyzing three-story substructures, and the displacement unknowns in the overall analysis were the mixing factors of all floors.

The method was further extended [59] by introducing global distribution factors to model the unevenly distributed column axial deformations away from the ground. Vertical nodal displacements and rotations about two horizontal axes are given by

$$w_i = \sum_{l_1=1}^{3}\sum_{l_2=1}^{3}(\beta^L_{il_1l_2}\cdot\delta^L_{kl_1l_2}) + \sum_{l_1=1}^{3}\sum_{l_2=1}^{3}(\beta^G_{il_1l_2}\cdot\delta^G_{kl_1l_2})$$

$$\theta_{xi} = \sum_{l_1=1}^{3}\sum_{l_2=1}^{3}(\alpha^L_{xil_1l_2}\cdot\delta^L_{kl_1l_2}) + \sum_{l_1=1}^{3}\sum_{l_2=1}^{3}(\alpha^G_{xil_1l_2}\cdot\delta^G_{kl_1l_2})$$

$$\theta_{yi} = \sum_{l_1=1}^{3}\sum_{l_2=1}^{3}(\alpha^L_{yil_1l_2}\cdot\delta^L_{kl_1l_2}) + \sum_{l_1=1}^{3}\sum_{l_2=1}^{3}(\alpha^G_{yil_1l_2}\cdot\delta^G_{kl_1l_2})$$

where α_{xi}, α_{yi} and β_i are the displacement distribution factors of node i at the kth floor level, $\delta_{kl_1l_2}$ are generalized coordinates and, the superscript L denotes local and G denotes global. It is reported in [59] that, with the combination of the local and global distribution factors, the accuracy is improved for buildings having more than ten stories. However, the global distribution factors are determined by analyzing the whole structure by the so called two-level finite element method, which is not a simple job for tall building structures. For an N story building, the total number of displacement unknowns is 21N. The method was refined in [60] by including floor out-of-plane rigid body displacements in the distribution factors, and was applied to the case study of a 32-story core-frame structure. The calculation of the global distribution factors is avoided in [60] and the number of unknowns is reduced to either 12N or 15N depending on the choice of the analysis scheme.

Similar to the finite strip method [20] and the generalized coordinate method [61], this method simplifies the analysis by reducing the number of unknowns, whereas it differs from the preceding plane frame and membrane analogies in that the nodal displacement patterns are determined by preliminary calculations instead of by certain prescribed functions. It can be seen from the above that the number of unknowns is only related to the number of stories in a building in this method, irrespective of the number of nodes at the floor levels. Compared to standard finite element analysis, the required computation is effectively reduced.

2.1.3 Characteristics of the present finite story method

By comparison to the distribution factor method described in the previous section, the finite story method (FSM) proposed herein has the following characteristics:

(1) The vertical nodal displacements and the nodal rotations about the two horizontal axes are defined as direct linear combinations of floor slab displacements without additional generalized coordinates. Correspondingly, nodal displacement fields are defined as nodal displacement patterns due to unit relative floor slab displacements. The magnitudes of the nodal displacements are obtained by multiplying each nodal displacement field by the corresponding relative floor slab displacement and adding up all components. Thus, the principal unknowns in a structural analysis are reduced to only the floor slab displacements themselves, i.e. 5N for an N story building under lateral loads.

(2) For dynamic analysis, the computational effort in condensing out the unwanted degrees-of-freedom is eliminated because the displacement unknowns in an overall analysis are the floor slab displacements only. Generally, by assuming floor slabs to be in-plane rigid, a full 3-D static analysis involves 3(N+n) degrees-of-freedom, where n represents the total number of nodes in the building. In order to obtain the natural frequencies by this approach, a technique such as static condensation or the Guyan

reduction method must then be employed to reduce the overall stiffness and mass matrices to the 3N dynamic degrees-of-freedom. Thus, the number of degrees-of-freedom is different in the static and dynamic analyses when employing the standard finite element method (FEM), while this difference does not exist in the method presented herein.

(3) The continuity of nodal vertical displacements and nodal rotations about the two horizontal axes at the floor levels along a building height is maintained in determining the nodal displacement fields, thus permitting the influence of accumulated deformations from the bottom to the top of a building to be included. The finite two-story segments isolated from the building in determining the nodal displacement fields involve restrained boundary conditions only for the horizontal displacements and the rotations about the vertical axis, whereas conditions for the nodal vertical displacements and the rotations about the two horizontal axes involve specified values (at ground level they are fixed).

2.2 Finite story method based on nodal displacement fields

2.2.1 Assumptions

Because rigorous analytical solutions for 3-D tubular structures are not feasible, assumptions are always imposed on real physical systems to obtain analytical models which are both capable of correctly representing the real systems and are mathematically manageable. It is conventionally assumed that structures are within the linear elastic stage, so that structural responses under combined loads can be obtained by superposing responses to individual load actions; floor slabs are in-plane rigid, out-of-plane stiffness is negligible, and the building is fixed at the ground level. There are two additional assumptions made herein. As in [57-60], relative nodal displacement patterns for vertical nodal displacements and rotations about the two horizontal axes at floor levels corresponding to floor slab displacements are assumed to be governed by the structural characteristics of the immediately adjacent stories, with the influence of the loading

conditions and deformations of the indirectly connected stories assumed to be of little consequence.

The second additional assumption is that the floor slabs undergo rotations about the horizontal axes as rigid plates producing vertical nodal displacements that are linearly distributed. This assumption is introduced in order to model cantilever action and also to meet the rigid-body mode requirement for the convergence of displacement fields. Although sufficiently accurate for the calculation of lateral displacements and dynamic properties of tall building structures, this assumption also implies that the shear lag feature shown in Figure 2.1 is only reflected in nodal displacement fields corresponding to floor slab in-plane displacements, but not included in the nodal displacement fields corresponding to the out-of-plane rotations. Thus this limitation would need to be relaxed if accurate member forces are also expected in the analysis.

2.2.2 Theory of the method

Floor slabs are considered in-plane rigid, with horizontal nodal displacements u, v and rotations θ_z about the vertical axis at each floor level given by:

$$\begin{aligned} u_i &= u_k - y_i\theta_{zk} \\ v_i &= v_k + x_i\theta_{zk} \qquad\qquad k = 1, 2, \ldots, N \\ \theta_{zi} &= \theta_{zk} \end{aligned} \tag{2.1}$$

where x_i, y_i are the coordinates of node i at the kth floor level and u_k, v_k and θ_{zk} represent the kth floor slab in-plane displacements.

For the in-plane rigid assumption associated with equation (2.1), the total number of degrees-of-freedom in a standard finite element method becomes 3(N+n). Since the number of nodes n of a structure is much larger than the number of stories, the large computational effort for tall building structural analysis is due mainly to the 3n

degrees-of-freedom. Obviously, reducing this effort in a 3-D analysis invokes the problem of modeling the 3n nodal degrees-of-freedom, i.e. nodal vertical displacements and rotations about the two horizontal axes.

Since the overall behavior of a building subjected to arbitrary lateral loads involves shear, bending and torsion simultaneously, depicting this response by rigid body displacements of the floor slabs allows the vertical displacement and the rotations about the two horizontal axes of an arbitrary node i at the kth floor to be expressed as

$$\begin{aligned} w_i &= \sum_{j=1}^{5} \beta_i^{(j)} D_{kj} \\ \theta_{xi} &= \sum_{j=1}^{5} \alpha_{xi}^{(j)} D_{kj} \qquad \begin{matrix} i = 1,2,\ldots,m \\ k = 1,2,\ldots,N \end{matrix} \\ \theta_{yi} &= \sum_{j=1}^{5} \alpha_{yi}^{(j)} D_{kj} \end{aligned} \tag{2.2}$$

where

$$\{D_k\} = [D_{k1}, \ \ldots \ , D_{k5}]^T = [u_k \ v_k \ \theta_{zk} \ \theta_{xk} \ \theta_{yk}]^T$$

in which u_k, v_k, θ_{zk}, θ_{xk} and θ_{yk} are the floor slab rigid-body displacements which represent the generalized coordinates of the structure at the kth floor level; $\beta_i^{(j)}$, $\alpha_{xi}^{(j)}$, $\alpha_{yi}^{(j)}$ (j=1,...,5) are the displacement distribution coefficients for node i at the kth floor corresponding to generalized displacement coordinate D_{kj}; D_{kj} denotes the j type displacement of floor slab k; and m denotes the total number of nodes of this floor. For all the nodes at one floor level, the coefficients $\beta_i^{(j)}$, $\alpha_{xi}^{(j)}$, and $\alpha_{yi}^{(j)}$ represent the nodal displacement fields of that floor. The physical meaning of these coefficients is exposed by letting only one of the five generalized coordinates be unity, and constraining the other four to be zero in equation (2.2). For instance, setting D_{k2}, D_{k3}, D_{k4}, D_{k5} to zero, and D_{k1} to unity establishes the vertical nodal displacements at the kth floor as $\beta_i^{(1)}$. At the

same time, the nodal rotations about the two horizontal axes x and y are $\alpha_{xi}^{(1)}$ and $\alpha_{yi}^{(1)}$ (i=1,2,...,m), respectively.

Theoretically, the present FSM is a two-stage interpolation. First, the infinite degrees-of-freedom of structural members are interpolated from finite ones at element nodes. This is standard in the FEM where displacements at nodes are the unknowns while, for any point within an element, displacements are obtained through some given shape functions. In the second stage, nodal displacements at each floor level are further interpolated from generalized coordinates of that floor. Only the generalized coordinates are the unknowns in an overall analysis, which are constant at floor levels but vary from floor to floor. If nodal displacement fields are preliminarily determined, based on equations (2.1) and (2.2), the total potential energy of a whole building structure will be a function of the generalized coordinates, and by the total potential energy principle

$$\begin{aligned} \Pi &= \sum_{k=1}^{N} \Pi_k (D_{k1}, \ldots, D_{k5}) \qquad && j = 1, \ldots, 5 \\ \frac{\partial \Pi}{\partial D_{kj}} &= 0 && k = 1, 2, \ldots, N \end{aligned} \tag{2.3}$$

thus allowing all the generalized coordinates to be determined by 5N equations.

The method can also be visualized as a displacement transformation. The displacement vector $\{\bar{d}_i\}$ in the local coordinate system of node i at the kth floor level is transformed into $\{d_i\}$ in the global coordinate system:

$$\{\bar{d}_i\} = [T_i] \{d_i\} \tag{2.4}$$

where

$$\{\bar{d}_i\} = [\bar{u}_i \ \bar{v}_i \ \bar{w}_i \ \bar{\theta}_{xi} \ \bar{\theta}_{yi} \ \bar{\theta}_{zi}]^T$$

$$\{d_i\} = [u_k \ v_k \ \theta_{zk} \quad w_i \ \theta_{xi} \ \theta_{yi}]^T$$

and $[T_i]$ is the coordinate transformation matrix which includes equation (2.1), and given in Appendix III. Vector $\{d_i\}$ denotes the constrained nodal displacements in the global coordinate system which are partitioned into two parts: the first - u_k, v_k, θ_{zi} - represents the rigid body displacements of the kth floor slab and the second part - w_i, θ_{xi}, θ_{yi} - contains the vertical displacement and the rotations about the horizontal axes.

The vector of generalized coordinates at the kth floor is also partitioned into two parts

$$\{D_k\} = \left[D_{k1} \quad D_{k2} \quad D_{k3} \mid D_{k4} \quad D_{k5}\right]^T = \left[D_{kI} \mid D_{kII}\right]^T \tag{2.5}$$

Writing equation (2.2) in matrix form and comparing $\{d_i\}$ with $\{D_k\}$ lead to

$$\begin{Bmatrix} d_{i1} \\ d_{i2} \end{Bmatrix} = \begin{bmatrix} I & 0 \\ g_1 & g_2 \end{bmatrix} \begin{Bmatrix} D_{kI} \\ D_{kII} \end{Bmatrix} \tag{2.6}$$

where [I] is a 3x3 identity matrix and $[g_1]$, $[g_2]$ are nodal displacement transformation matrices. For the whole structure

$$\begin{Bmatrix} d_1 \\ d_2 \end{Bmatrix} = \begin{bmatrix} I & 0 \\ G_1 & G_2 \end{bmatrix} \begin{Bmatrix} D_I \\ D_{II} \end{Bmatrix} \tag{2.7}$$

in which

$$\{D\} = [D_I \; D_{II}]^T = [D_{11} \; D_{21} \ldots D_{NI} \mid D_{1II} \; D_{2II} \ldots D_{NII}]^T$$

$$\{d\} = [d_1 \; d_2]^T = [d_{11} \; d_{21} \ldots d_{N1} \mid d_{12} \; d_{22} \ldots d_{N2}]^T$$

where [G] is a displacement transformation matrix assembled from $[g_1]$ and $[g_2]$ of all nodes. By energy conservation, the overall stiffness matrix corresponding to $\{D\}$ is obtained:

$$[K^*] = [G]^T [K] [G]$$

$$= \begin{bmatrix} K_{11} + G_1^T K_{21} + K_{12} G_1 + G_1^T K_{22} G_1 & K_{12} G_2 + G_1^T K_{22} G_2 \\ G_2^T K_{21} + G_2^T K_{22} G_1 & G_2^T K_{22} G_2 \end{bmatrix} \tag{2.8}$$

in which [K] is the overall stiffness matrix of the 3-D FEM corresponding to {d}. The order is 5Nx5N for $[K^*]$ and 3(N+n)x3(N+n) for [K].

Because the second stage interpolation of equation (2.2) involves only vertical nodal displacements and nodal rotations about the horizontal axes, a unique condensed overall stiffness matrix $[K^{**}]$ of order 3Nx3N (corresponding to $\{D_I\}$ in equation (2.7)) can be obtained from either $[K^*]$ or [K] of equation (2.8):

$$\begin{aligned} [K^{**}] &= (K_{11} + G_1^T K_{21} + K_{12} G_1 + G_1^T K_{22} G_1) \\ &\quad - (K_{12} G_2 + G_1^T K_{22} G_2) (G_2^T K_{22} G_2)^{-1} (G_2^T K_{21} + G_2^T K_{22} G_1) \\ &= K_{11} - K_{12} K_{22}^{-1} K_{21} \end{aligned} \tag{2.9}$$

This ensures good solutions for horizontal motions, rotations about the vertical axis and natural frequencies.

In natural frequency calculations, the inertial effects of the mass at the floor levels are considered for the two components of translation and rotation about the vertical axis only, with no contribution about the horizontal axes. Consistent mass matrices of beam and column elements undergo the same displacement transformation as element stiffness matrices.

2.2.3 Nodal displacement fields

Previously in equation (2.2), nodal displacement fields were defined as nodal displacement patterns arising from unit generalized coordinates. However, in order to determine the nodal displacement fields approximately by analyzing two-story segments

of the building, the displacement distribution coefficients; $\beta_i^{(j)}$, $\alpha_{xi}^{(j)}$, $\alpha_{yi}^{(j)}$ are redefined to represent nodal displacement patterns corresponding to unit relative generalized coordinates. Figure 2.4 shows the definition of vertical nodal displacement fields $\beta^{(j)}$ (j = 1, 2, 3). With the definition $\Delta D_{kj} = D_{kj} - D_{k-1j}$, it can be seen that the curve for $\beta^{(1)}$ represents the vertical nodal displacement pattern due to $\Delta D_{k1} = 1$ ($\Delta D_{kj} = 0.0$; j = 2, 3, 4, 5), whereas that for $\beta^{(2)}$ is due to $\Delta D_{k2} = 1$ ($\Delta D_{kj} = 0.0$; j = 1, 3, 4, 5), and so on. These curves are obtained by analyzing a two-story substructure as shown in Figure 2.5. The nodal displacement fields $\alpha_{xi}^{(j)}$ and $\alpha_{yi}^{(j)}$ are defined in a similar way and represent patterns of nodal rotations about the horizontal axes. Correspondingly, equation (2.2) is modified as follows:

$$
\begin{aligned}
w_i &= \sum_{j=1}^{5} \beta_i^{(j)} \Delta D_{kj} \\
\theta_{xi} &= \sum_{j=1}^{5} \alpha_{xi}^{(j)} \Delta D_{kj} \qquad \begin{matrix} i = 1, 2, \ldots, n \\ k = 1, 2, \ldots, N \end{matrix} \\
\theta_{yi} &= \sum_{j=1}^{5} \alpha_{yi}^{(j)} \Delta D_{kj}
\end{aligned}
\tag{2.10}
$$

According to the first basic assumption, nodal displacement fields at the floor levels are assumed to be determined primarily by the structural properties and load conditions of adjacent stories. A two-story segment is therefore isolated from an original building in order to determine the nodal displacement fields at the kth floor. This process is depicted in Figure 2.5, which shows that the bottom of the substructure starts from the ends of columns immediately above the (k-1)th floor slab and the top of the substructure terminates at the (k+1)th floor including the slab.

Certain boundary conditions are imposed on the two-story substructure according to the definition of nodal displacement fields. At the top, a non-zero component of floor displacement is imposed and the other floor displacements are restrained. At the bottom

level, horizontal displacements u_{k-1}, v_{k-1} and rotation θ_{zk-1} about the vertical axis are restrained while, for the other three degrees-of-freedom (w, θ_x, θ_y) of each node, computed displacement conditions are imposed. Thus, at the ground level conditions are fixed and at the other floor levels nodal displacements at the (k-1)th floor from the previous analysis of a two-story segment are input. The latter introduce the influence of the unevenly distributed nodal vertical displacements due to torsion and/or bending which accumulated from the building bottom. At the same time, this also maintains continuity of nodal rotations about the horizontal axes at floor levels.

Under the above boundary conditions, nodal displacement patterns corresponding to unit relative generalized coordinates are the required nodal displacement fields which are given by

$$\begin{aligned} \beta_i^{(j)} &= \frac{w_i}{D_{kj}} \\ \alpha_{xi}^{(j)} &= \frac{\theta_{xi}}{D_{kj}} \qquad\qquad j = 1, 2, 3 \\ \alpha_{yi}^{(j)} &= \frac{\theta_{yi}}{D_{kj}} \qquad\qquad i = 1, 2, \ldots, m \end{aligned} \tag{2.11}$$

for j = 4, 5, nodal displacement fields corresponding to θ_{xk} and θ_{yk} do not need to be computed since they are determined only by the nodal locations along the horizontal axes. Thus the calculation of the first three nodal displacement fields is carried out from the bottom to the top of a building.

It is to be expected that distinct changes in relative nodal displacement patterns of a slender building structure will occur only when stories are encountered which have appreciably different material properties, geometric properties or boundary conditions. Thus, for buildings with setbacks the calculation needs to include the transfer floor levels. For uniform buildings, on the other hand, the results to follow show that acceptable

solutions are obtained by calculating nodal displacement fields only at the first three floor levels and applying the mean values from these to the other levels. Such results are denoted by FSM* in the numerical examples.

The equilibrium equations for the above two-story segments are given by

$$\begin{bmatrix} k_{mm} & k_{ms} \\ k_{sm} & k_{ss} \end{bmatrix} \begin{Bmatrix} d_m \\ d_s \end{Bmatrix} = \begin{Bmatrix} d_m \\ 0 \end{Bmatrix} \tag{2.12}$$

where $\{d_m\}$ represents the imposed displacements which include in-plane displacements u, v, θ_z at the (k+1)th floor level as well as all the nodal displacements at the (k-1)th floor level; $\{f_m\}$ denote the forces corresponding to $\{d_m\}$ and; $\{d_s\}$ contains the nodal displacements w, θ_x, θ_y at the kth and (k+1)th floor levels. The latter are obtained by solving

$$[k_{ss}]\{d_s\} = -[k_{sm}]\{d_m\} \tag{2.13}$$

The number of equations in (2.13) is 3L+3, where L denotes the total number of nodes at the kth plus (k+1)th floor levels. Three cases (j = 1, 2, 3) are calculated at the same time in equation (2.13), so that $\{d_s\}$ is of order (3L+3)x3.

2.2.4 Overall structural analysis

For a 3-D beam element, equation (2.10) yields the nodal displacements written as

$$\begin{Bmatrix} d_i \\ d_j \end{Bmatrix} = [g_b] \begin{Bmatrix} D_{k-1} \\ D_k \end{Bmatrix} \tag{2.14}$$

whereas for a 3-D column element

$$\begin{Bmatrix} d_i \\ \\ d_j \end{Bmatrix} = [g_c] \begin{Bmatrix} D_{k-2} \\ D_{k-1} \\ D_k \end{Bmatrix} \tag{2.15}$$

in which the transformed beam and column displacement vectors are

$$\{d_b\} = [u_k \quad v_k \quad \theta_{zk} \quad w_i \quad \theta_{xi} \quad \theta_{yi} \mid u_k \quad v_k \quad \theta_{zk} \quad w_j \quad \theta_{xi} \quad \theta_{yi}]^T$$
$$\{d_c\} = [u_{k-1} \quad v_{k-1} \quad \theta_{zk-1} \quad w_i \quad \theta_{xi} \quad \theta_{yi} \mid u_k \quad v_k \quad \theta_{zk} \quad w_j \quad \theta_{xi} \quad \theta_{yi}]^T$$

and $[g_b]$, $[g_c]$ are transformation matrices of nodal displacement distribution coefficients, given in the Appendix IV. Thus, energy conservation leads to the following stiffness and consistent mass matrices for beams and columns corresponding to the generalized coordinates at floor levels

$$[k_b^*] = [g_b]^T [k_b] [g_b] \qquad [k_c^*] = [g_c]^T [k_c] [g_c] \tag{2.16}$$

$$[m_b^*] = [g_b]^T [m_b] [g_b] \qquad [m_c^*] = [g_c]^T [m_c] [g_c] \tag{2.17}$$

where $[k_b]$, $[k_c]$, $[m_b]$ and $[m_c]$ are the normal element stiffness and mass matrices in the global coordinate system. In the famed tube, the deep spandrel beams are rigidly connected to the columns. While the total length of each element is measured from center to center of joints, the ends within the finite joints are considered to be flexurally undeformable, and as the result, elements are with rigid arms at the ends. However, the axial deformations of columns are still based on the total lengths of the elements. The element matrices $[k_b]$, $[k_c]$, $[m_b]$ and $[m_c]$ are obtained by the following transformations:

$$\begin{aligned} [k_b] &= [T_b]^T [R_b]^T [\bar{k}_b] [R_b] [T_b]^T \\ [k_c] &= [T_c]^T [R_c]^T [\bar{k}_c] [R_c] [T_c]^T \end{aligned} \tag{2.18}$$

$$[m_b] = [T_b]^T [\bar{m}_b] [T_b]^T$$
$$[m_c] = [T_c]^T [\bar{m}_c] [T_c]^T \tag{2.19}$$

in which [T] is the coordinate transformation matrix; [R] is the rigid end transformation matrix; $[\bar{k}]$ and $[\bar{m}]$ are element stiffness and mass matrices in element local coordinates and; subscript b and c stand for beam and column, respectively. All matrices on the right hand of above equations are listed in the Appendix I, II and III.

The equilibrium and dynamic characteristic equations for the building are built by assembling the overall stiffness and mass matrices from the above element matrices to yield

$$[K^*] \{D\} = \{P^*\} \tag{2.20}$$

$$\left| [K^*] - \omega^2 [M^*] \right| = 0 \tag{2.21}$$

where $\{P^*\}$ represents lateral forces and moments acting at floor levels, and ω denotes the natural frequencies of vibrations of the building. Nodal displacements corresponding to $\{D\}$ are obtained from equations (2.1) and (2.10).

The overall stiffness matrix and mass matrix can also be established by utilizing the substructure technique, which will be more efficient in saving computer time if the building is uniform over most stories. This procedure will be described in Chapter 5.

2.3 Numerical examples

To illustrate the validity of the simplified procedure proposed herein, four numerical examples are presented. Each was calculated by both the commercial FEM program NISA and a FORTRAN computer program designed according to the present FSM.

2.3.1 Unsymmetric 20-story space frame

The 20-story unsymmetric space frame structure analyzed by Leung and Wong [59] is employed. Figure 2.6 shows the plan layout of the structure. All members have identical cross section 0.3x0.3 m; story heights are 5.0 m. Young's modulus E = 210 GPa and the shear modulus G = 80.8 GPa. Static response under lateral load of 1.0×10^3 kN, which is applied at node 1 in the X direction at each floor level, and natural frequencies and modes of vibrations are computed. Translational floor mass is 0.253×10^4 kg, with corresponding mass moment of inertia about the vertical axis = 0.545×10^5 kg m^2.

Floor in-plane displacements at node 1 and rotations about the vertical axis are listed in Table 2.1 in comparison with results from 3-D FEM. The maximum difference between the two solutions is 4.4% for displacement u, 1.3% for v, and 4.5% for rotation θ_z. Table 2.2 shows natural frequencies obtained by FSM and FEM. The first, second and the third frequencies correspond to the first primarily translational modes of this torsionally coupled structure in the two perpendicular directions and the torsion dominated mode, respectively. The other three frequencies are associated with the corresponding second modes of these vibrations. The maximum difference between the two calculations is 6.2%.

The number of independent degrees-of-freedom (DOFs) in 3-D FEM is 48 at each floor, with a total of 960, whereas in the present FSM, it is 5 per floor for a reduced total of 100. The CPU time is 126.5 sec, approximately one-half of the 242.8 sec required by FEM for the above displacement and frequency calculation. Actually, the greater the number of nodes at the floor levels, the more efficient the method becomes in terms of computer storage and CPU. The following two examples demonstrate this point.

2.3.2 Small scale model of a 20-story framed tube

A small scale (1:30) model of a 20-story framed tube structure adopted from [62] is studied, in which the behavior of the model under lateral load was tested. The plan

dimension of the model is 494x667 mm, and the total height is 2.0 m. Figure 2.7 shows the plan and elevation. A point load 1.5 kN was applied at the origin at the top level of the model in the Y direction. Elasticity modulus E is 2.2×10^4 MN/m^2, and Poisson's ratio is taken as 0.2 in the calculation.

Lateral displacements at floor levels are shown in Figure 2.8 in comparison with results from FEM and experiment carried out by Pocanschi and Olariu [62]. The solutions denoted by FSM* is obtained by calculating nodal displacement distribution coefficients only at the first three floor levels, as described in Section 2.2.3. It is seen that the lateral displacements obtained by the FSM and FEM are very close; the top drift is 31.5 mm by FSM vs. 34.8 mm by FEM.

The shear forces in columns in the first and fourth stories are given in Figure 2.9. Similar correlation as above is seen for column shear force distributions. It is also seen that the plane frame action in the frame panels parallel to the load direction are well predicted by the present method.

2.3.3 Symmetric 30-story framed tube

The 30-story framed tube structure from [20] is analyzed. Figure 2.10 shows the plan layout of the building. Both the story height and the column spacing are 3.66 m. Young's modulus E = 0.239×10^5 MPa; shear modulus G = 0.99×10^4 MPa and; mass density is 2.4×10^3 kg/m^3. Geometric properties of members are listed in Table 2.3. Translational mass and mass moment of inertia about the vertical axis at floor levels are 5.604×10^5 kg and 1.702×10^8 kg $\cdot$ m^2, respectively. Two static load cases, and natural frequencies and modes of vibration are studied.

Load case one: The structure is subject to uniformly distributed torque of 720.6 kN $\cdot$ m/m. In the present FSM calculation, the uniformly distributed torque is replaced by equivalent concentrated torques 2.637×10^3 kN $\cdot$ m applied at floor levels.

Figure 2.11 shows rotations about the vertical axis. It is seen that the rotational responses of the floor slabs are almost identical for both methods. The top floor rotation is 0.548×10^{-4} rad by the present FSM and 0.557×10^{-4} rad by FEM, thus differing by only 1%. Figures 2.12(a) and 2.12(b) show column shear forces Fx and Fy in comparison with results of FEM. Column 1 and 6 are in the frame panel parallel to the X-direction and their values represent the envelope of Fx in the panel. Similarly, column 6 and 9 belong to the Y-direction panel, and yield the envelope for Fy in this panel. It can be seen that the results of the FSM solution agree well with those of FEM upon the whole, except that 17-19% overestimation of shears for column 6 in the second story. Some discrepancy in the topmost few stories can also be observed; however, since the shear in those stories is small in magnitudes, the FSM results can be deemed as acceptable here also.

Shear forces of spandrel beams at floors 1, 10, 20 and 30 are shown in Figure 2.13 for a quarter of the building cross-section. Node 6 is a corner of the framed tube as shown in Figure 2.10. Although shear forces in the bottom stories are most important, the results indicate that very close agreement exists between the present FSM and FEM at all levels.

Load case two: Uniformly distributed lateral load of 2.0 kN per floor in the Y direction is applied at floor levels. The building deflection is shown in Figure 2.14. The maximum drift at the top is 0.480 m by FSM, and 0.495 m by FEM.

Figures 2.15 show the shear force (F_y) distribution in columns in the first and the second stories. The corresponding bending moments about the X axis in columns in the first two stories are given in Figure 2.16. It can be seen that the member forces in the first story obtained by FSM agree well with FEM solutions, while in the second story greater discrepancy appears. The reason for this discrepancy in member forces is attributed to the approximation in modeling shear lag which is included only in the shear deformation mode in determining nodal displacement fields.

Natural frequencies and vibration modes: Figure 2.17 shows the first 6 natural frequencies and corresponding mode shapes obtained by both methods. The first three frequencies correspond to the first modes of vibration in the Y-direction, the X-direction and rotation about the Z axis, respectively, The next three frequencies correspond to the associated second modes of these vibrations. The tabular data for the frequencies show a maximum difference 5.7% which occurs for the fundamental mode between the calculations by FSM* and FEM. As noted previously, results denoted by FSM* are obtained by calculating nodal displacement fields only at the first three floor levels. This additional simplification introduces no additional errors in either floor rotations or member forces of the building under applied torque already presented in Figure 2.11 - 2.13, but further reduces considerably computer CPU compared with FSM which calculates nodal displacement fields at every other floor in this example.

The CPU time required for the eigenvalue problem of this example by the present FSM method (suppose nodal displacement fields have already been determined in static calculations, so that the CPU for nodal displacement fields is not included) is 184.2 sec about one-tenth of 1971.6 sec by FEM. To obtain the whole solution requires 489.6 sec by FSM if the nodal displacement fields are calculated at every other floor level, compared with 3456.3 sec by FEM. If the nodal displacement fields are calculated only three times (solutions denoted by FSM* in Figure 2.17), CPU time is 271.6 sec, or roughly 8/100 of that for FEM and 5/9 for FSM.

2.3.4 Unsymmetric 30-story framed tube

To examine application of the method in a more general case, an unsymmetrical framed tube structure is created from the preceding example by modifying one of the Y-direction panels, i.e. the left panel has fewer columns and the following changed geometric properties: (a) for all columns - $A=0.675\ m^2$, $I_x=3.70\times10^{-2}\ m^4$, $I_y=3.70\times10^{-2}$

m^4, $J=1.72x10^{-2}$ m^4; (b) for all spandrel beams - $A=0.390$ m^2, $I_y=5.33x10^{-2}$ m^4, $I_z=3.02x10^{-3}$ m^4, $J=1.027x10^{-2}$ m^4. The plan view of the structure is shown in Figure 2.18.

Although asymmetric in stiffness, the center of mass is located at the centroid of the rectangular cross-section. Translational mass and mass moment of inertia about the vertical axis at each floor level are $5.6x10^5$ kg and $1.707x10^8$ kg m^2, respectively. Thus, the structure is unsymmetric in the Y-direction along which a uniformly distributed lateral load Fy = 400.3 kN is applied at each floor level. In determining the torsionally uncoupled nodal displacement patterns for the unsymmetric framed tube corresponding to floor displacements in the FSM model, the origin of the local coordinate system of the two-story segment is located approximately at x = 4.11 m in the overall coordinate system, which is the shear center of a single story in this uniform building.

Figures 2.19 and 2.20 show floor slab displacement components in the Y-direction and rotations about the vertical axis, respectively. The results show that floor rotations by FSM and FEM are almost coincident over the entire height of the building, although the lateral displacements do not agree quite as well at the upper floor level. Comparisons of the frequencies and actual mode shapes obtained by FSM and FEM are presented in Figure 2.21, where it can be seen that good agreement is achieved for both sets of data. The maximum difference in the frequency predictions is 5.9% and occurs for the fundamental mode. The mode shapes shown refer to the floor origins and are normalized in individual component vectors. A top view of the associated first 6 vibration mode shapes is shown in Figure 2.22. Since the structure is symmetric in the X-direction, mode shapes 2 and 5 are solely translational, whereas modes 1, 3, 4 and 6 are torsionally coupled. Among the latter, it can been seen from Figure 2.22 that modes 1 and 4 are dominated by lateral motion whereas modes 3 and 6 involve primarily torsional oscillation.

By the present method, the number of independent DOFs for this 3-D unsymmetrical structure is 150 in the overall analysis and 204 in determining nodal displacement fields, contrasted with 3060 DOFs by standard 3-D FEM. The CPU time by FSM is 397.6 sec, versus 2161 0 sec for the FEM.

Although the foregoing examples represent space frame and framed tube structures, the proposed FSM procedure can also be readily applied to other kinds of structures, such as bundled tubes and tube-in-tubes with or without setbacks. For uniform buildings, whether computation of nodal displacement fields is carried out at every floor level or only for the lowermost three stories dose not produce any obvious differences in the results for floor slab rotations about the vertical axis and natural frequencies, even though it does have some influence on lateral deflections and member forces.

2.4 Summary

The finite story method (FSM), an approximate approach based on nodal displacement fields, has been proposed for tall buildings subject to lateral loads. The characteristics of the FSM are described in comparison with the displacement distribution factor method, with which the present method shares the concept of distribution factors. Additional assumptions to those general in tall building structural analysis, the analytical modeling, and the procedure of the finite story method are also described. It is shown that the condensed overall stiffness matrix corresponding to floor in-plane displacements (U, V and θ_z) obtained by the FSM is identical with that obtained by the standard FEM. In general, compared with 3-D FEM the present method reduces storage requirements and saves much computer time in solving equilibrium equations, condensing out DOFs and extracting eigenvalues, although it doe take time in the determining nodal displacement fields.

The present FSM has been applied to the analysis of a space frame and several framed tube structures under bending and torsion. These numerical examples demonstrate that the present method is effective in predicting the static responses and the dynamic characteristics of such structures. The computational work is significantly reduced for determining displacements, natural frequencies and modes of vibration, making the proposed procedure an attractive one for implementation on personal computers.

Before extending the FSM to the analysis of tube-in-tube structures, core tubes are studied in the following Chapter. Based on a review of previous research on core tubes under torsional actions and thin-wall beam theory, the core tube is modelled by a thin-wall beam with equivalent closed section. This simplified model of core tubes is compatible with the present finite story method, thus allowing the method to be applied to tube-in-tube structures in later stages of this work.

Table 2.1 Floor displacements of unsymmetric space frame

Floor Level	FSM			FEM		
	u	v	θ_z	u	v	θ_z
20	3.859	-1.561	0.295	4.035	-1.580	0.309
19	3.800	-1.552	0.293	3.976	-1.573	0.306
18	3.732	-1.538	0.289	3.905	-1.558	0.302
17	3.651	-1.517	0.285	3.808	-1.535	0.296
16	3.555	-1.488	0.279	3.699	-1.505	0.289
15	3.443	-1.451	0.271	3.574	-1.467	0.280
14	3.314	-1.407	0.262	3.433	-1.421	0.270
13	3.168	-1.354	0.252	3.275	-1.366	0.259
12	3.006	-1.294	0.240	3.310	-1.305	0.247
11	2.828	-1.225	0.227	2.911	-1.236	0.233
10	2.634	-1.149	0.213	2.707	-1.158	0.218
9	2.424	-1.065	0.196	2.486	-1.072	0.201
8	2.199	-0.973	0.179	2.251	-0.979	0.183
7	1.959	-0.873	0.160	2.001	-0.878	0.163
6	1.704	-0.765	0.140	1.738	-0.769	0.142
5	1.436	-0.649	0.119	1.461	-0.653	0.120
4	1.153	-0.526	0.096	1.172	-0.528	0.097
3	0.859	-0.392	0.072	0.870	-0.396	0.073
2	0.554	-0.258	0.047	0.557	-0.257	0.047
1	0.239	-0.114	0.021	0.239	-0.113	0.021

(Unit: deflection, m; rotation, rad)

Table 2.2 Natural frequencies of unsymmetric space frame (Hz)

Mode number	FSM	FEM	Difference(%)
1	0.586	0.551	6.4
2	0.598	0.570	4.9
3	0.707	0.675	4.7
4	1.786	1.712	4.3
5	1.815	1.736	4.6
6	2.139	2.045	4.6

Table 2.3 Member properties of 30-story symmetric framed tube

Member	Area (m^2)	Shear Area (m^2)	Moment of Inertia (m^4)	Torsion Constant (m^4)
Interior column	0.337	0.281	$I_x=0.261\times10^{-2}$ $I_y=0.344\times10^{-1}$	0.860×10^{-2}
Corner column	0.674	0.562	$I_x=0.370\times10^{-1}$ $I_y=0.370\times10^{-1}$	0.172×10^{-1}
Spandrel beam	0.368	[illegible]	$I_y=0.447\times10^{-1}$ $I_z=0.285\times10^{-2}$	0.958×10^{-2}

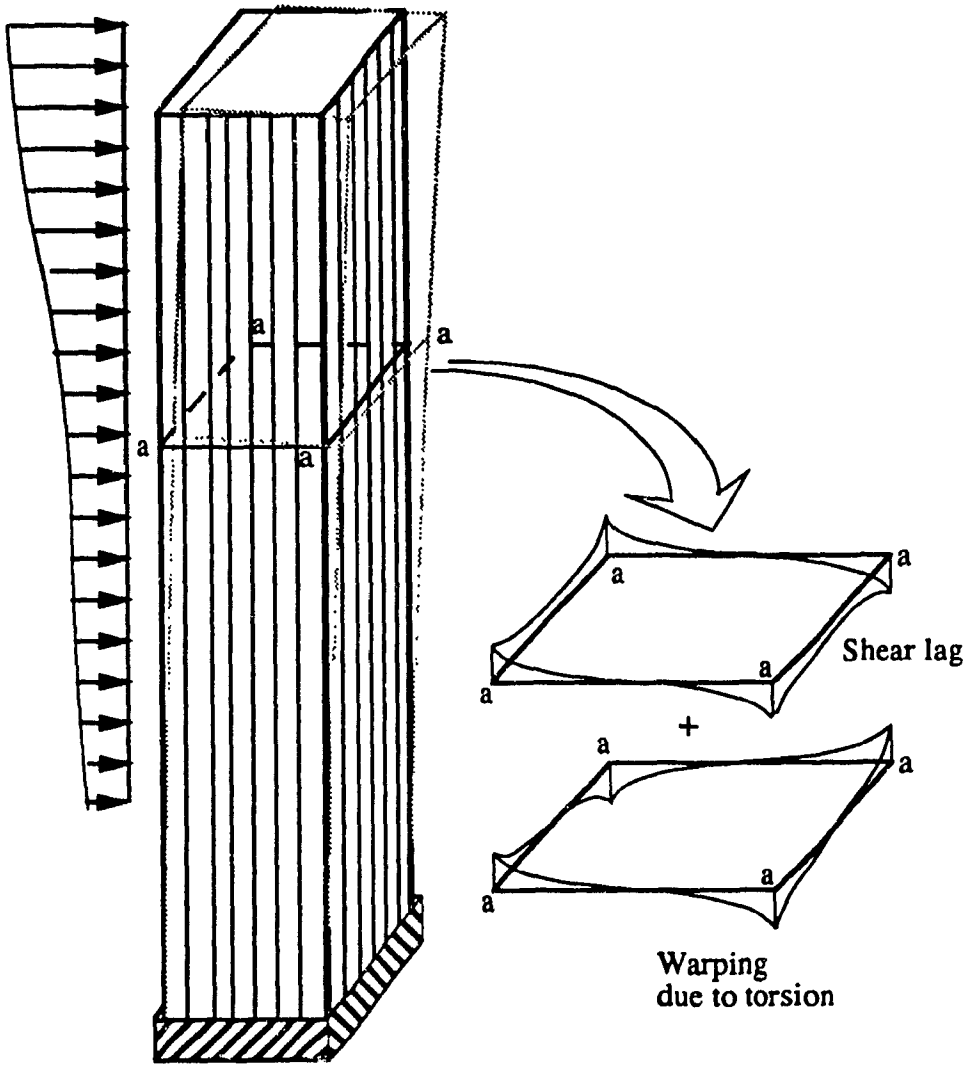

Figure 2.1 Framed tube structure under arbitrary lateral loading

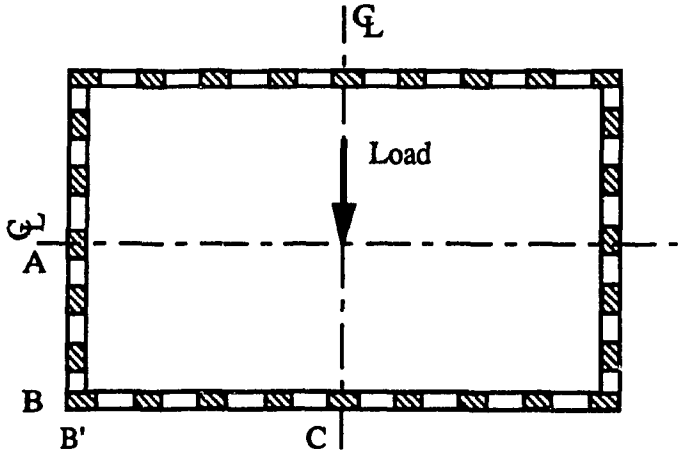

(a) Doubly symmetric framed tube under lateral load

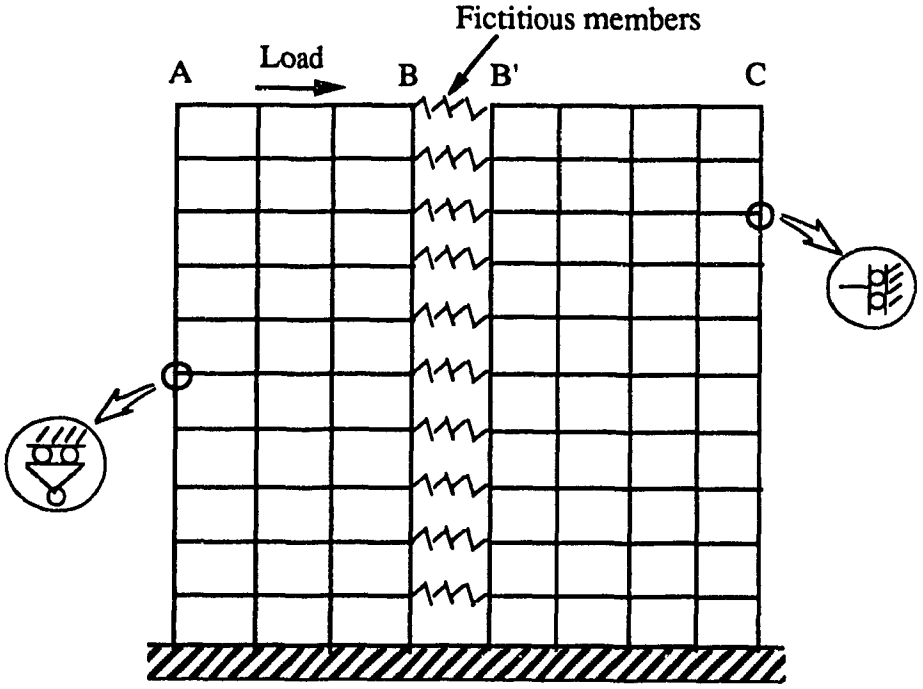

(b) Equivalent plane system

Figure 2.2 Equivalent plane system for doubly symmetric framed tube

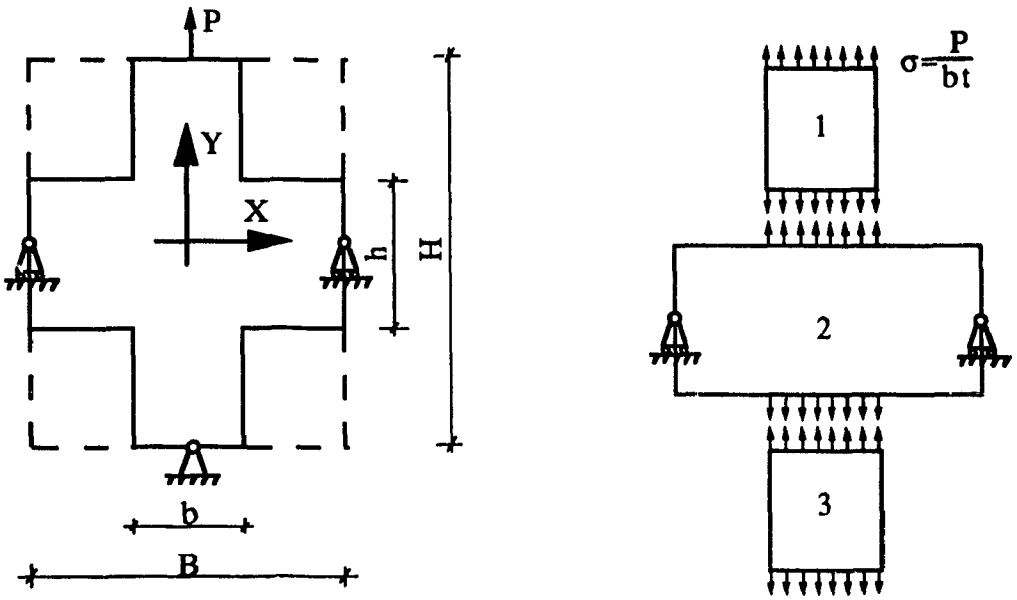

(a) Element analysis for equivalent E_y

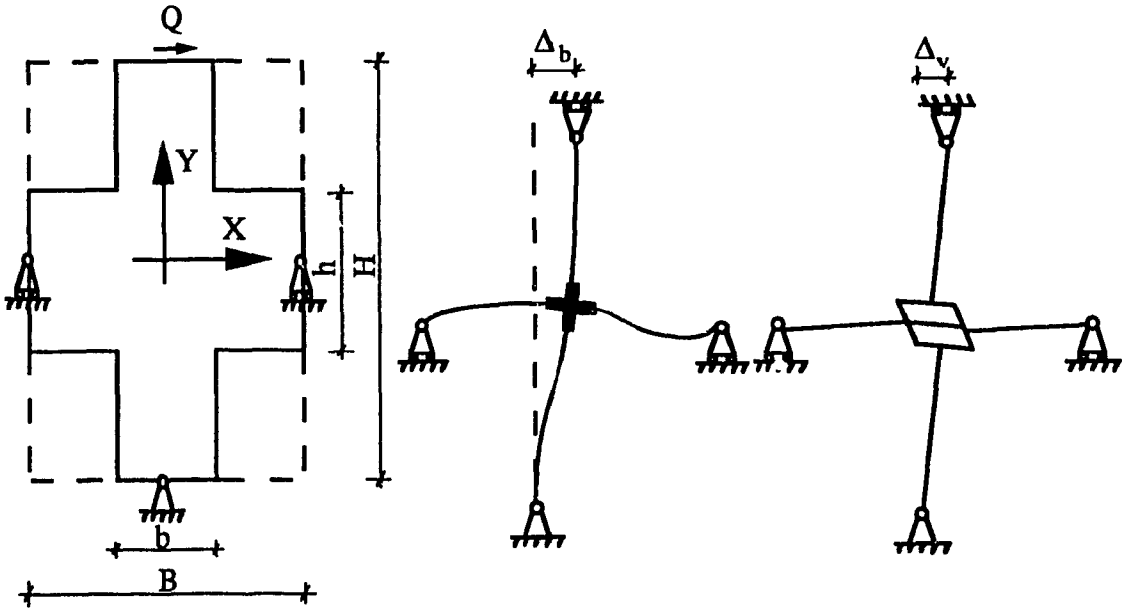

(b) Element analysis for equivalent G_{xy}

Figure 2.3 Orthotropic membrane analogy for uniform framed tube

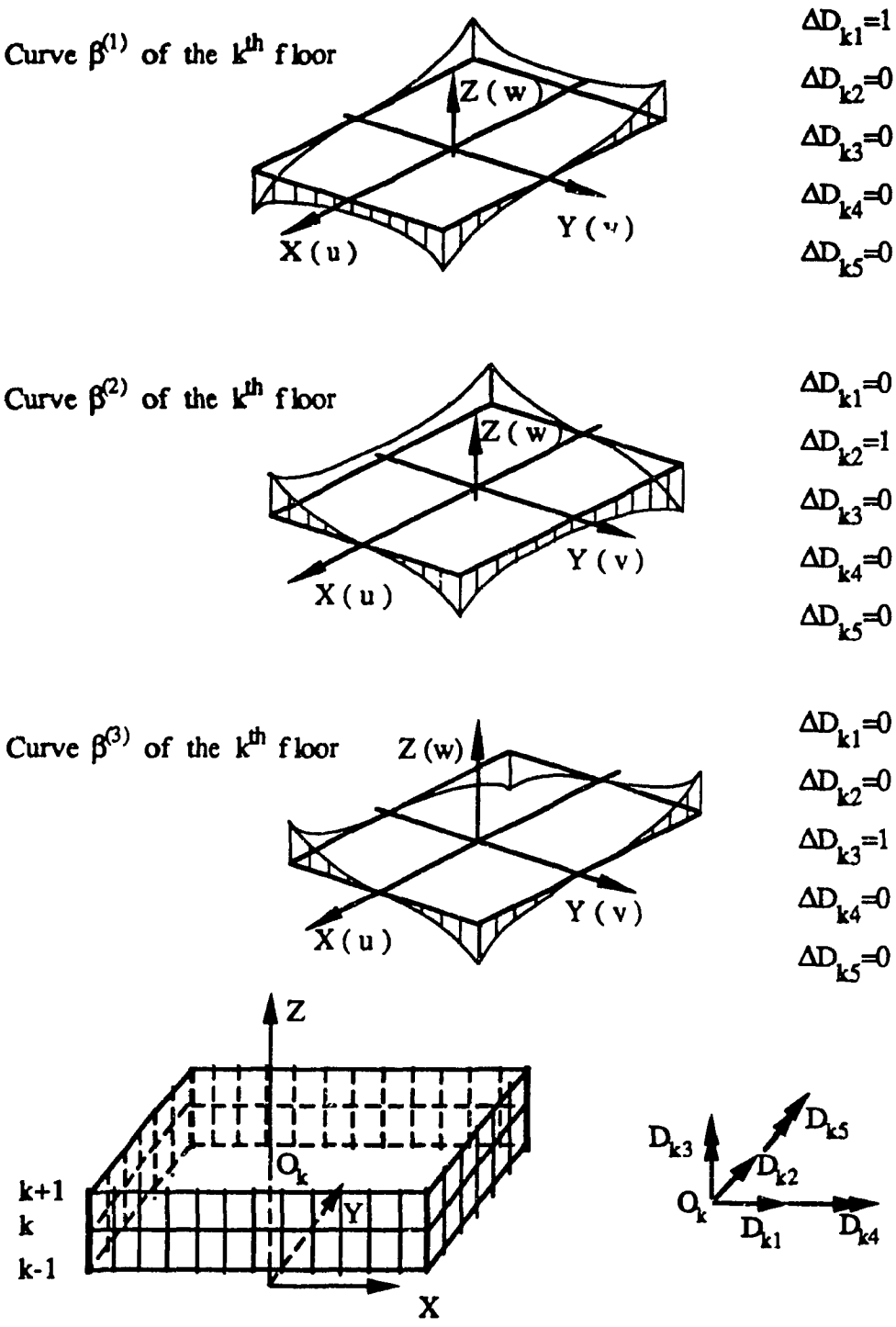

Figure 2.4 Definition of nodal displacement fields

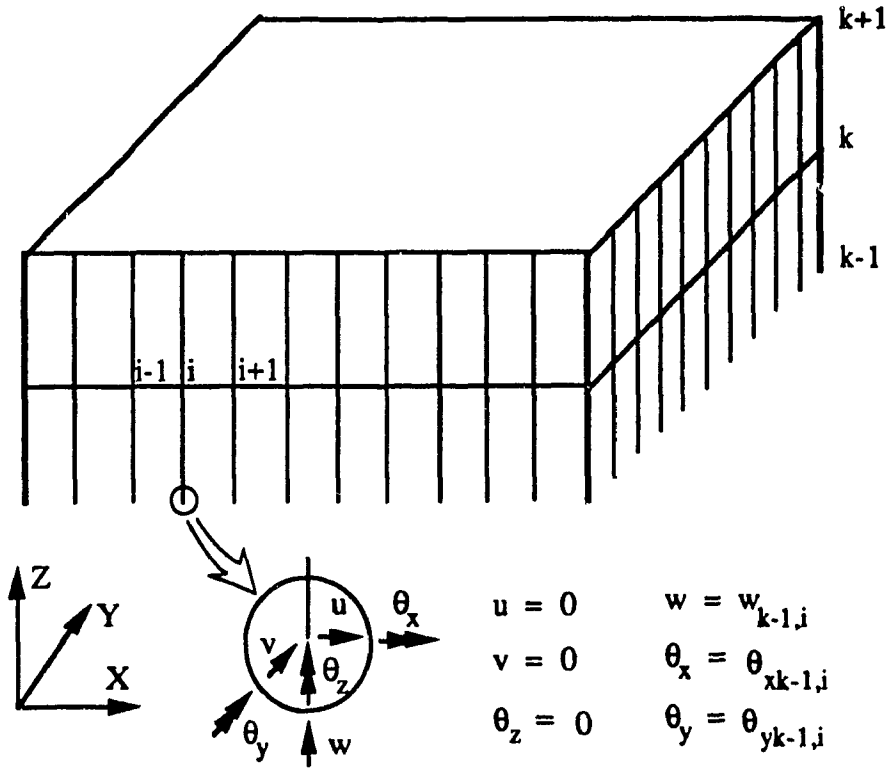

Figure 2.5 Two-story segment for determining nodal displacement fields

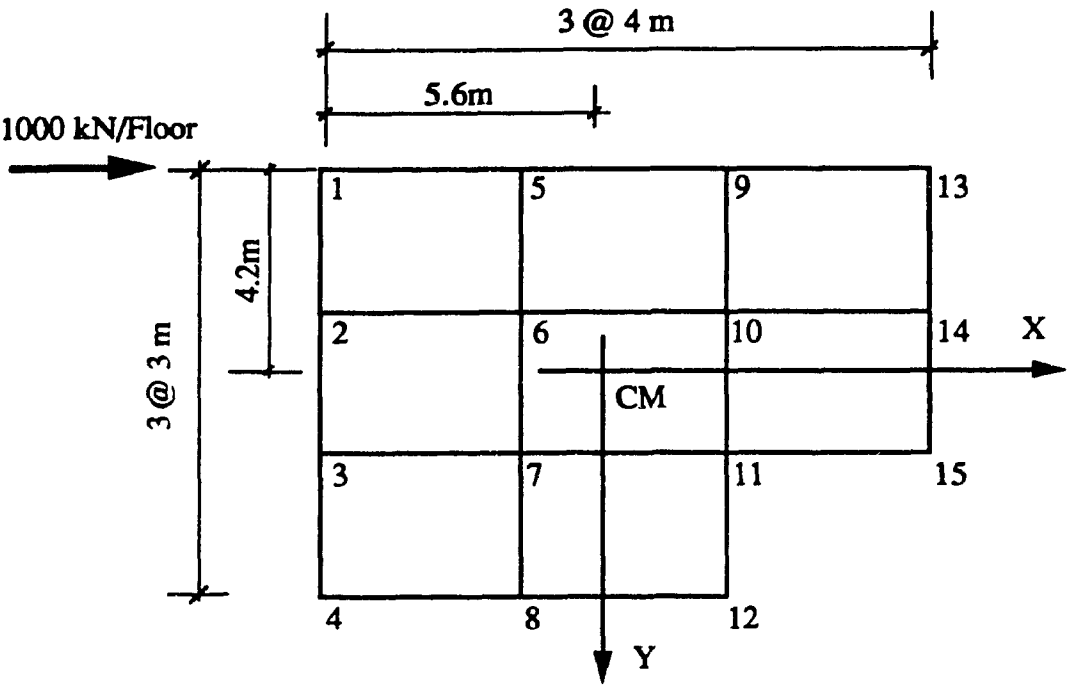

Figure 2.6 Plan layout of unsymmetric 20-story space frame

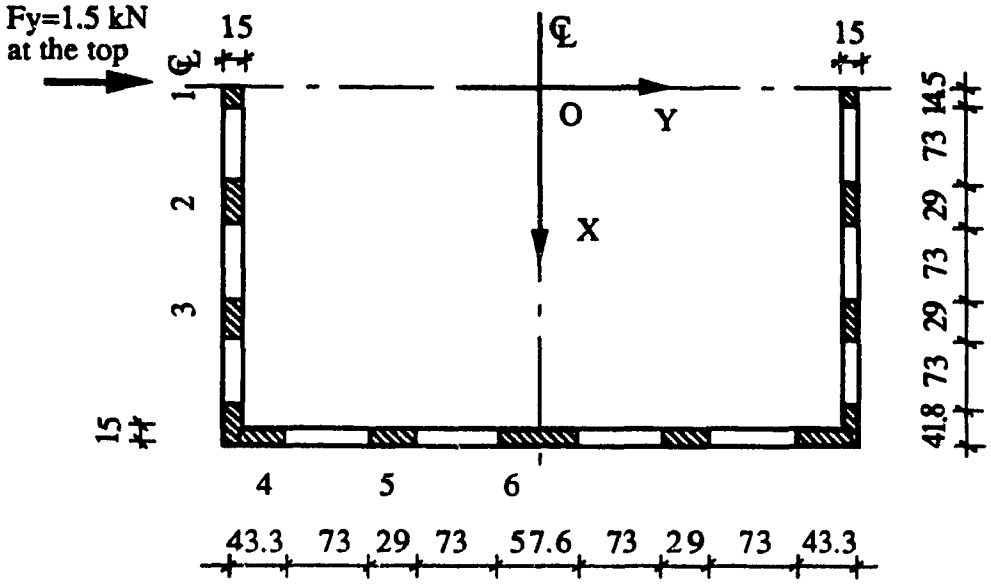

(a) Plan Layout (mm)

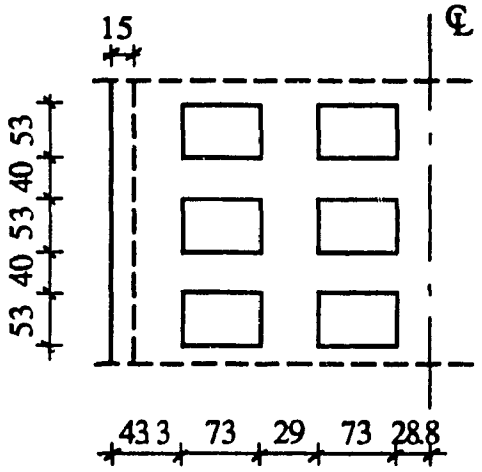

(b) Elevation (mm)

Figuer 2.7 Geometrical dimensions of 20-story framed tube model

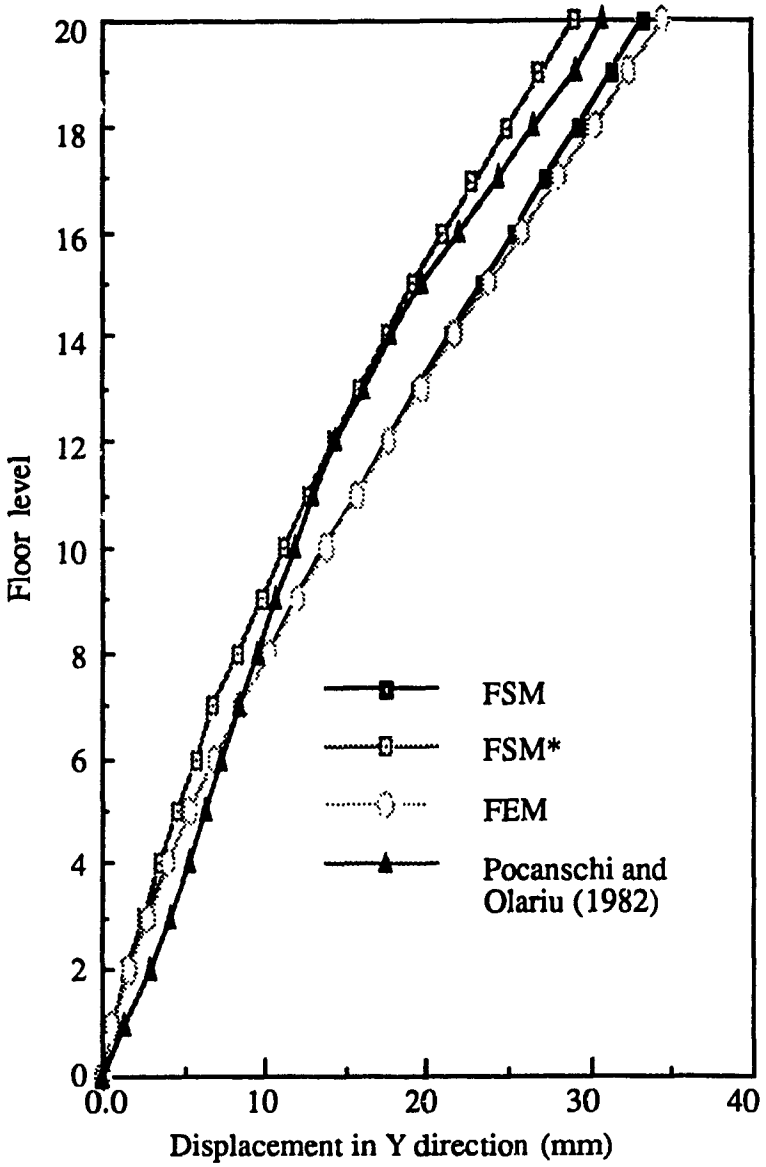

Figure 2.8 Lateral displacements of 20-story model framed tube

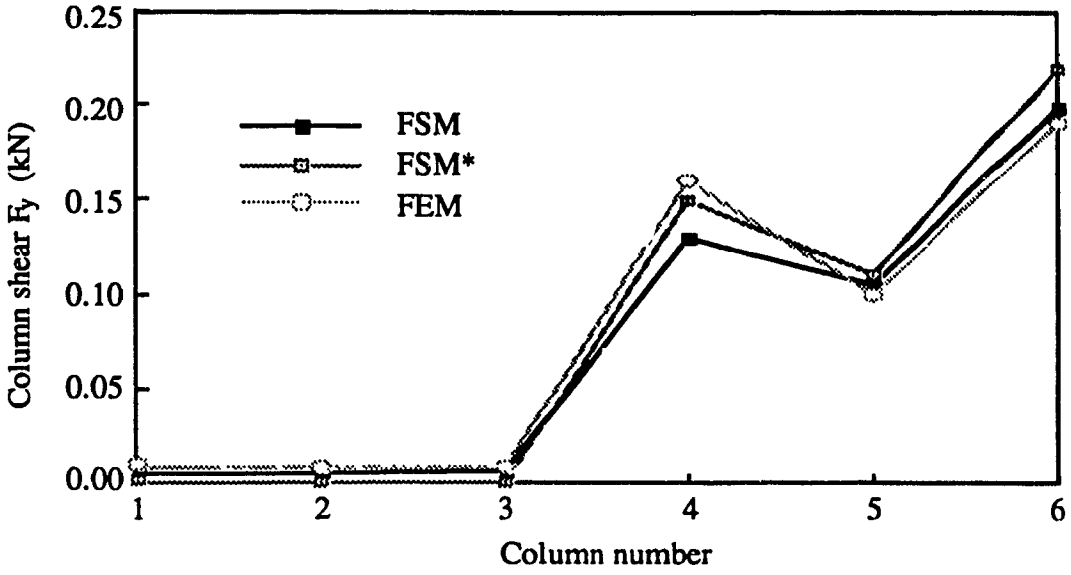

(a)

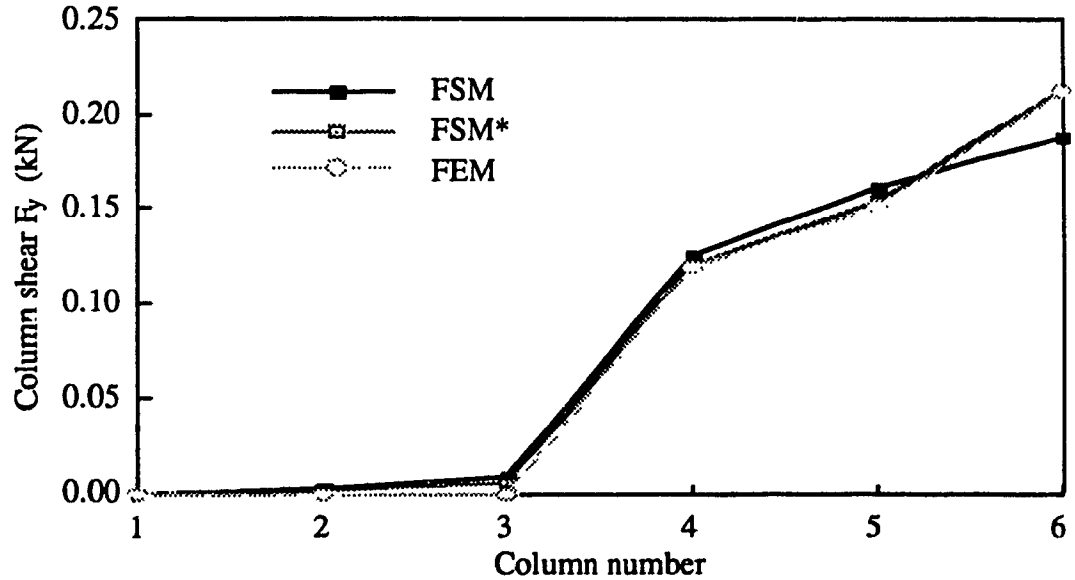

(b)

Figure 2.9 Column shear force distribution for 20-story model framed tube: (a) first story; (b) fourth story

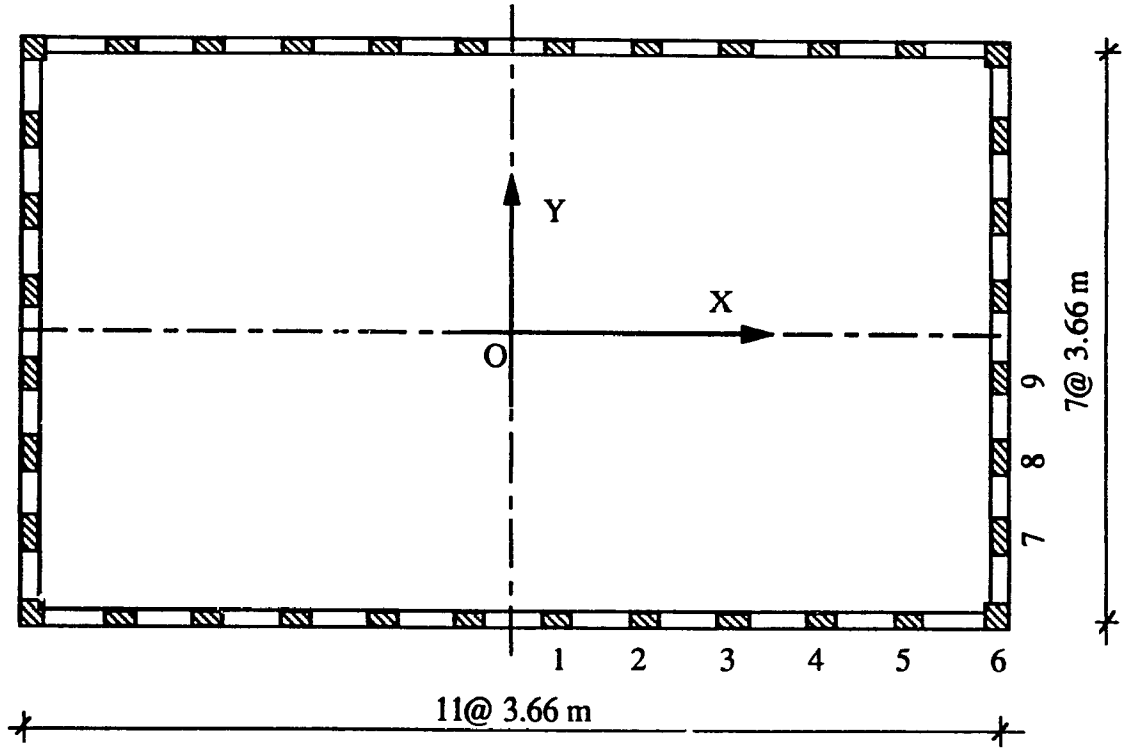

Figure 2.10 Plan layout of symmetric 30-story framed tube structure subject to: (1) pure torsion; (2) lateral loading

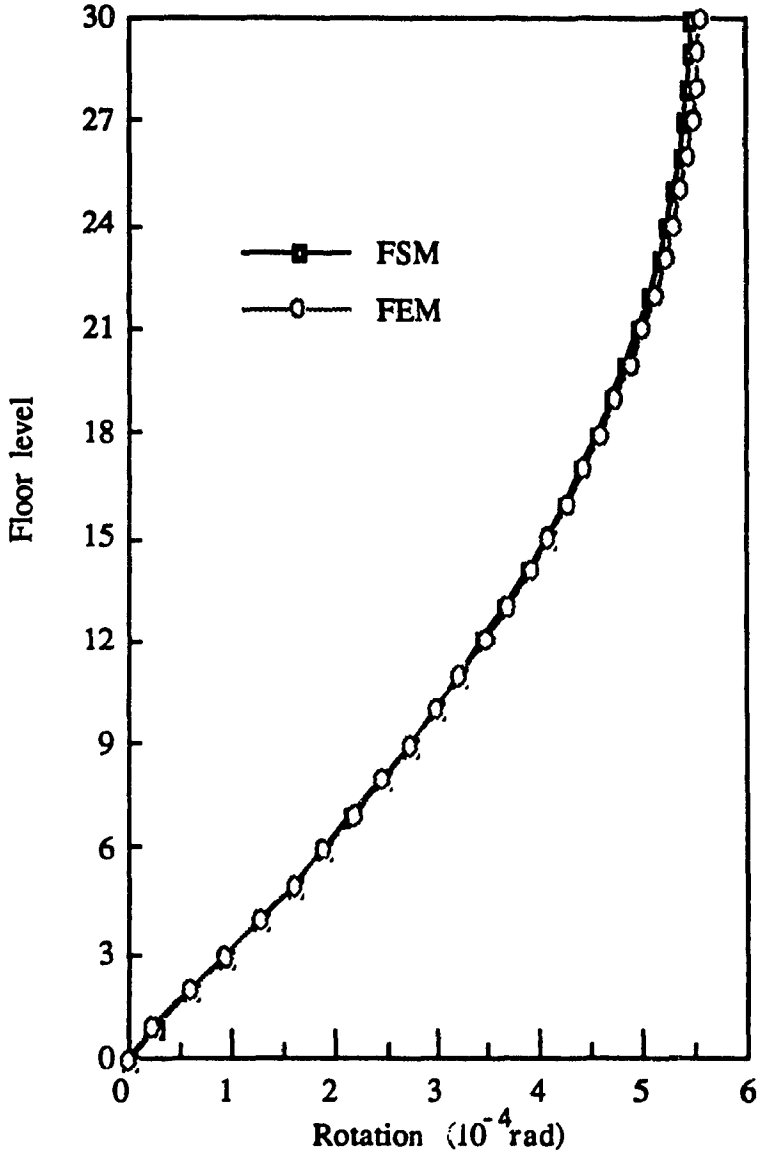

Figure 2.11 Floor rotations for symmetric 30-story framed tube

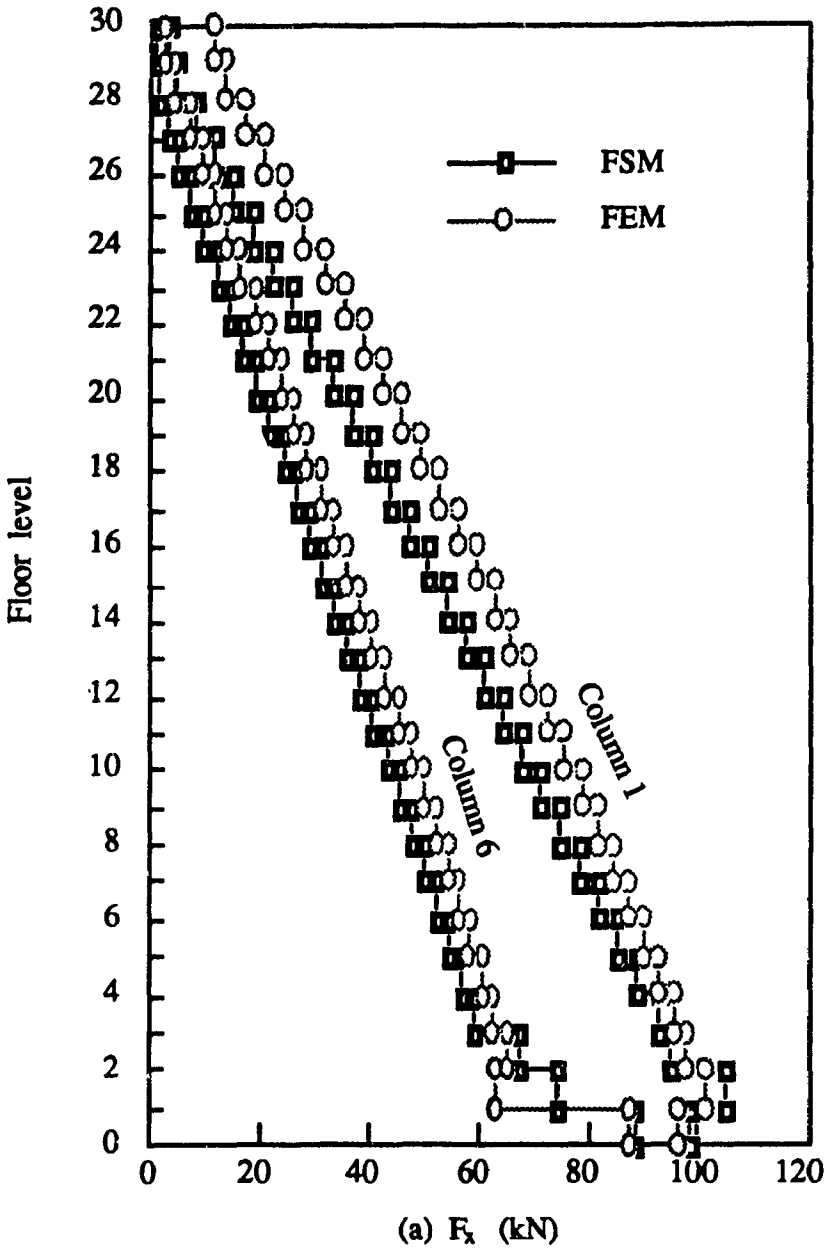

Figure 2.12 Shear forces in columns for symmetric 30-story framed tube

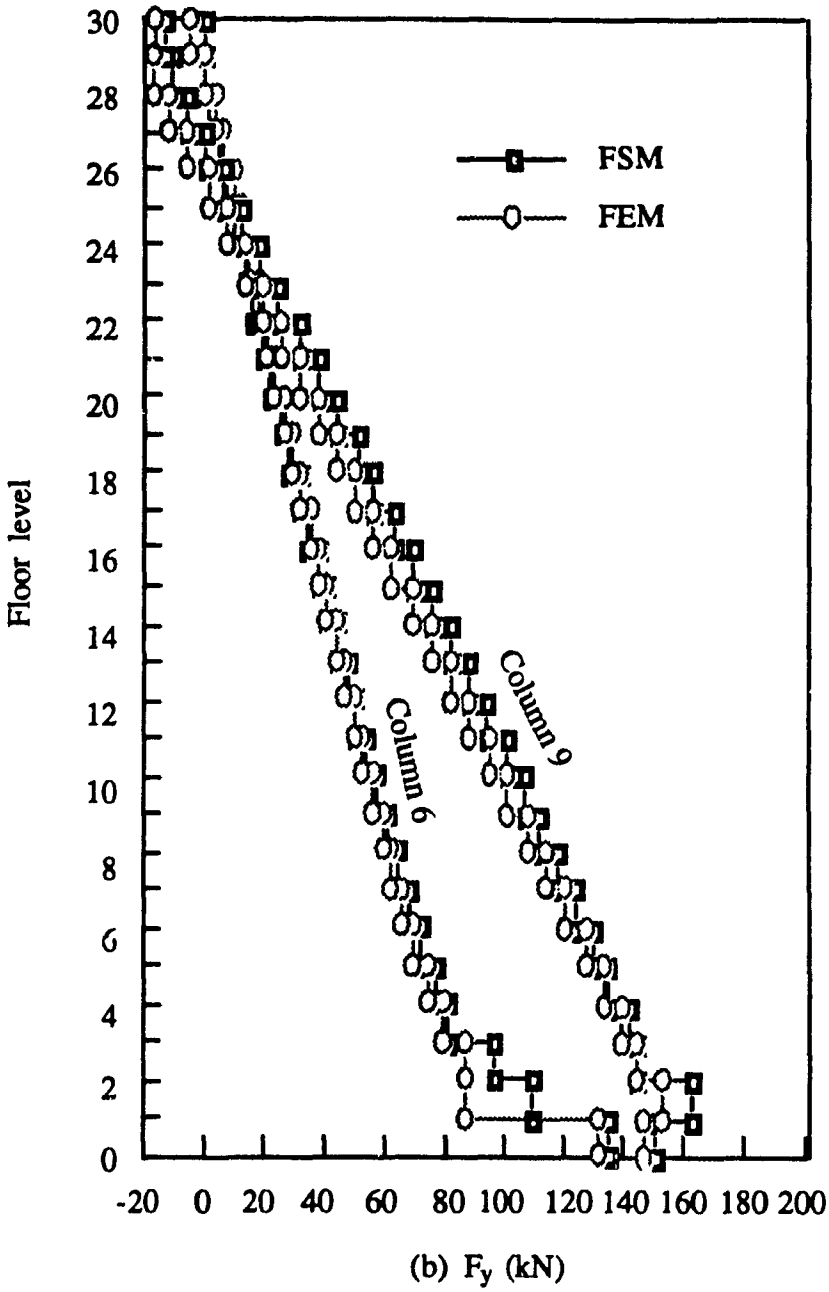

Figure 2.12 (Continued)

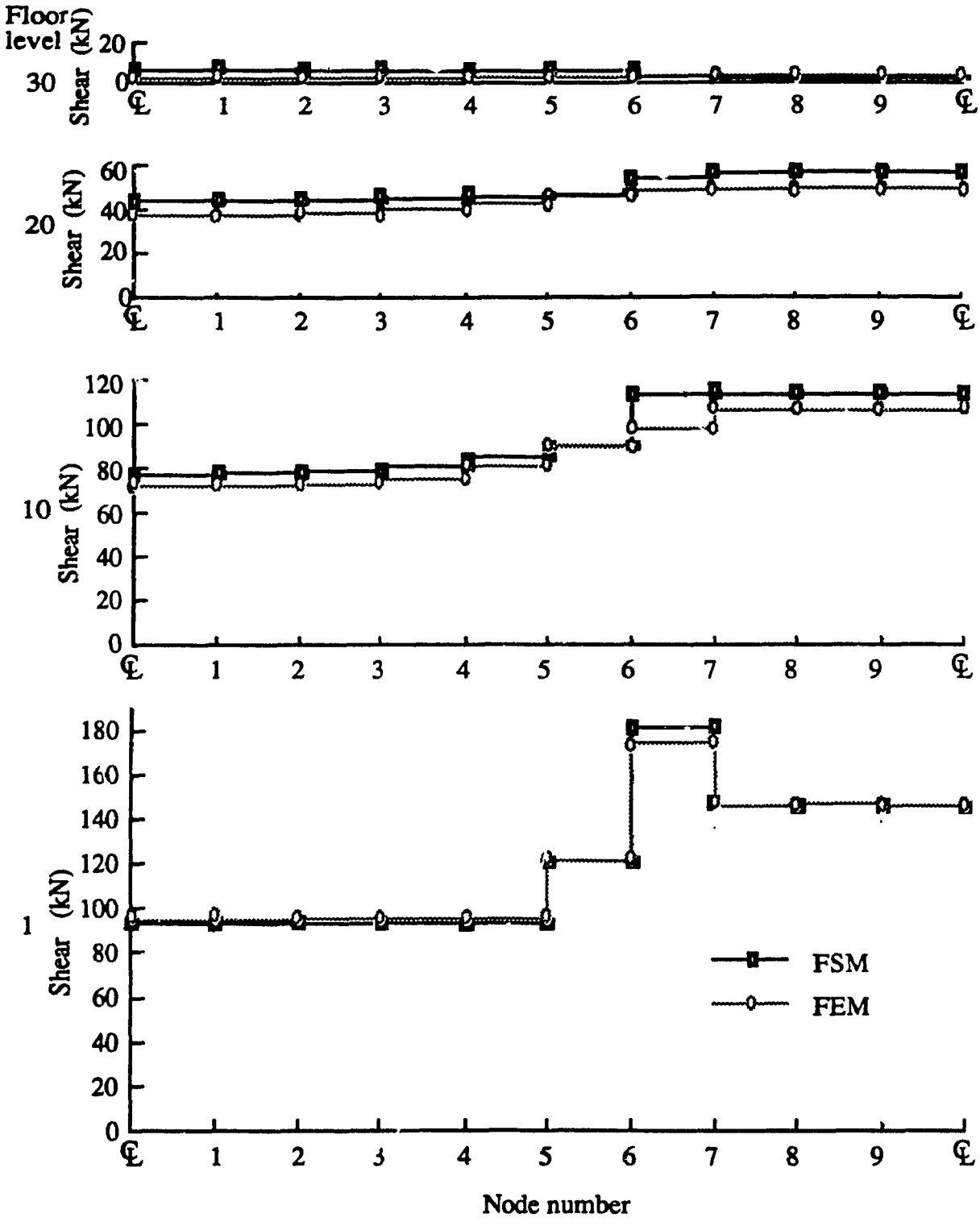

Figure 2.13 Shear forces in spandrel beams of symmetric 30-story framed tube

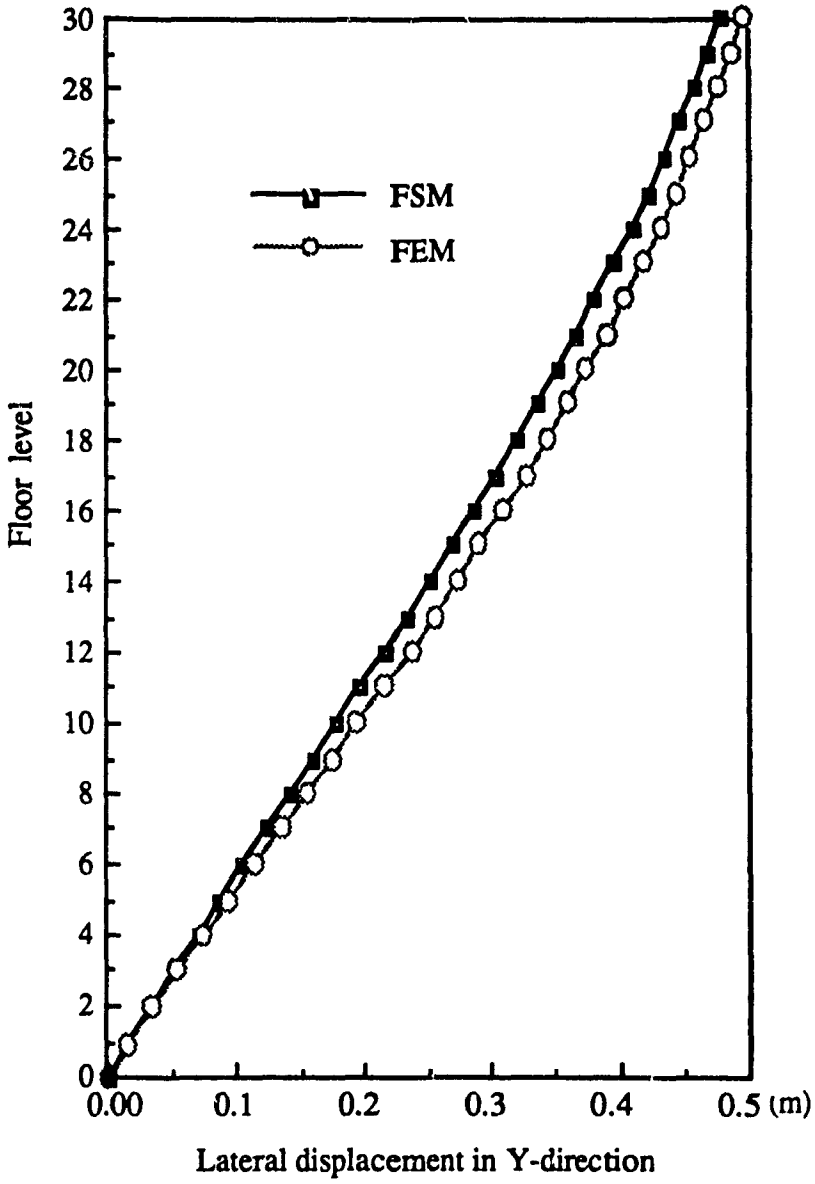

Figure 2.14 Lateral displacements for symmetric 30-story framed tube

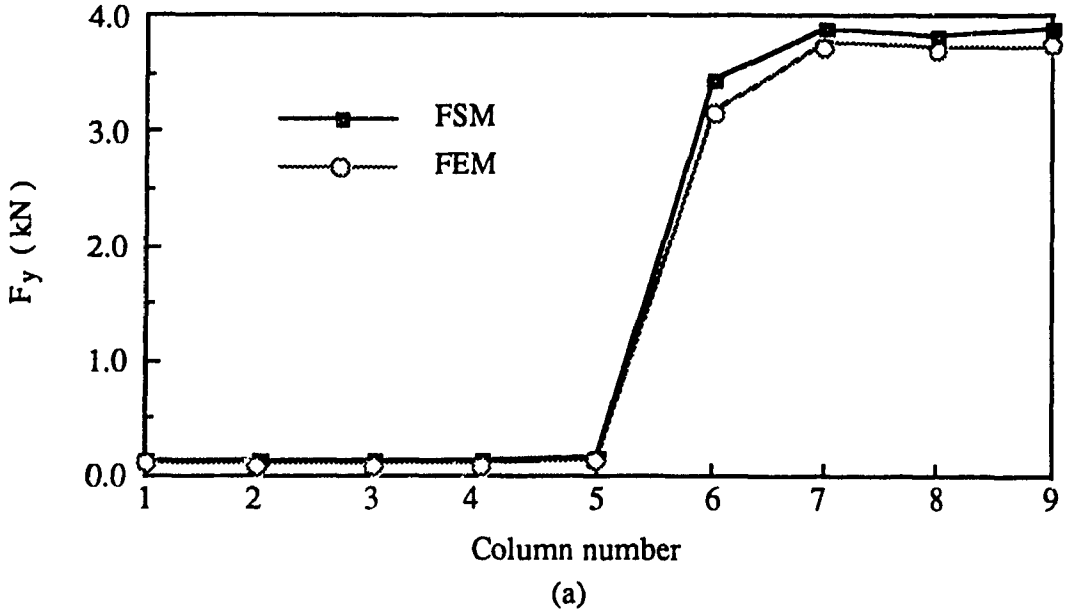

(a)

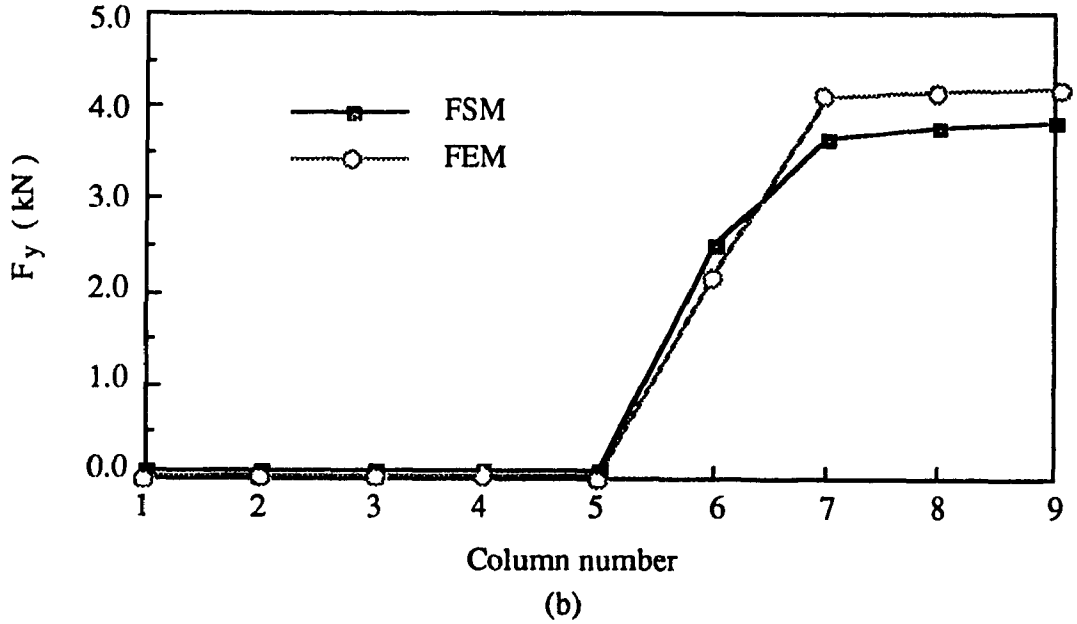

(b)

Figure 2.15 Column shear forces for symmetric 30-story framed tube under lateral load: (a) first story; (b) second story

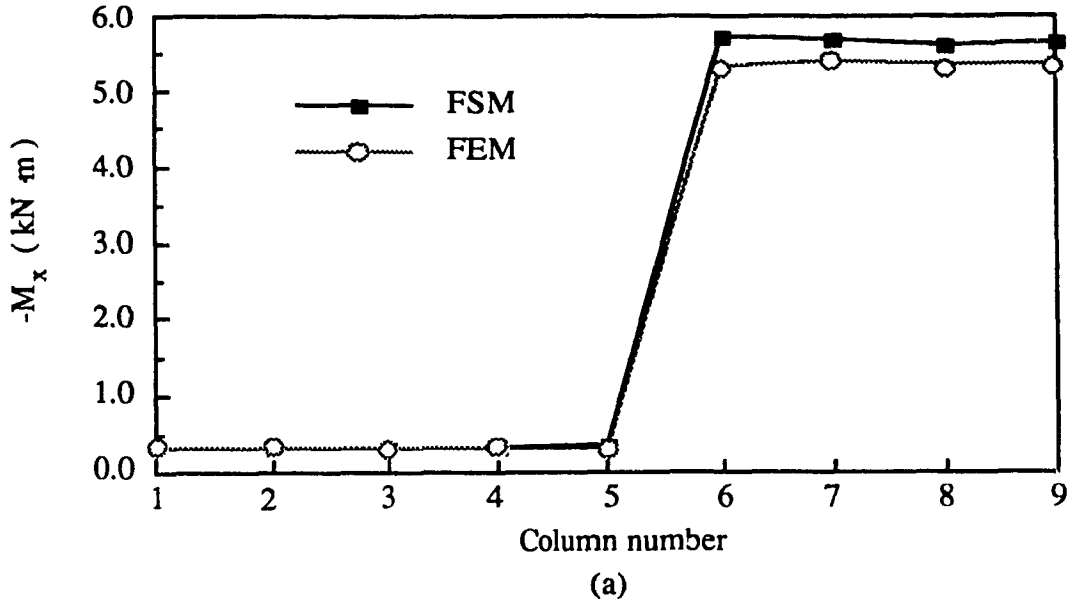

(a)

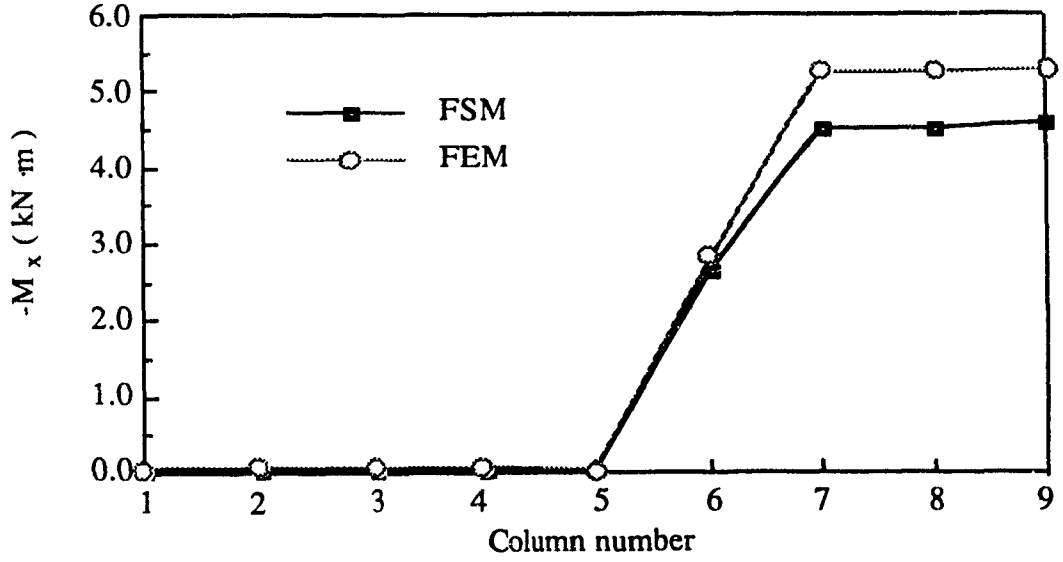

(b)

Figure 2.16 Column bending moments for symmetric 30-story framed tube under lateral load: (a) first story; (b) second story

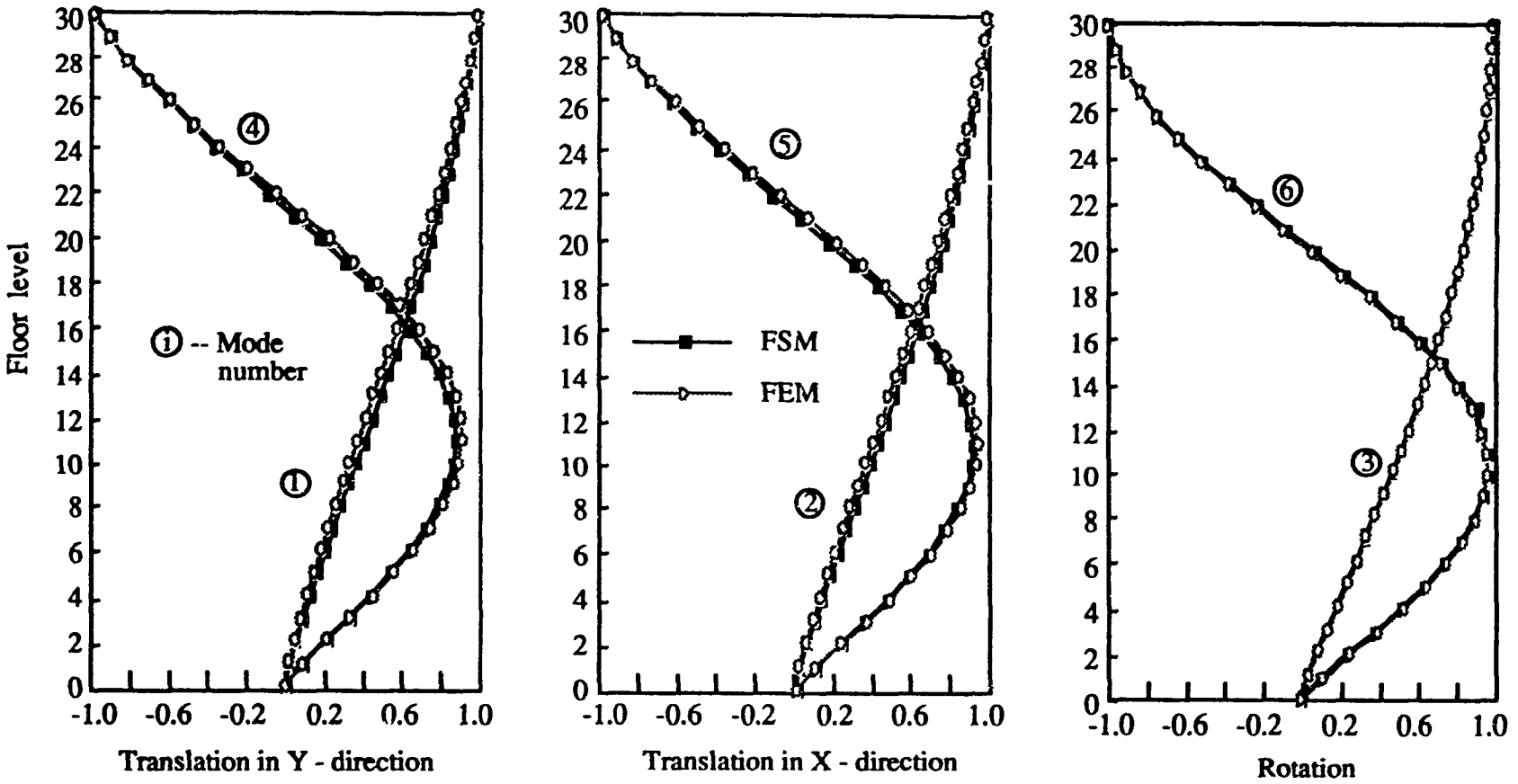

Natural frequency (Hz)

Mode	1	2	3	4	5	6
FSM	0.445	0.572	0.754	1.363	1.747	2.271
FSM*	0.463	0.589	0.750	1.412	1.797	2.259
FEM	0.438	0.581	0.792	1.394	1.798	2.382

Figure 2.17 Natural frequencies and modes of vibration for symmetric 30-story framed tube

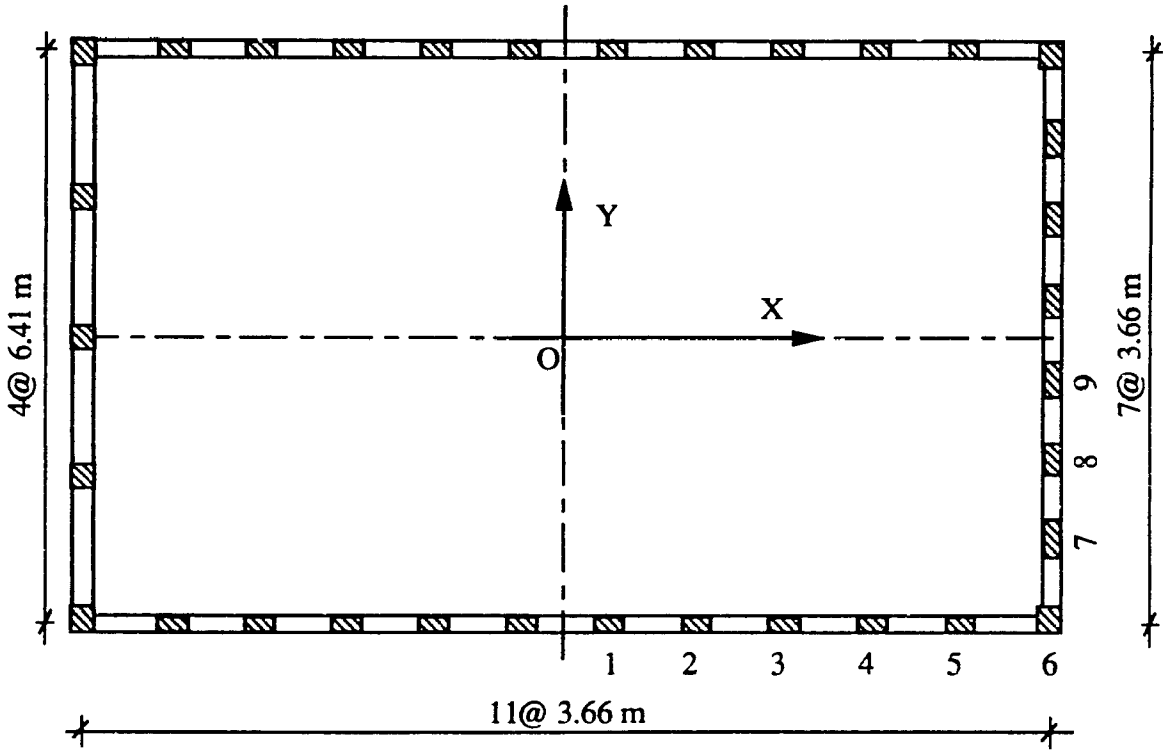

Figure 2.18 Plan layout of unsymmetric 30-story framed tube structure subject to lateral loading

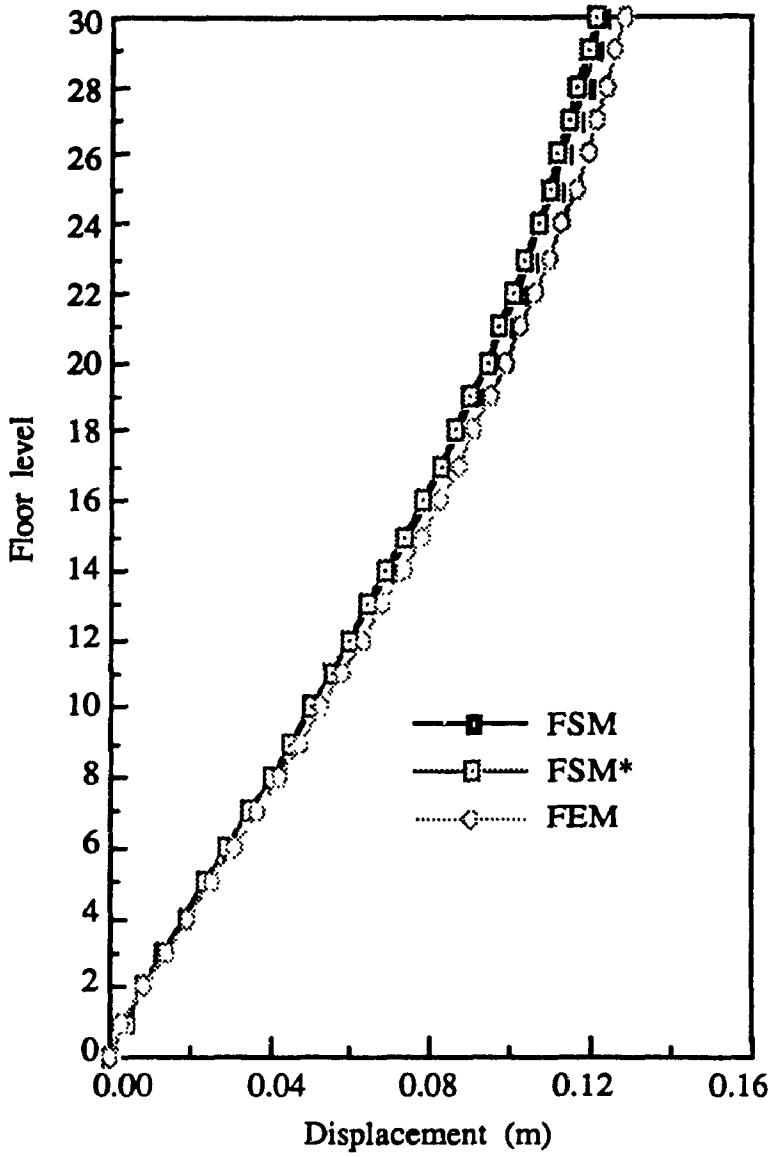

Figure 2.19 Y- direction lateral displacements of unsymmetric 30-story framed tube

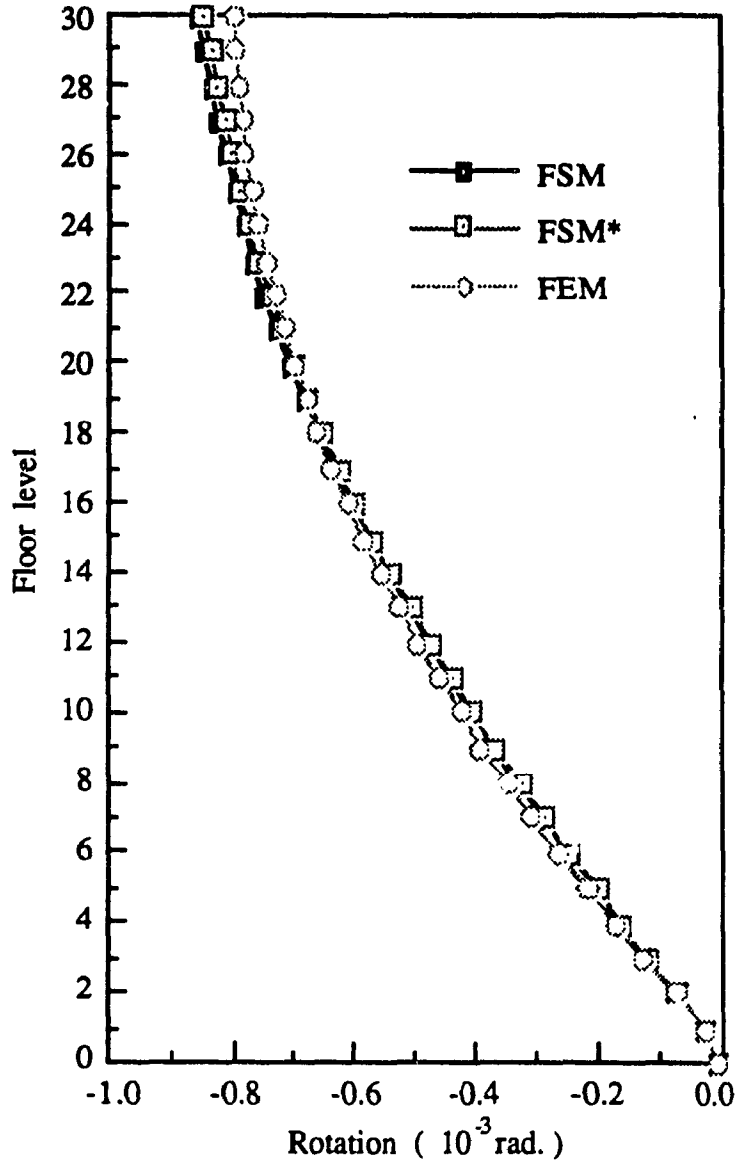

Figure 2.20 Floor rotations of unsymmetric 30-story framed tube

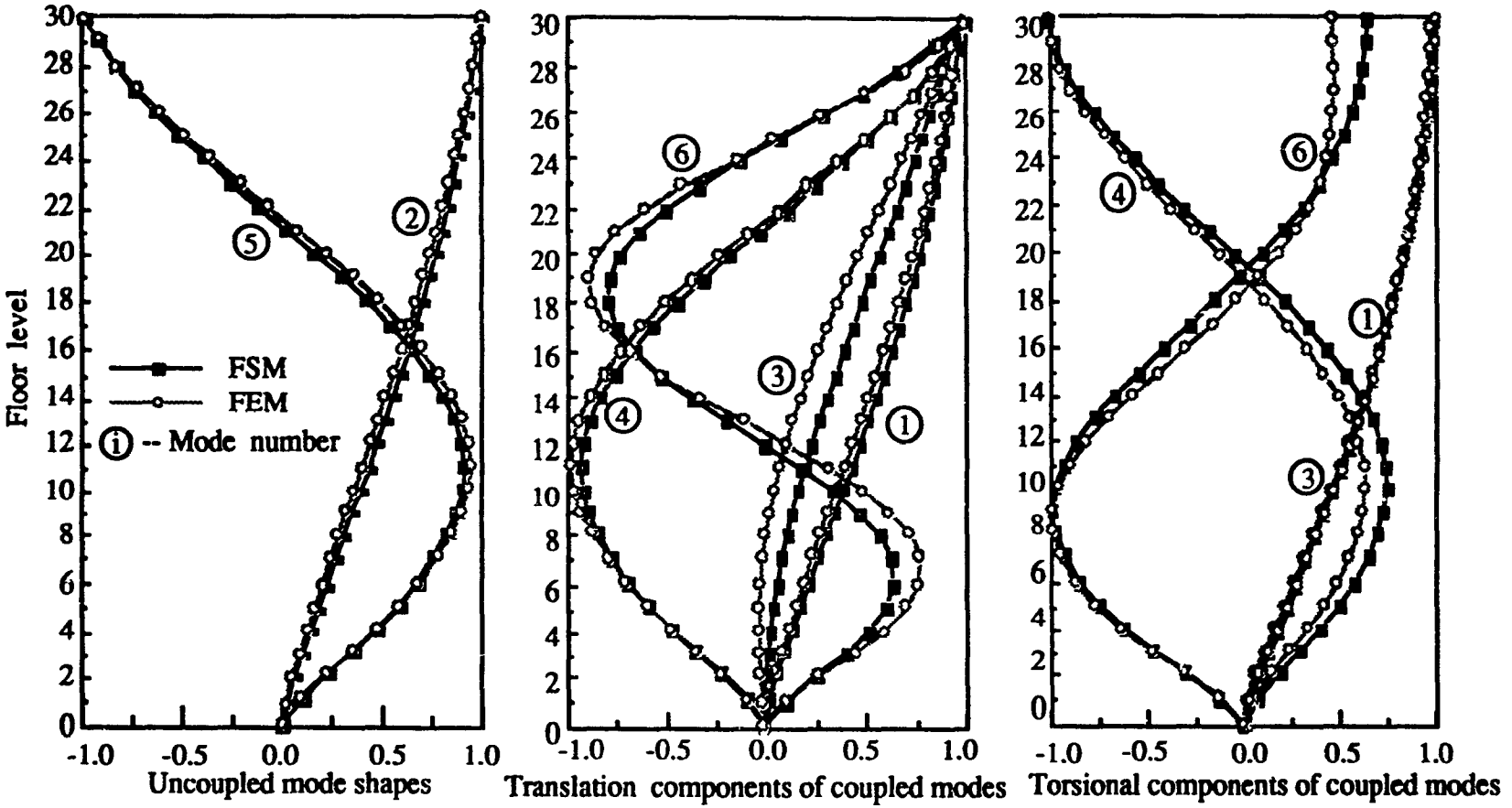

Natural frequency (Hz)

MODE	1	2	3	4	5	6
FSM	0.389	0.588	0.701	1.181	1.789	2.089
FSM*	0.400	0.601	0.704	1.216	1.830	2.110
FEM	0.378	0.576	0.729	1.190	1.789	2.137

Figure 2.21 Natural frequencies and modes of vibration for unsymmetric 30-story framed tube

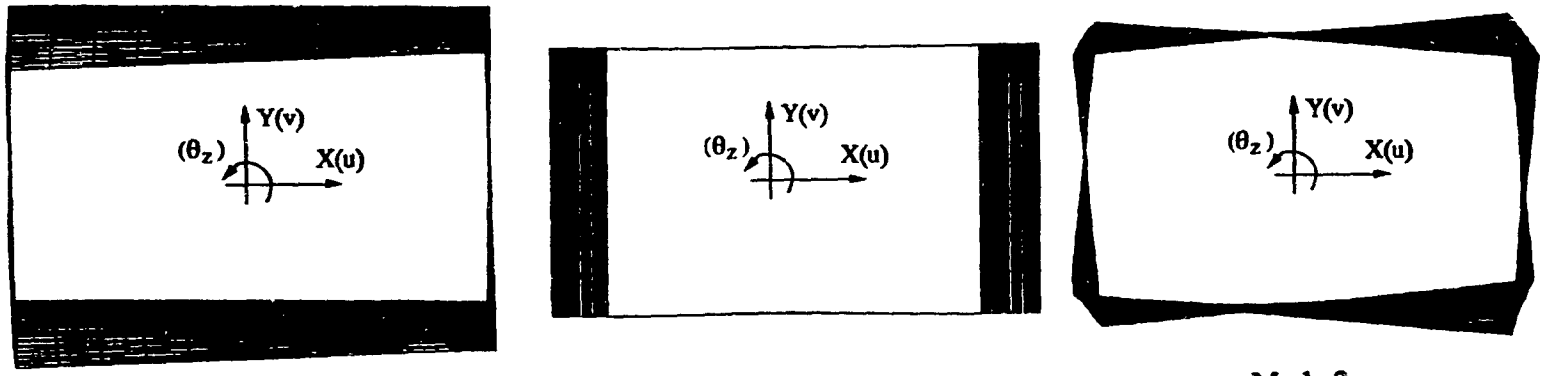

Mode 1 Mode 2 Mode 3

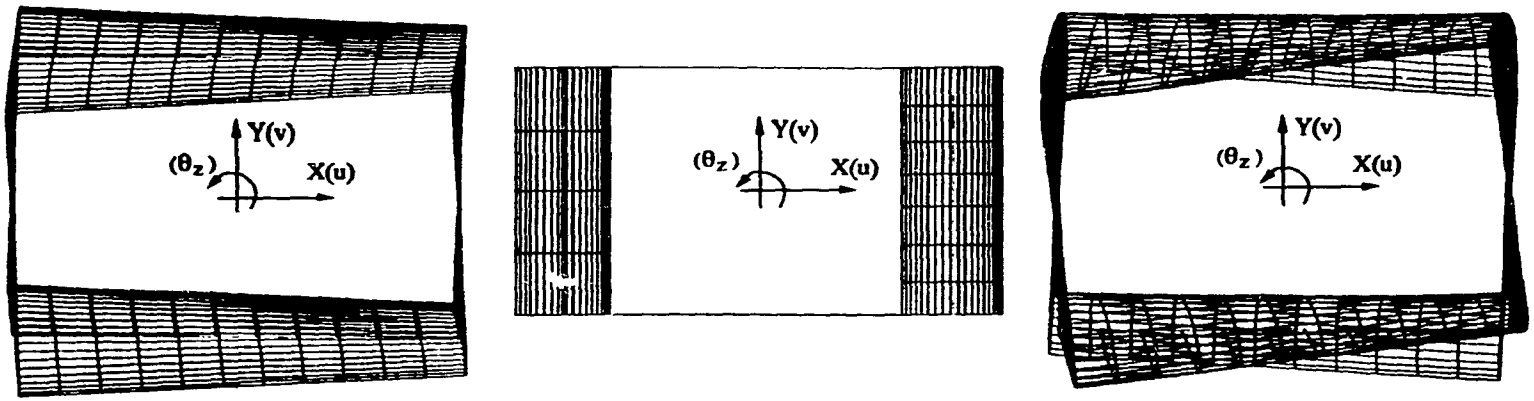

Mode 4 Mode 5 Mode 6

Figure 2.22 Top view of vibration modes (FEM) for unsymmetric 30-story framed tube

Chapter 3
Core Tube Structures

3.1 Introduction

In the preceding Chapter, framed tubes under lateral loads and their dynamic properties have been analyzed by the present finite story method. The method is based on nodal displacement fields obtained from two-story segments and intended for approximate shear, bending and torsion components of global deformations. The effectiveness of the method has been demonstrated for static and dynamic examples of either symmetric or unsymmetric framed structures. In order to extend the method to tube-in-tube structural analysis, the core tube structural behavior under lateral loads is now studied. The aim of this core tube analysis is to incorporate the analytical model of the core tube with the foregoing method for framed tube structures, in order to apply the present finite story method to the structural analysis of tube-in-tube systems.

Tall building core tubes under torsion fall in the general warp-restrained category, and their structural modeling has been of great interest to both engineers and researchers, [24-44]. In addition to a brief review of the characteristics of the torsional behavior of thin-walled beams and the available literature on core tubes, the features of the present matrix-based method are compared with other existing methods for core tubes. The torsion and warping related stiffness coefficients of a core tube modeled as a thin-walled beam are then derived based on available analytical solutions, from which the extended story-wise stiffness matrix of the core tube is formed. The numerical results compare

favorably with other solutions, including full finite element modeling, and demonstrate the high efficiency and acceptable accuracy of the method.

3.1.1 Definition of thin-walled beam members

A beam or column is distinguished from other kinds of structural members in that its cross-section dimensions are not of the same scale as that of length. Beam and column members can be further cataloged into two kinds: one in which the two perpendicular dimensions of the cross-section are of the same scale and; the other in which the orthogonal dimensions differ greatly. The latter are referred to as a thin-walled beams. The definition of such beams is therefore given by [63]

$$b/t \geq 10 \qquad l/b \geq 10 \tag{3.1}$$

where t is the thickness, b is the linear dimension of the cross-section, and l denotes the length of the member. In this study, only straight thin-walled beams which are the most common in tall building structures are studied.

3.1.2 Characteristics of core tube structural behavior under torsion

Tall building core tube structures are cataloged as thin-walled structures due to the large ratios of the building height to the linear dimensions of the cross-section, and of the linear dimension to the wall thickness. In most cases, core tubes are perforated in rows for access doors, which makes their structural behavior more complicated than that of thin-walled structures with completely open or closed sections. To model core tube structures correctly, it is essential to recognize the characteristics of these structures in response to loadings.

From a structural point of view, a core tube may constitute the only supporting system of a building, or it may be incorporated with other structural components to form a

lateral load resistant system. If a core tube is subjected to lateral loads and the resultant of the loads is offset from the shear center, torsion will be induced. Unlike general cantilever structures in which cross-sections remain plane after the structure has deformed, the core tube responds to torsion actions with cross-sectional warping deformation, which may induce corresponding stresses of a magnitude similar to those due to bending [37]. Thus, warping behavior of these structural forms needs to be considered in engineering practice. Other structural responses of a core tube under lateral loads, namely bending, shear and axial deformations, are the same as for general cantilever structures.

The torque applied on a core tube is resisted in closed sections by circulating, wall-twisting and warping shear stresses and in open sections by wall-twisting and warping shear stress only. In terms of torques, the external torque is resisted by St. Venant torque and the so-called bending-twisting moment (warping resistance). The latter is the torque component associated with warping deformation. Which one of these components plays the most important role depends on the cross-sectional shape of the core tube. For circular or regular polygon closed sections the bending-twisting moment is zero, while for open sections the bending-twisting moment may assume considerable portions. A typical concrete core structure becomes a partially closed tube structure due to penetrations for door openings or service systems. When the penetrations are small and arranged in a staggered manner, the overall behavior resembles that of a closed tube and the effect of the openings may therefore be ignored in preliminary design. For cores with door openings which occur in a vertical row, the effect of openings must be taken into account and both St. Venant torque and bending-twisting need be considered in the equilibrium conditions.

3.1.3 Existing methods of core tube structural analysis

The modeling of core tubes consisting of alternating segments possessing closed and open cross-sections is generally approached by assuming either open sections with

braces at the floor levels or equivalent closed sections [28]. For either of these structural models, both continuous approaches and discrete procedures are available. Continuous approaches derive the governing differential equations according to equilibrium conditions of the entire tube, and allow analytical solutions and hand calculations; however, incorporating the core tube with exterior structural components becomes inconvenient since the latter are usually treated by discrete formulations such as finite element or matrix methods. The discrete procedures, on the other hand, are known to have advantages in dealing with complex loading and boundary conditions, and also lend themselves readily to computerized analysis of super-structural systems. These two kinds of approaches are reviewed separately in the following paragraphs.

Continuous approach:

Extensive use of the continuous approach has been made in tall building core tube structural analysis since late the 60's. Rosman [24] applied Vlasov's thin-walled beam theory to analyze torsional behavior of perforated concrete core tubes. The study concerned deflections, internal forces under different load cases, as well as periods of free vibration of core tubes with doubly symmetric cross-sections. In this analysis, the lintel beams at floor levels are replaced by equivalent laminas, and the structure is idealized into a uniform closed shaft; however, the sectorial properties of the cross-section were still determined according to open channel sections. Tso and Biswas [31, 32] presented a three-dimensional method of analysis for non-planar coupled walls in which the bending, shear, twisting, warping and axial deformations of the shear walls were considered. In the analytical model, the connecting beams are also replaced by a uniform connecting laminas, and the sectorial properties are determined accordingly.

A typical structural model for core tubes proposed by Stafford Smith and Taranath [37], and Heidebrecht and Stafford Smith [27], which was naturally developed from two-dimensional analysis of coupled shear walls, is to consider these structures as

consisting of open section channel shear walls connected by lintel beams or slabs at floor levels. The geometric properties of the cross-sections are based on the open channel walls, whereas the warping constraint exerted by lintel beams or floor slabs is taken into account by incorporating the associated bimoments into the corresponding warping stiffness coefficients of the walls [37], or modifying the St. Venant torsional constant of open sections [30].

Most of the above methods are based on Vlasov's theory established for open sections, wherein the shear deformation in middle surfaces of the walls is not considered; therefore, the accuracy of these methods may questionable for cases with deep lintel beams at the floor levels. Khan and Stafford Smith [28] examined the shift of the effective shear center of open cross-sections due to the existence of lintel beams. It was shown that, with increasing depth of the lintels, the shear center shifts and shear deformations become more pronounced. Rutenberg, Shtarkman and Eisenberger [30] described and compared the merits and limitations of several continuous methods, including some models in which shear deformations were also considered.

Discrete approach:

With the development of computer techniques, discrete approaches for tall building core tubes have become prevalent. In the standard finite element analysis, shear wall panels can be modeled by plane stress elements or thin-shell elements, while the undeformed cross-sections are modeled by means of rigid links or auxiliary beams at floor levels [6]. For core tubes with lintel beams, the lintel beams can be replaced by an equivalent continuum and treated as wall panels. In addition to the standard elements mentioned above, some specially developed elements have also been reported. Examples comprise a super-element which modeled the core tube in one story by a three-dimensional subassemblage of two-dimensional shell elements [42], a strain-based element which spans several stories and which performed well in both shear and bending

deformation modes [21], and a generalized thin-walled beam element in which both displacement and strain fields were employed [43]. The merit of the finite element method is that it does not require preliminary determination of the location of the shear centers, nor do most of its applications require the calculation of the geometrical sectorial properties of the cross-section.

An alternative discrete approach is the general matrix method. The warping distortion of the cross-section is considered as an additional degree-of-freedom at joints of members, and the corresponding member stiffness coefficients are determined based on Vlasov's thin-walled beam theory. The derived member stiffness matrix was employed with the transfer matrix method to examine core tube structural behavior in [37-39]. The method solves tall building core tube problems by using recursive compatibility conditions without assembling the overall structural stiffness matrix. Another approach based on the general matrix method for core tube structures [36] modeled the core tube as individual piers of core walls connected by lintel beams at floor levels. Because each pier was idealized as a one-dimensional member at the shear center of the represented wall, the ends of connecting beams were extended to the shear centers of walls. This was realized by means of the in-plane rigid diaphragm assumption for floor slabs in assembling the story stiffness matrix. The overall structural stiffness matrix was obtained by assembling story matrices. Compared with the finite element method, the matrix method provides concise member stiffness matrices, but requires thin-walled beam theory as well as the calculation of geometrical sectorial properties.

3.2 Concept and formulation of thin-walled beam theory

3.2.1 Warp-restrained torsion

For a thin-walled beam subjected to a uniform torque, if all cross-sections of the beam are permitted to warp freely, the magnitude of warping and the lengths of

longitudinal fibers do not change. Consequently, the shear stress distribution is the same at all cross-sections, and no normal stress is produced. This situation occurs only if the thin-walled structure is straight and without any longitudinal restraint. All longitudinal fibres are still straight, but the cross-sections are warped.

If the support or load conditions do not allow a thin-walled beam to warp freely, torsion becomes warp-restrained. In this case, the magnitude of warping varies along the member axis, longitudinal fibres experience elongation or compression, and both normal and shear stress are generated by the non-uniform warping of cross-sections. A typical example is a thin-walled I beam fixed at one end and subjected to a torque at the other. The warping varies from zero at the fixed end to a maximum at the free end, while the two flanges bend in opposite directions, thus giving rise to warp-restrained torsion being referred to as bending twisting.

3.2.2 Sectorial properties of thin-walled beams

In his work on the behavior of thin-walled beams, Vlasov [63] introduced sectorial properties of thin-walled beams in addition to the St. Venant's cross-sectional properties, which permitted the analysis of warp-restrained torsion. The thin-walled beam theory has been widely applied in the aerospace industry and the definitions of sectorial properties have been generalized based on Vlasov's original work of open sections, so that they are valid for either open or closed sections [33, 64].

The sectorial coordinate of a cross-sections is the basic quantity in thin-walled beam analysis. In the cross-section shown in Figure 3.1a, C denotes the centroid of the section; CX and CY are principal axes in the Cartesian system; O_1 represents an arbitrary pole in the CXY plane; M_1 located at the middle surface is the origin; r is the perpendicular distance from O_1 to M where the sectorial coordinate is to be determined and; s is the curvilinear coordinate of the middle surface measured from the origin M_1.

Any point in the middle surface can be measured by the axial coordinate z and the curvilinear coordinate s. The sectorial coordinate $\bar{\omega}$ at M is defined by

$$\begin{aligned} \bar{\omega}(s) &= \int_0^s r\,ds && \text{for open sections} \\ \bar{\omega}(s) &= \int_0^s r\,ds - \frac{\Omega}{\oint_s \frac{ds}{t}} \int_0^s \frac{ds}{t} && \text{for closed sections} \end{aligned} \tag{3.2}$$

The first term on the right hand side of the sectorial coordinate for closed-sections is the same as that for open-sections introduced by Vlasov. The thickness t can be a function of s; Ω is twice the area enclosed by the middle surface of the cross-section. For open-sections Ω is zero.

Similar to the St. Venant geometric properties, there are sectorial properties which are given below:

$$\begin{aligned} I_{\bar{\omega}x} &= \int_s t\bar{\omega}y\,ds, & I_{\bar{\omega}y} &= \int_s t\bar{\omega}x\,ds \\ S_{\bar{\omega}} &= \int_s t\bar{\omega}\,ds, & I_{\bar{\omega}} &= \int_s t\bar{\omega}^2\,ds \end{aligned} \tag{3.3}$$

If the pole and origin are chosen to satisfy the following conditions

$$S_{\bar{\omega}} = 0, \qquad I_{\bar{\omega}x} = 0, \qquad I_{\bar{\omega}y} = 0 \tag{3.4}$$

the corresponding pole and the origin become the principal pole and the principal origin of the cross-section. The principal pole coincides with the shear center of the cross-section and the principal origin is a point on the wall contour where $\bar{\omega} = 0$. Under these conditions, $I_{\bar{\omega}}$ is the principal sectorial moment of inertia. The procedure for calculating the principal sectorial moment of inertia [63, 33] is summarized in Appendix V.

3.2.3 Basic assumptions and governing differential equation

The equilibrium conditions of elastic thin-walled beam theory are essentially based on one fundamental assumption: the cross-sectional shape does not change as the beam deforms. There are two approaches for warping displacements of thin-walled beams under torsion: (1) Vlasov approach [63]

$$w(s, z) = w(0, z) - \bar{\omega}\, \theta_z' \tag{3.5}$$

and (2) Umanisky - Benscoter's approach [30, 33, 64]

$$w(s, z) = w(0, z) - \bar{\omega}\, \beta'(z) \tag{3.6}$$

in which $\bar{\omega}$ is the afore-defined principal sectorial coordinate, and $w(0, z)$ is a constant. Both are based on the common assumption that the warping displacement pattern of a section varies as the sectorial coordinate diagram of the section, while the magnitude of the distribution varies along longitudinal axis of the member [33, 63, 64]. The two approaches differ in the manner in which the magnitude varies. Vlasov considered that the warping displacement varies along the longitudinal axis directly with the rate of the twist angle θ_z'; whereas Umanisky and Benscoter assumed it to vary as another function β', the so-called warping function. The latter allows shear deformation in wall panels to be included, whereas in Vlasov's thin-walled beam theory for open sections, the shear deformation of the thin walls is neglected. Since tall building core tube structures consist of segments with alternately open and closed sections, modeling the structural behavior based on the theory for open sections may give erroneous results for the location of the shear center [28] and, consequently, also for sectorial moment of inertia, rotation and stresses.

Based on the Umanisky - Benscoter assumption, the governing differential equation of the thin-walled beam subjected to distributed torque $m_z(z)$ is established as [30, 33, 64]

$$\theta_z''''(z) - a^2\theta_z''(z) = \frac{\mu m_z(z)}{EI_{\bar{\omega}}} - \frac{m_z''(z)}{G(I_p + J_o)} \tag{3.7}$$

in which θ_z is the angle of rotation; primes denote differentiation with respect to coordinate z along the member longitudinal axis; E = the modulus of elasticity; G = the shear modulus; and

$$a^2 = \mu\frac{G(J_o + J_c)}{EI_{\bar{\omega}}} = \mu\frac{GJ}{EI_{\bar{\omega}}}, \qquad \mu = 1 - \frac{J_c + J_o}{I_p + J_o} \tag{3.8}$$

in which $J = J_c + J_o$, the torsional constant of the core tube given by the sum of the Bredt and St. Venant constants, respectively; I_p is the tangent second moment of inertia; and μ is a dimensionless section constant, the so-called warping characteristic parameter representing the warping performance [33]. For circular or regular polygon sections with uniform thickness, $\mu = 0$ and the bending-twisting moment is also zero. On the other hand, for open sections $\mu = 1.0$. It should be noted that the bending-twisting moment increases as the value of μ increases.

3.2.4 Solution for torsion related displacements and forces

For cantilever beams fixed at $z = 0$ and free at $z = l$, and subjected to intensity of distributed torque m_z = constant, the solution of governing equation (3.7) is

$$\theta_z = \theta_{z0} + \frac{\mu \sinh az}{a}\cdot\beta'_0 + \frac{1-\cosh az}{GJ}\cdot B_{\bar{\omega}0} + \frac{az - \mu\sinh az}{aGJ}\cdot M_{z0} - \frac{m_z}{a^2GJ}\left(1 + \frac{a^2z^2}{2} - \cosh az\right) \tag{3.9}$$

$$\beta' = \cosh az\cdot\beta'_0 - \frac{a\sinh az}{\mu GJ}\cdot B_{\bar{\omega}0} + \frac{1-\cosh az}{GJ}\cdot M_{z0} + \frac{m_z}{\mu aGJ}\left((1-2\mu)az - \sinh az\right) \tag{3.10}$$

$$B_{\bar{\omega}} = -\frac{GJ \cdot \mu \sinh az}{a} \cdot \beta'_0 + \cosh az \cdot B_{\bar{\omega}0} + \frac{\mu \sinh az}{a} \cdot M_{z0} - \frac{m_z}{a^2}(1 - 2\mu + \cosh az) \tag{3.11}$$

$$M_z(z) = M_{z0} - m_z z \tag{3.12}$$

3.3 Thin-walled beam modeling for core tube structures

In this Section, the core tube in each story of a building is modeled as a thin-walled beam element and represented by its extended stiffness matrix so that the core tube can be incorporated into the finite story method (FSM) based on nodal displacement fields described as in Chapter 2. The original structure with alternating open and closed sections is replaced by one with equivalent closed section, with the thickness of the assumed connecting continuum based on equivalent in-plane flexibility of the lintel beams as formulated by Khan and Stafford Smith [28]:

$$t_1 = h^{-1}\left[\frac{l}{12I_b}\frac{G}{E} + \frac{1.2}{A_b}\right]^{-1} \tag{3.13}$$

in which A_b and I_b are area and moment of inertia of the lintel beam, respectively; h is the story height and; l denotes span of the lintel beam.

As a corollary to the assumption of an equivalent closed section, shear deformation in wall panels and the warping characteristic parameter are included in the torsion related stiffness coefficients. Thus, although the coefficients obtained in this study are based on the governing equation for warp-restrained torsion of thin-walled beams with closed sections, open sections can be viewed as a special case in which the thickness of the equivalent membrane for lintel beams is zero and the warping parameter μ = 1.0. The method is therefore applicable to core supported structures with completely open, closed or a mix of open and closed sections.

3.3.1 Stiffness matrix of thin-walled beam element

From the cross-section warping distortion of thin-walled beams given by equation (3.6), it is clear that at a specific section, w is proportional to the sectorial coordinate $\bar{\omega}$ with the factor $(-\beta')$. The latter is taken as a measure of warping, which becomes the seventh degree-of-freedom at beam ends in addition to the usual six for solid beams. The member force corresponding to the β' is the bimoment $B_{\bar{\omega}}$ which is defined by

$$B_{\bar{\omega}} = \int_A \bar{\omega} \cdot \sigma_{\bar{\omega}} dA \tag{3.14}$$

where $\sigma_{\bar{\omega}}$ is the normal warping stress and; A denotes the cross-section area of the beam.

To derive stiffness coefficients corresponding to twist and warping, consider a beam only loaded at its ends i and j, i.e. $m_z(z) = 0.0$. Equation (3.7) becomes homogeneous, and equations (3.9-3.12), expressed in terms of the end rotations θ_i, θ_j; end torques M_{zi}, M_{zj}; bimoments $B_{\bar{\omega}i}$ and $B_{\bar{\omega}j}$ and; the corresponding warping deformations β'_i, β'_j, are given in matrix form by

$$\begin{Bmatrix} \theta_{zj} \\ \beta'_j \\ \dfrac{M_{zj}}{GJ} \\ \dfrac{B_{\bar{\omega}j}}{GJ} \end{Bmatrix} = \begin{bmatrix} 1 & \dfrac{\mu}{a}\sinh al & l-\dfrac{1}{a}\sinh al & 1-\cosh al \\ 0 & \cosh al & 1-\cosh al & -\dfrac{\mu}{a}\sinh al \\ 0 & 0 & 1 & 0 \\ 0 & -\dfrac{\mu}{a}\sinh al & \dfrac{1}{a}\sinh al & \cosh al \end{bmatrix} \begin{Bmatrix} \theta_{zi} \\ \beta'_i \\ \dfrac{M_{zi}}{GJ} \\ \dfrac{B_{\bar{\omega}i}}{GJ} \end{Bmatrix} \tag{3.15}$$

In the equation (3.15), by letting θ_{zi}, β'_i, θ_{zj}, β'_j have unit values in turn with all other displacements zero, member forces M_{zi}, $B_{\bar{\omega}i}$, M_{zj}, and $B_{\bar{\omega}j}$ can be obtained to yield the required stiffness coefficients. The equilibrium equation in matrix form for the warp-restrained member subjected to end torques becomes

$$\begin{Bmatrix} M_{zi} \\ B_{\bar{\omega}i} \\ M_{zj} \\ B_{\bar{\omega}j} \end{Bmatrix} = [k_r] \begin{Bmatrix} \theta_i \\ \beta'_i \\ \theta_j \\ \beta'_j \end{Bmatrix} \tag{3.16}$$

where

$$[k_r] = \overline{GJ} \begin{bmatrix} \frac{a}{\mu}\sinh al & 1-\cosh al & -\frac{a}{\mu}\sinh al & 1-\cosh al \\ & l\cosh al - \frac{\mu}{a}\sinh al & \cosh al - 1 & \frac{\mu}{a}\sinh al - l \\ & & \frac{a}{\mu}\sinh al & \cosh al - 1 \\ & (Symm) & & l\cosh ah - \frac{\mu}{a}\sinh al \end{bmatrix} \tag{3.17}$$

$$\overline{GJ} = \frac{GJ}{\sqrt{2-2\cosh al + \frac{al\sinh al}{\mu}}} \tag{3.18}$$

and l is the length of element. The difference between the above form of matrix $[k_r]$ and the corresponding torsion and warping related stiffness matrix derived for open sections is the inclusion of μ. For beams with open sections, μ=1.0 and $[k_r]$ degenerates into that based on Valsov's theory for open sections. In cases of core tube structures with lintel beams that are relatively deep, the shear deformation in wall panels becomes significant. Additionally, stiff lintel beams cause a shift in the shear center which also notably affects the displacements and warping stresses [28]. Stiffness coefficients derived for open sections are therefore less suitable in such situations, whereas the present stiffness coefficients for closed sections reflect more realistically the foregoing effects of the lintel beams.

For a story-height segment of the core tube structure subjected to a combination of bending, shear, axial and torsional loadings, the complete member stiffness matrix for the warp-restrained condition is established in the coordinate system shown in Figure 3.2. The origin O of the system is located at the shear center of the cross-section, which is also the principal pole of the cross-section. Axes OX and OY are parallel to the principal axes C$\overline{X}$ and C$\overline{Y}$. Point C denotes the geometric centroid of the cross-section.

The coordinate transformation from the principal axes to the member local axes is based on the assumption that the cross-section is in-plane undeformed. Expressed in terms of the displacement coordinates of Figure 3.2, the extended nodal displacement vector of the element becomes

$$\{d\} = [\ u_i\ v_i\ w_i\ \theta_{xi}\ \theta_{yi}\ \theta_{zi}\ \beta'_i \mid u_j\ v_j\ w_j\ \theta_{xj}\ \theta_{yj}\ \theta_{zj}\ \beta'_j\ ]^T \tag{3.19}$$

The corresponding complete stiffness matrix for this member, extended from the usual order 12x12 to 14x14, is given below:

$$[k] = \begin{bmatrix} k_{ii} & k_{ij} \\ k_{ji} & k_{jj} \end{bmatrix} \tag{3.20}$$

where

$$[k_{ii}] = \begin{bmatrix} c_1 & & & & & & \\ 0 & c_2 & & & & & \\ 0 & 0 & c_3 & & & (Symm) & \\ 0 & -c_5 & -y_s c_3 & c_7 + y_s^2 c_3 & & & \\ c_4 & 0 & x_s c_3 & -x_s y_s c_3 & c_9 + x_s^2 c_3 & & \\ 0 & 0 & 0 & 0 & 0 & c_{10} & \\ 0 & 0 & 0 & 0 & 0 & c_{11} & c_{12} \end{bmatrix} \tag{3.21}$$

$$[k_{ji}] = \begin{bmatrix} -c_1 & 0 & 0 & 0 & -c_4 & 0 & 0 \\ 0 & -c_2 & 0 & c_5 & 0 & 0 & 0 \\ 0 & 0 & -c_3 & y_s c_3 & x_s c_3 & 0 & 0 \\ 0 & -c_5 & y_s c_3 & c_7 + y_s^2 c_3 & 0 & 0 & 0 \\ c_4 & 0 & -x_s c_3 & x_s y_s c_3 & c_9 - x_s^2 c_3 & 0 & 0 \\ & & 0 & 0 & 0 & -c_{10} & -c_{11} \\ 0 & 0 & 0 & 0 & 0 & c_{11} & c_{13} \end{bmatrix} \tag{3.22}$$

$$[k_{jj}] = \begin{bmatrix} c_1 & & & & & & \\ 0 & c_2 & & & & & \\ 0 & 0 & c_3 & & & (Symm) & \\ 0 & c_5 & -y_s c_3 & c_6 + y_s^2 c_3 & & & \\ -c_4 & 0 & x_s c_3 & -x_s y_s c_3 & c_8 + x_s^2 c_3 & & \\ & & 0 & 0 & 0 & c_{10} & \\ 0 & 0 & 0 & 0 & 0 & -c_{11} & c_{12} \end{bmatrix} \tag{3.23}$$

in which

$$\begin{aligned} &c_1 = \frac{12EI_y}{l^3}, \quad c_2 = \frac{12EI_x}{l^3}, \quad c_3 = \frac{EA}{l}, \quad c_4 = 0.5lc_1 \\ &c_5 = 0.5lc_2, \quad c_6 = \frac{4EI_x}{l}, \quad c_7 = 0.5c_6, \quad c_8 = \frac{4EI_y}{l} \\ &c_9 = 0.5c_8, \quad c_{10} = \overline{GJ}\frac{a}{\mu}\sinh\ al, \quad c_{11} = \overline{GJ}(1 - \cosh\ al) \\ &c_{12} = \overline{GJ}(l\ \cosh\ al - \frac{a}{\mu}\sinh\ al), \quad c_{13} = \overline{GJ}(\frac{a}{\mu}\sinh\ al - l) \end{aligned} \tag{3.24}$$

and x_s, y_s specify the location of the shear center O with respect to the centroid C. Equations (3.20 - 3.24) are for core tubes which are uniform in each story. The stiffness coefficients in equation (3.20) for shear, bending and axial deformations remain the same

as those for ordinary beams, while the coefficients related to torsion and warping are from equation (3.17).

3.4 Numerical Examples

Three illustrative examples are presented involving symmetric and unsymmetrical core tubes subject to either torsional actions or lateral loads. The accuracy of the results obtained by the present modeling is examined by comparing with reported other matrix method solutions or with data generated using the commercially available finite element software NISA.

3.4.1 Symmetric core tube subjected to concentrated torque at the top

Re-analyzed herein is the small scale model core tube studied earlier by Liauw and Leung [38], and Gendy, Saleeb and Chang [43] employing, respectively, the transfer matrix method with different state vectors immediately below and above the lintel beams, and generalized one-dimensional thin-walled finite beam elements with specially defined displacement and strain interpolation functions for torsional behavior. This 20-story structure is doubly symmetric and under the action of unit torque M_z applied at the top. Figure 3.3 shows the plan layout of the model. The story height = 62.2 mm, lintel beam depth = 9.5 mm, and thickness of shear wall panels and lintel beams = 6.2 mm. Young's modulus E = 29.65×10^2 MPa and shear modulus G = 11.03×10^2 MPa. The lintel beams are replaced by an equivalent continuum with thickness of t_1 = 0.13 mm, resulting in the sectorial coordinate diagram is shown in Figure 3.4 where the corresponding sectorial moment of inertia $I_{\bar{\omega}} = \oint_A \bar{\omega}^2 \, dA = 5.98 \times 10^{10}$ mm^6 for the equivalent closed section.

The floor slab in-plane rotations θ_z and the variation of bimoment $B_{\bar{\omega}}$ along the building height obtained by the present model are compared with solutions from [38, 43]

in Figures 3.5 and 3.6, respectively. Figure 3.5 shows that the agreement of rotations is very close between the present method and that of [43], with a difference of 6.3% at the top. Similar good agreement is also evident in Figure 3.6 for the distribution of bimoment $B_{\bar{\omega}}$ over the lower half of the structure. Over the uppermost portion, however, the present method (whether story-wise or continuous approach) shows different behavior for the bimoment. The solution denoted continuous approach is obtained according to the formula $B_{\bar{\omega}} = \mu M_z \sinh a(L-z) / (a \cdot \cosh aL)$ given in [33]. By this formula, the bimoment distribution along the axis of the structure subjected to concentrated torque at the free end is controlled by the function $\sinh a(L-z)$, in which L is the total length of the beam and z is the axial coordinate. Thus, for $z \leq L$, the bimoment does not cross over the zero line and, at the top of the structure, the bimoment under the given loading condition of this problem should theoretically vanish, which are both correctly predicted by the present method.

3.4.2 Asymmetric core tube under uniformly distributed lateral load

To demonstrate the performance of the present model for a core tube, with or without lintel beams and undergoing flexural torsion in addition to bending deformation, an asymmetric 15-story core supported structure is considered. This structure has previously been analyzed by Stafford Smith and Taranath [37] employing the assembled stiffness matrix for the core treated as an open section, with the warping stiffness contributed by the lintel beams added separately. The plan view of the structure and the applied lateral load are shown in Figure 3.7. The story height = 3.81 m, lintel beam depth = 0.457 m, Young's modulus E = 2.76×10^4 MPa and shear modulus G = 1.20×10^4 MPa. The lintel beams are replaced by an equivalent continuum with thickness of t_l = 1.78 mm, which leads to the sectorial moment of inertia $I_{\bar{\omega}} = 2.78 \times 10^2$ m^6 for the equivalent closed section. Since the structure is modeled by end-loaded thin-walled subsystems, the

uniformly distributed load is transformed into concentrated loads of 6.95 kN applied at the floor levels (3.48 kN at the top) and passing through the geometric centroid O of the centrally located core tube.

Floor rotations and bimoments along the building height are shown in Figure 3.8 and 3.9 and compared with solutions from [37], respectively. Since the analysis in [37] modeled the core as open section constrained by lintel beams at floor levels, shear deformation in the wall panels was not included. Presented also are the results obtained by the FEM software NISA for the floor rotations θ_z only, since the corresponding data for bimoments $B_{\bar{\omega}}$ are not obtainable from such programs. In this FEM analysis, the core tube is modeled by a quite fine mesh: 342 four-noded thin-shell elements per story, where the 3.05 m long and 0.457 m deep lintel beams are modeled by six 0.508 x 0.457 m elements. The elements are formed by superimposing plane stress and thin plate behavior. These elements have six degrees-of-freedom per node, but possess no rotational stiffness normal to the element middle surface.

Examining the accuracy for the core with lintel beams, Figure 3.8 shows that the rotation at the top is $3.53\text{x}10^{-3}$ rad by the present method, $2.95\text{x}10^{-3}$ rad in [37] and $3.41\text{x}10^{-3}$ ra l by FEM, yielding a difference of 0.9% between the displacement solutions by the present model and NISA. In terms of computing efficiency, the number of DOFs by NISA is 34848 in contrast to only 90 for the present method. It is interesting to note that neglecting shear deformation, as represented by the results from [37], introduces only 8.7% error in top rotation in this example since the lintel beam is only 12% of the story height, but the effect of shear will of course become more significant as the lintel beam depth increases. On the other hand, analyzing this example as open section, i.e. without lintel beams at floor levels, results in a much larger top floor rotation, i.e. $14.4\text{x}10^{-3}$ rad by the present method, $12.8\text{x}10^{-3}$ rad in [37] and $14.4\text{x}10^{-3}$ rad by FEM. Evidently, the lintel beams constrain the torsional warping of the cross-section to increase significantly the overall torsional rigidity of the core tube.

Figure 3.9 compares the bimoments obtained by the present model with those from [37]. Since the magnitude of normal warping stress $\sigma_{\bar{\omega}}$ varies with the bimoment along the longitudinal axis, the close match between the results observed in Figure 3.9 indicates that the variation of $\sigma_{\bar{\omega}}$ is well predicted by the present core model over the full height of the structure.

The distribution of the normal stresses at the base of the structure for the case with lintel beams is compared with the results from [37] in Figure 3.10, also with good agreement. The final values are obtained by superimposing the stress components due to bending and flexural torsion, which allows assessing the relative importance of the roles of these separate deformation modes. As done previously in [37], inspecting the distributions of the two stress components in Figure 3.10 demonstrates that the maximum normal stress due to warping is slightly more than double that due to bending in this example, thus confirming the aforementioned usefulness of methods such as the present in identifying the significance of warping in the total stress computations.

3.4.3 Non-uniform core tube under uniformly distributed torque

A non-uniform core tube under torque $M_z = 1.89 \times 10^4$ kN · m at each floor level is analyzed. The cross-section is the same as in the example of Section 3.4.2 but with wall thickness and the moment of inertia of lintel beams increased to 0.61 m and $2I_b$, respectively, in the first five stories. Figure 3.11 shows the elevation of the structure. Material properties remain the same as before. This structure differs from that of [27] in that the latter has a strengthened lintel beam (with moment of inertia = $4I_b$) at the top level. The sectorial coordinate diagram of the lower segment (the first five stories) is shown in Figure 3.12, which is obtained based on the equivalent continuum for lintel beams with the thickness t_l = 3.56 mm.

Figure 3.13 shows the variation of floor rotations along the building height in comparison with results from [27]. It is seen that the rotations for non-uniform and uniform cross-sections agree quite well for the present model and that of [27]. At the top, the floor rotation is reduced from 0.0165 rad to 0.0125 rad, about 24%, due to the strengthening of wall thickness and lintel beams in the first five stories. Figure 3.14 shows the corresponding comparison for bimoments. The discrepancy in the top few stories between the two solutions for the non-uniform section in both Figures 3.13 and 3.14 is due to the different lintel beams at the top level. Figure 3.13 also indicates that, by increasing the wall thickness in the first few stories, the overall rotations are reduced notably; in comparison, the influence of increasing the strength of the top lintel beam is local and limited to only a few of the uppermost stories.

3.5 Summary

A structural model based on the matrix method for tall building core tube structural analysis has been developed. The modeling is an extension of the continuous approach for core tube structures modeled as thin-walled beams.

The obtained analytical model is applicable to thin-walled structures with either open or closed sections. For the latter, shear deformations in the middle surfaces of wall panels are included. The thickness of walls can be changed story-wise but the shear center of each story segment remains the same. Numerical examples confirm the reliability and efficiency of this extended thin-wall beam model in comparison with finite element modeling and other methods of analysis. With the same accuracy for warping deformation and stresses as continuous methods achieved by the structural model for core tubes in this Chapter, this model for core tubes will be incorporated with the present FSM in the next Chapter to analyze tube-in-tube structures.

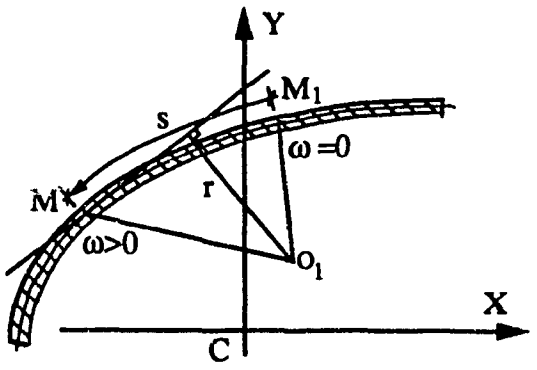

(a) Sectorial coordinate at M based on pole O_1 and origin M_1

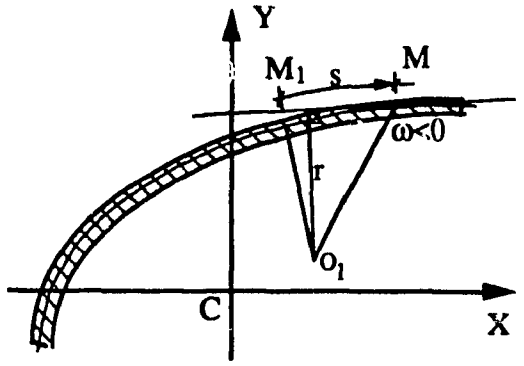

(b) Negative sectorial coordinate

Figure 3.1 Definition of sectorial coordinate

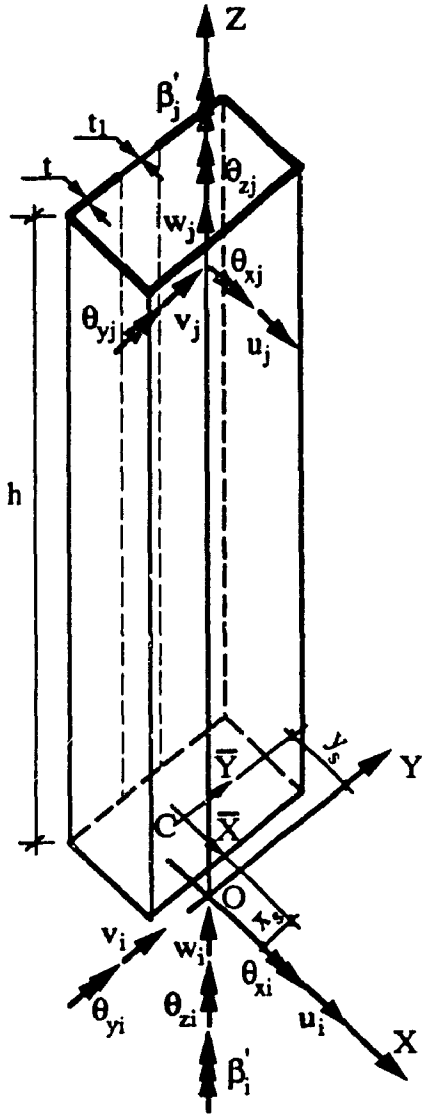

Figure 3.2 Coordinate system for thin-walled core element

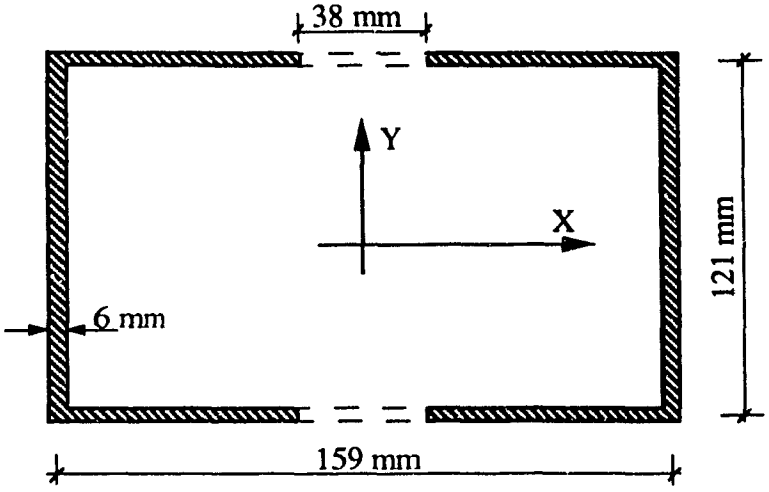

Figure 3.3 Plan of symmetric 20-story core tube under concentrated torque at top

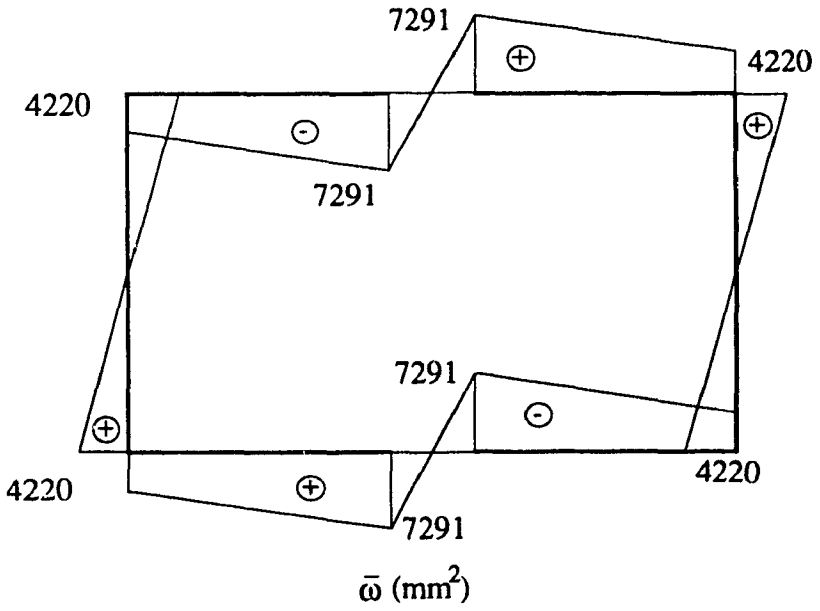

Figure 3.4 Sectorial coordinate diagram for symmetric 20-story core tube

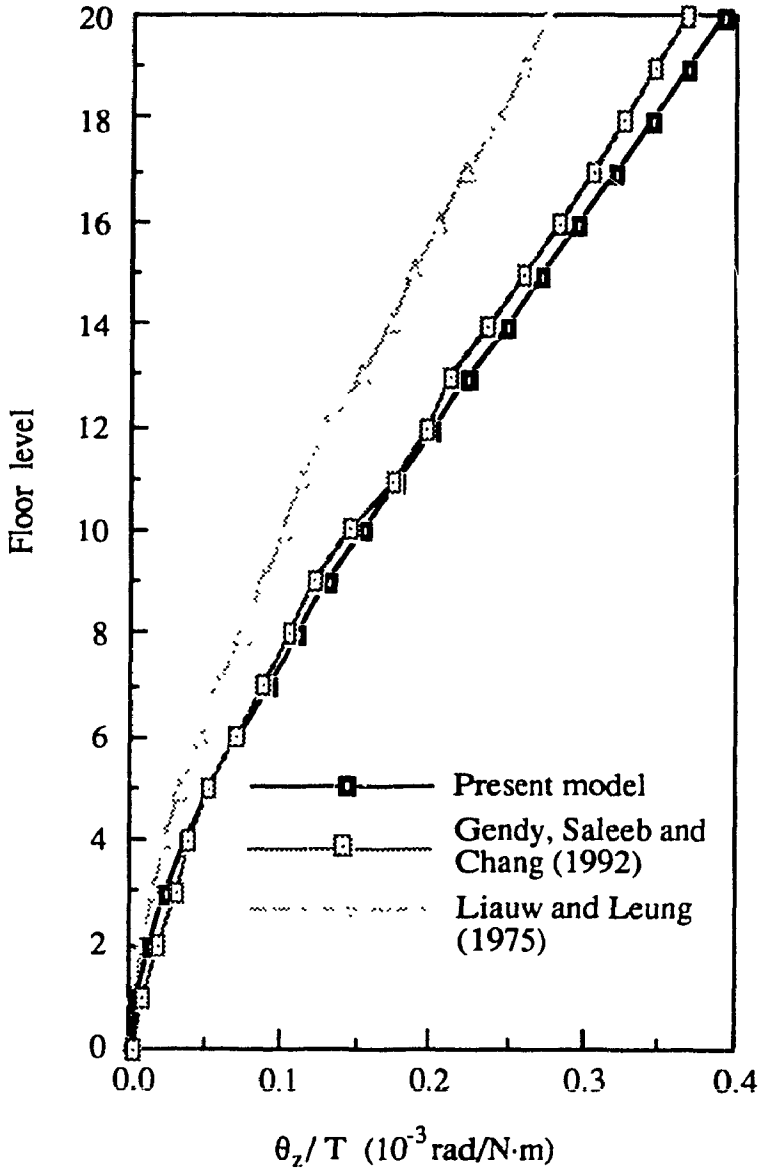

Figure 3.5 Floor rotations for symmetric 20-story core tube

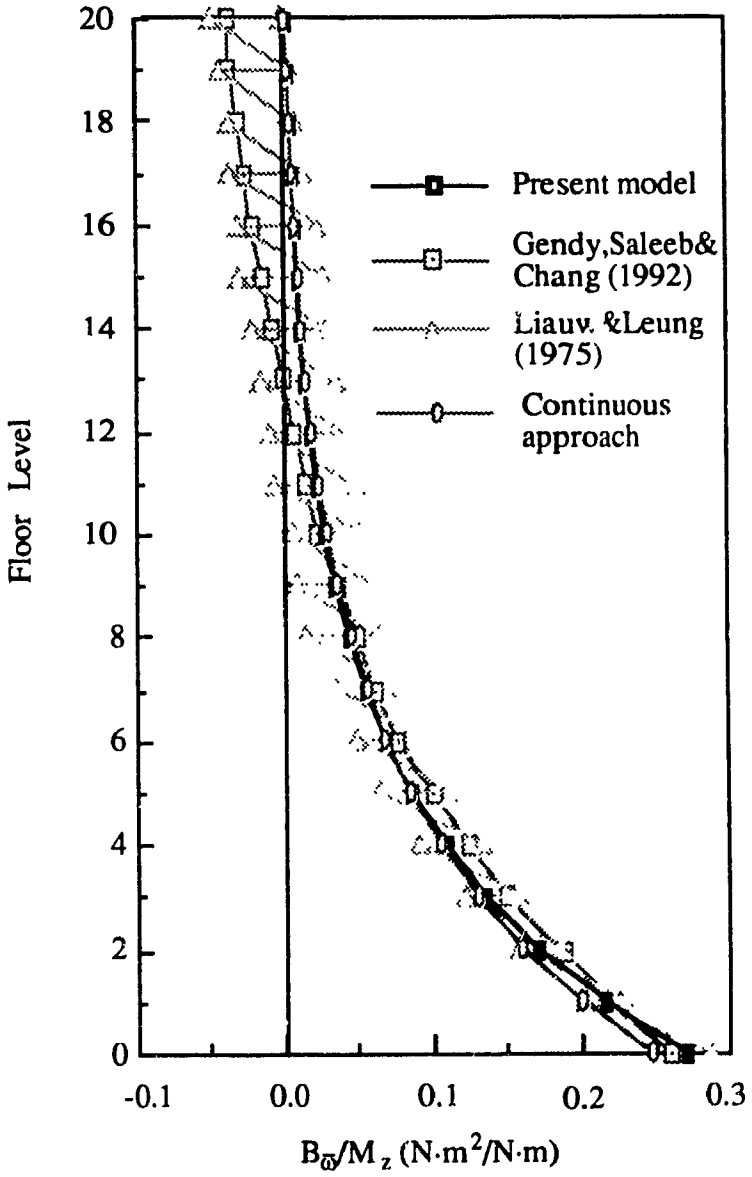

Figure 3.6 Variation of bimoments for symmetric 20-story core tube

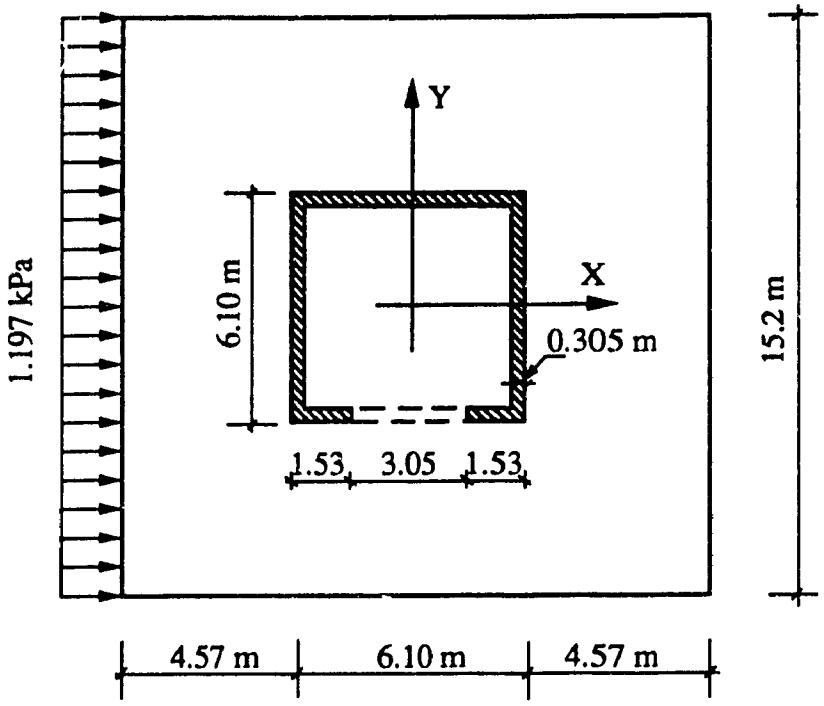

Figure 3.7 Plan view of asymmetric 15-story core-supported structure under lateral load

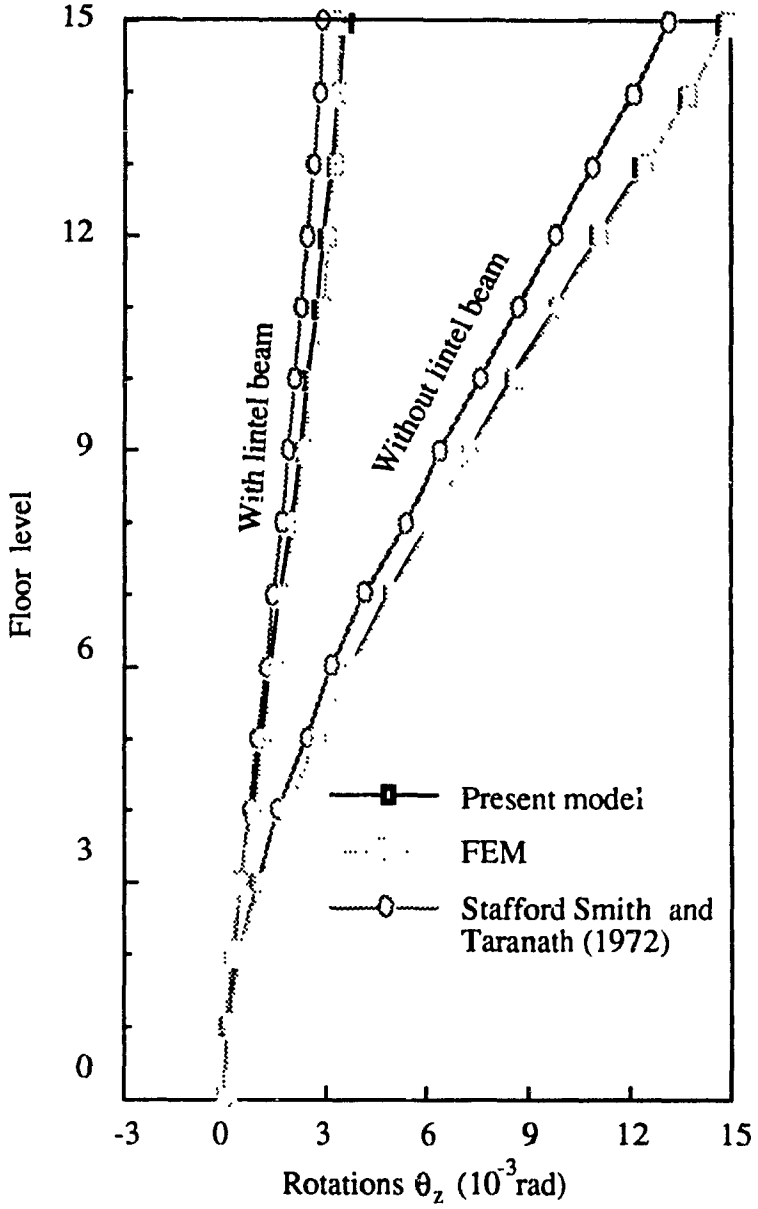

Figure 3.8 Floor rotations for asymmetric 15-story core-supported structure

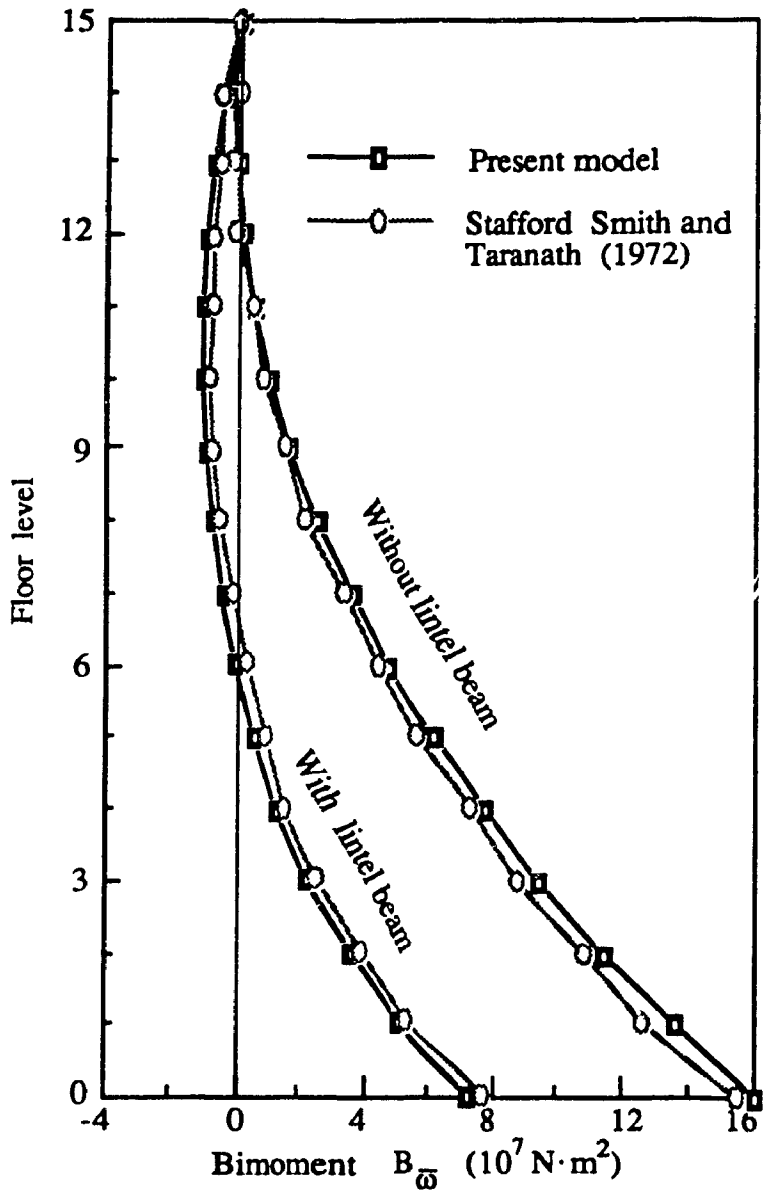

Figure 3.9 Variation of bimoments along the building height for asymmetric 15-story core supported structure

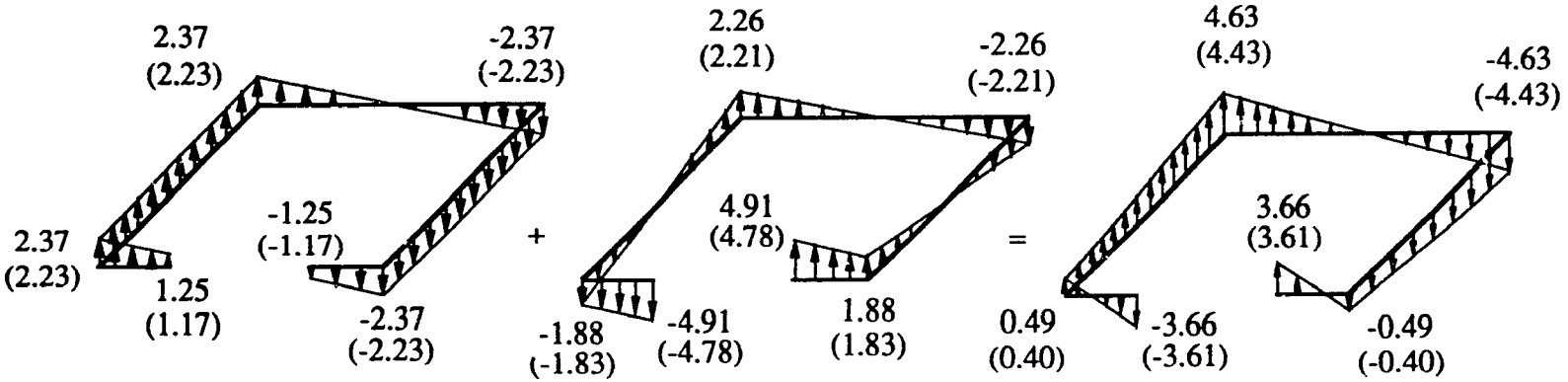

** Present model

(**) Stafford Smith and Taranath (1972)

Figure 3.10 Normal stress distributions at ground level of asymmetric 15-story core-supported structure

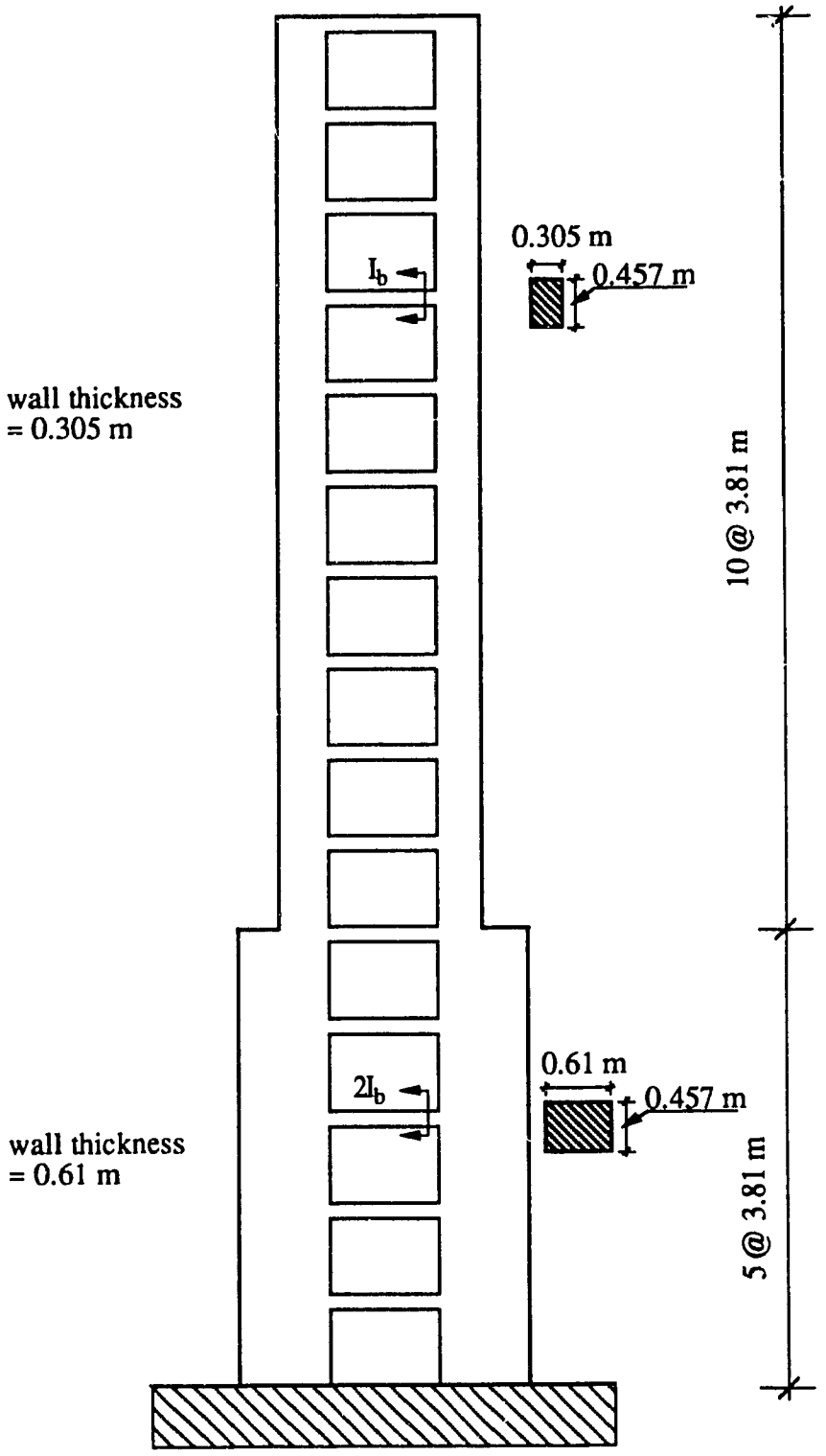

Fig. 3.11 Elevation of non-uniform core tube under uniformly distributed torque

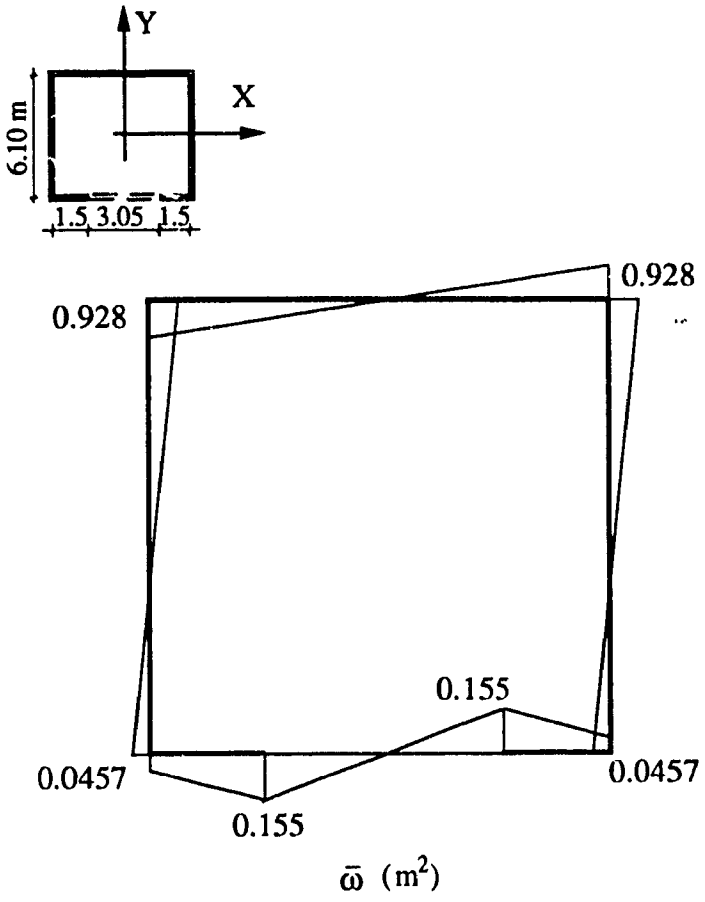

Figure 3.12 Sectorial coordinate diagram for non-uniform core tube

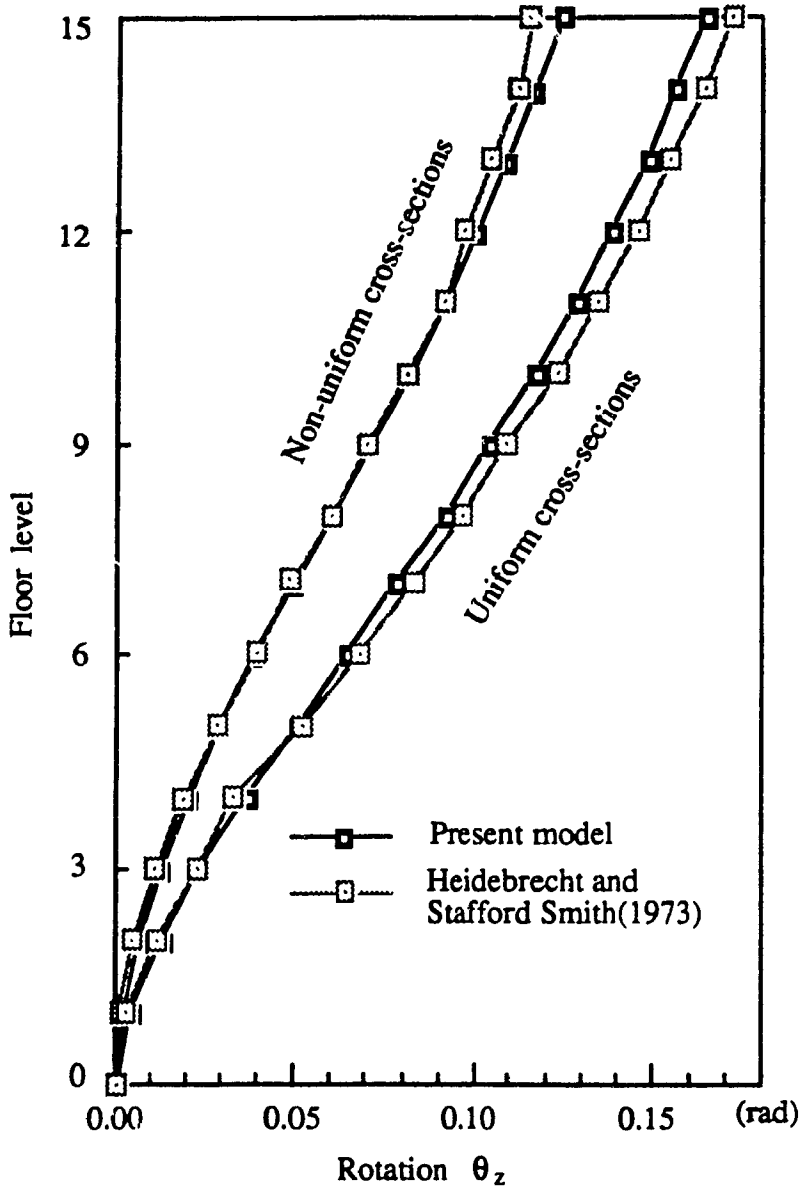

Figure 3.13 Floor rotations for non-uniform core tube structure

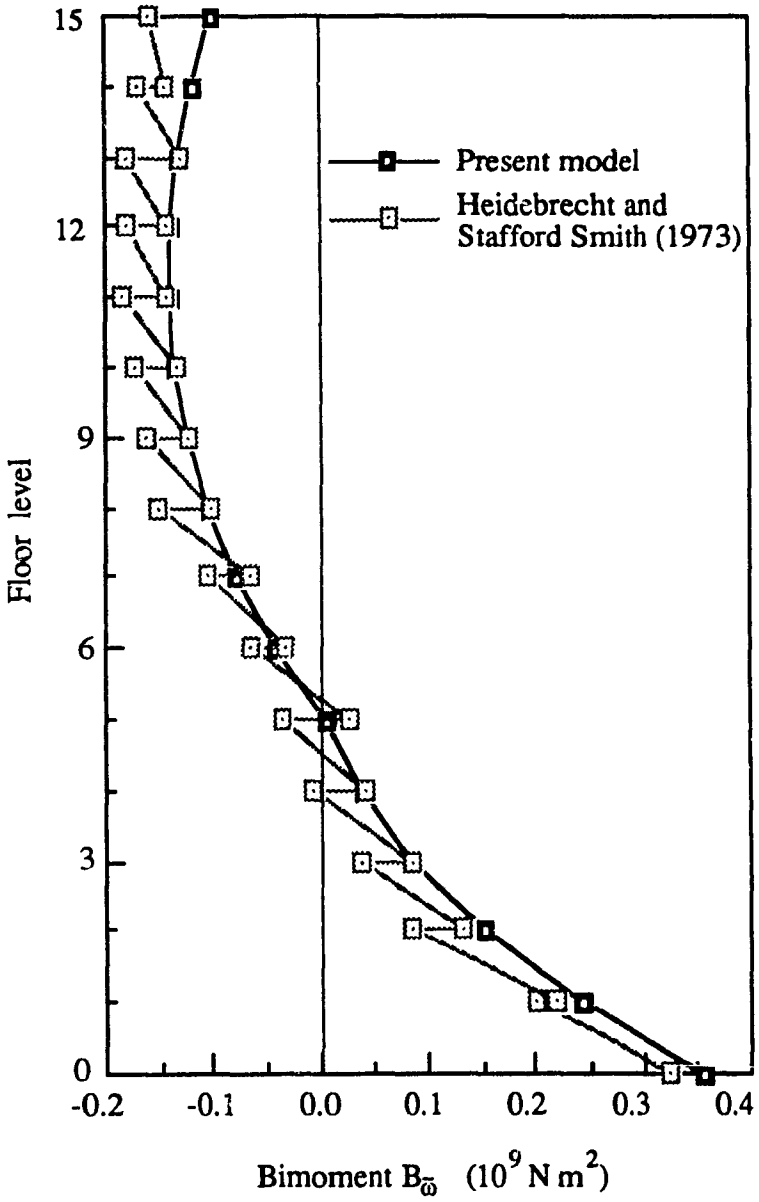

Figure 3.14 Variation of bimoments along the building height for non-uniform core tube

Chapter 4

Tube-in-Tube Structures

4.1 Introduction

In Chapter 2, the finite story method is presented for framed tube structural analysis. The assumptions in the method, definition of nodal displacement fields and procedure of the analysis were described To apply the FSM to the analysis of tube-in-tube structures, the core tubes are modeled by thin-walled beams, and the basic concept and formulation of thin-walled beam theory are reviewed in Chapter 3.

This Chapter extends the above finite story method by incorporating the modeling of core tubes as thin-walled beam elements in 3-D analysis for displacements, natural frequencies and modes of vibration of tall building tube-in-tube structures. Structures and structural behavior under lateral loads are described. Existing simplified methods of analysis are reviewed and the extended analysis procedure is presented. Numerical examples include both a symmetric structure under torsion action, and an unsymmetric tube-in-tube structure under lateral loading. The dynamic properties of the latter structure are also computed in order to verify the effectiveness of the present analytical model for response to dynamic loading. The results are compared with full finite element modeling in order to establish the accuracy and efficiency of the present FSM in modeling tube-in-tube structural systems.

4.1.1 Characteristics of tube-in-tube structures and their behavior under lateral loads

The framed tube or the core tube may be used individually to resist all lateral loads; however, it is common in design to place a tubular core inside a peripheral framed tube. The inner core tube and the outer framed tube are connected by floor slabs and perform as a unit forming the tube-in-tube system, also referred to as hull-core structures.

Tube-in-tube structures are essentially shear wall-frame interactive systems, with the outer framed tube possessing much greater stiffness than a conventional rigid frame. There may be one or more core tubes located inside the frame tube; the area enclosed by the core tube can occupy up to a quarter of the total plan area; and the overall system can comprise a multiple of this basic tube-in-tube forms. Two typical examples are the 38-story Brunswick office building in Chicago, shown in Figure 4.1a, and the 64-story Hope Well Tower in Hong Kong shown in Figure 4.1b.

Generally, the framed tube plays the dominant role in responding to external loads because of its much greater plan dimensions, while the core is flexural weak in overall bending due to its usual proximity to the neutral axis. Similar to shear wall-frame systems, the two different subsystems are tied together to perform as a unit in resisting lateral loads, and the interaction between the core tube and the framed tube augments the lateral load resistance of the whole system. Under lateral loads, shear is carried by the core tubes as well as by the in-plane rigidity of the frame panels, whereas the overturning moment is resisted primarily by the framed tube which responds in tension and compression of columns and racking of spandrel beams.

Torsion in these systems occurs due to unsymmetrical structural arrangements or lateral load distributions. Even a structural system designed to be symmetric may behave as an unsymmetric system due to various unforeseen factors such as variation in construction methods and later changes made to the structural components [45]. If a building structure is unsymmetric in one direction, the lateral displacements in that

direction are coupled with the torsional deformation. On the other hand, if the asymmetry is in both perpendicular directions, the structural response will be torsionally coupled in both directions. Only a three-dimensional (3-D) analysis is capable of predicting the behavior of such systems.

4.1.2 Existing simplified methods of tube-in-tube structural analysis

Although extensive attention has been paid to simplifying the structural analysis of framed tubes and core tubes separately, little research has been reported on simplified procedures for tube-in-tube structures. Coull and Subedi [11] adapted the equivalent plane frame technique, originally developed by them for framed tube structural analysis, to the analysis of tube-in-tube structures under lateral loads. The method analyzes tube-in-tube structures by means of 2-D frame computer programs and is effective in modeling the static response, although it is limited to doubly symmetric systems. Stafford Smith and Crowe [58] proposed a hand method for estimating the frequency of free vibration of tall buildings. The method is efficient and improves the accuracy of frequency calculations over procedures in codes of practice for uniform symmetric buildings. Other approaches such as the finite strip method [20] and the strain-based finite element method [21] can be applied to tube-in-tube structures, although these methods have been applied only to core tube and frame structures, separately. A simplified approach, however, for predicting natural frequencies and modes of vibration of asymmetric tube-in-tube structures has not been devised. In view of the complex structural behavior of such a highly redundant structural system, there is an obvious need for developing an efficient method to determine static response to lateral loads, as well as for predicting the natural frequencies and modes of vibration, especially for preliminary design purposes.

4.2 Extension of FSM procedure

The theory and the analysis procedure of the finite story method based on nodal displacement fields for framed tube structures and the thin-walled beam modeling for core

tubes have been given in detail in the preceding Chapters; thus, only the significant steps of the present extension are given herein.

As in Chapter 2, the out-of-plane stiffness of floor systems is neglected in the analysis, while the in-plane stiffness is considered infinite. By this assumption, the building cross-sections remain plane when subjected to external loads, and the out-of-plane deformations of the core tube cross-section are uncoupled from those of the framed tube.

Based on the above, the tube-in-tube structure consisting of an exterior framed tube and interior core tubes is assumed to be connected by in-plane rigid floor slabs. Each of these vertical structural components, namely the framed tube and the core tubes, is considered as a structural subsystem, with each subsystem possessing five DOFs at each floor level. The overall structural stiffness and mass matrices are established in accordance with the foregoing floor slab assumption. Because the core tube is modeled by thin-walled beam elements between floor levels, the preliminary analysis of nodal displacement fields is necessary only for the exterior framed tube employing two-story segments at a time. Since the floor slabs are considered to be in-plane rigid diaphragms, the nodal displacements w^c, θ^c_{xk} and θ^c_{yk} of the core tube element, are uncoupled from the corresponding θ^f_{xk} and θ^f_{yk} of the framed tube. Thus, the number of DOFs of a tube-in-tube structure becomes $N(5+3N_S)$, where N denotes the number of stories in the building and N_S represents the total number of core elements.

For the framed tube, the vector of generalized displacement coordinates at the kth floor level (k = 1, 2,..., N) is expressed as

$$\{D^f\}_k = [D_{k1}\ D_{k2}\ D_{k3}\ D^f_{k4}\ D^f_{k5}\ ]^T = [U_k\ V_k\ \theta_{zk}\ \theta^f_{xk}\ \theta^f_{yk}]^T$$

in which U_k, V_k represent in-plane displacements in the X, Y directions, respectively; θ_{zk} denotes the floor rotations about the vertical axis; and θ^f_{xk} and θ^f_{yk} represent the framed tube rigid body rotations about the horizontal axes at the kth floor level, respectively. The

substructure stiffness matrix $[S^{f*}]_k$ and the mass matrix $[M^{f*}]_k$ of the kth story of the framed tube corresponding to the generalized displacement coordinates $\{D^f\}_k$ are formed by assembling the transformed stiffness matrices $[k_c^*]$, $[k_b^*]$ and mass matrices $[m_c^*]$, $[m_b^*]$ for columns and beams, respectively, as follows:

$$[S^{f*}]_k = \sum_1^{m_c} [k_c^*]_k + \sum_1^{m_b} [k_b^*]_k \tag{4.1}$$

$$[M^{f*}]_k = \sum_1^{m_c} [m_c^*]_k + \sum_1^{m_b} [m_b^*]_k \tag{4.2}$$

where m_c and m_b are the numbers of columns and beams in the kth story.

Supposing that there are m_w thin-walled beam elements modeling the core tube in the kth story, the corresponding displacement vector for the core at the kth floor level (k = 1, 2,..., N) is given by

$$\begin{aligned} \{D^c\}_k &= [D_{k1}\ D_{k2}\ D_{k3} \mid d_{k1}^c \ldots d_{km_w}^c]^T \\ &= [U_k\ V_k\ \theta_{zk} \mid\ w_1^c\ \theta_{x1}^c\ \theta_{y1}^c \ldots w_{m_w}^c \theta_{xm_w}^c\ \theta_{ym_w}^c]^T \end{aligned} \tag{4.3}$$

in which w_i^c, θ_{xi}^c and θ_{yi}^c denote the vertical displacement and the rotations about the orthogonal horizontal axes of the core tube elements ($i = 1, \ldots m_w$) at the kth floor level. The degrees-of-freedom at floor levels for warping deformations of thin-walled members are free of external loads, so that the order of the thin-walled beam element stiffness matrix in equation (3.20) is reduced to 12x12 by static condensation before entering the overall stiffness matrix. The resulting stiffness matrix corresponding to the vector of generalized coordinate $[D_{k-1}^c\ D_k^c]^T$ then becomes

$$[k_w] = \begin{bmatrix} k_{ii} & k_{ij} \\ k_{ji} & k_{jj} \end{bmatrix} \tag{4.4}$$

in which i and j denote the element ends at the (k-1)th and kth floor level, respectively. All sub-matrices in the equation (4.4) are of the order 6x6, i.e.

$$[k_{ii}] = \begin{bmatrix} c_1 & & & & & \\ & c_2 & & & (Symm) & \\ & & c_{10}+c_{11} & & & \\ & & & c_3 & & \\ & -c_5 & & -y_s c_3 & c_6+y_s^2 c_3 & \\ c_4 & & & x_s c_3 & -x_s y_s c_3 & c_8+x_s^2 c_3 \end{bmatrix} \tag{4.5}$$

$$[k_{ji}] = \begin{bmatrix} -c_1 & & & & & -c_4 \\ & -c_2 & & & c_5 & \\ & & -c_{10}-c_{11} & & & \\ & & & -c_3 & y_s c_3 & -x_s c_3 \\ & -c_5 & & y_s c_3 & c_6+y_s^2 c_3 & \\ c_4 & & & -x_s c_3 & x_s y_s c_3 & c_8-x_s^2 c_3 \end{bmatrix} \tag{4.6}$$

$$[k_{jj}] = \begin{bmatrix} c_1 & & & & & \\ & c_2 & & & (Symm) & \\ & & c_{10}+c_{11} & & & \\ & & & c_3 & & \\ & c_5 & & -y_s c_3 & c_6+y_s^2 c_3 & \\ -c_4 & & & x_s c_3 & -x_s y_s c_3 & c_8+x_s^2 c_3 \end{bmatrix} \tag{4.7}$$

where

$$c_1 = \frac{12EI_y}{l^3}, \quad c_2 = \frac{12EI_x}{l^3}, \quad c_3 = \frac{EA}{l}, \quad c_4 = 0.5lc_1$$

$$c_5 = 0.5lc_2, \quad c_6 = \frac{4EI_x}{l}, \quad c_7 = 0.5c_6, \quad c_8 = \frac{4EI_y}{l} \tag{4.8}$$

$$c_9 = 0.5c_8, \quad c_{10} = \overline{GJ}\frac{a}{\mu}\sinh\ al, \quad c_{11} = \frac{-2\overline{GJ}\,(1-\cosh\ al)}{l}$$

with x_s, y_s denoting the location of shear center O with respect to centroid C. For core elements possessing a shear center coincident with the centroid of the cross-section, x_s and y_s are zero. With the floor out-of-plane stiffness neglected, the equilibrium equation of the core tube element involves axial forces which are null for lateral load analysis. Thus, the order of equation (4.4) is reduced to 10x10, and the total number of DOFs of a tube-in-tube structure becomes $N(3+2N_s)$. The substructural stiffness matrix representing all the thin-walled elements of the core tube is then given by

$$[S^c]_k = \sum_{1}^{m_w} [k_w]_k \tag{4.9}$$

Combining now the subsystem stiffness matrices of equations (4.1) and (4.9) leads to the following standard form for the overall equilibrium equation for a tube-in-tube structure:

$$[K^*]\ \{D\} = \{P^*\} \tag{4.10}$$

in which

$$[K^*] = \sum_{k=1}^{N} ([S^{f*}]_k + [S^c]_k) \tag{4.11}$$

$$\{D\} = [D_1^f \quad D_2^f \ \ldots \ D_N^f \mid d_1^c \quad d_2^c \ \ldots \ d_N^c \ ]^T \tag{4.12}$$

where for the kth story

$$\{d_k^c\} = [w_1^c \ \theta_{x1}^c \ \theta_{y1}^c \ldots w_{m_w}^c \ \theta_{xm_w}^c \ \theta_{ym_w}^c]^T \tag{4.13}$$

and $\{P^*\}$ represents the external load vector corresponding to the overall vector of generalized coordinates {D}.

For dynamic analysis, the mass moments of inertia of the core tube corresponding to core vertical displacement w_i^c and flexural rotations θ_{xi}^c and θ_{yi}^c are relatively small, and consequently not sufficiently significant to define w_i^c, θ_{xi}^c and θ_{yi}^c as dynamic

degrees-of-freedom in computing the overall structural response. Hence, in dynamic analysis the order $N(5+3N_s)xN(5+3N_s)$ of the overall stiffness $[K^*]$ is reduced to 5Nx5N by eliminating the degrees-of-freedom of the core tube vertical displacements and rotations about the horizontal axes through static condensation.

4.3 Numerical examples

In this section, two illustrative examples involving symmetric and unsymmetrical tube-in-tube structures under the action of torsion and lateral loading, respectively, are presented. To examine the effectiveness of the FSM in predicting dynamic properties of torsionally coupled structures, the natural frequencies and modes of vibration of the unsymmetrical tube-in-tube structure are also examined.

4.3.1 Symmetric tube-in-tube structure under torsion

The structure is a symmetric 30-story tube-in-tube system subjected to torsion. The plan layout is shown in Figure 4.2. Young's modulus $E = 2.39x10^4$ MPa and shear modulus $G = 0.99x10^4$ MPa. The story height = 3.66 m and the lintel beam depth of the core tube = 1.22 m. Properties of members comprising the exterior framed tube are listed in Table 4.1. For the core tube, the thickness of equivalent continuum t_1 = 63.4 mm, which yields the sectorial coordinate diagram given in Figure 4.3 for which $I_{\bar{\omega}}$ = 44.1 m^6, while other properties are also given in Table 4.1. The structure is subjected to uniformly distributed external torque M_z = 3953 kN · m per floor with 1976 kN · m applied at the top of the building.

The system is analyzed by both the present FSM and NISA. In NISA the core tube is modeled by 50 of the four-noded thin shell elements per story, in which each lintel beam is modeled by only one shell element. The number of DOFs in NISA is 11754, whereas in FSM it is reduced to 210 in the overall analysis and 222 in the preliminary calculations for nodal displacement distribution coefficients.

Floor rotations of the structure under the applied torques are shown in Figure 4.4. At the top level the rotation θ_z is 8.22×10^{-4} rad by FSM and 7.86×10^{-4} rad by FEM, thus differing by 4.6%. Similar correlation exists for the distribution of column shear forces around the outer framed tube, as evidenced by Figure 4.5. This shows a maximum difference of 5.9%, which occurs for column 3. Figure 4.6 presents the distribution of these forces over the height of the building. It is seen that the results from the two methods are very close, indicating that the external torque distribution between the framed tube and the core tube is also correctly reported by the present FSM.

Since the dynamic properties of this structure without the core tube have previously been examined in Chapter 2, it is interesting to note the influence of the introduction of the core on these properties. For the framed tube only, the natural frequencies by FSM for the first six modes of vibration were 0.445, 0.572, 0.754, 1.363, 1.747, and 2.271 Hz. For the present tube-in-tube structure these become 0.425, 0.567, 0.755, 1.366, 1.806 Hz and 2.272 Hz, respectively, with an average difference of 5.8% for the six modes compared to corresponding FEM analysis. It is noteworthy that the effect expected for increase in stiffness arising from the introduction of the core is, more or less, offset by the additional mass associated with the core, thus resulting in the foregoing similarity in the frequencies.

4.3.2 Unsymmetric tube-in-tube structure under lateral load

Since the current FSM method exploits the fullest benefit for structures which cannot be modelled by equivalent 2-D procedures, this example involves an asymmetric structure for which lateral-torsional coupling always necessitates 3-D analysis. For such structures, the benefit of the current procedure is the greatly reduced input effort, accompanied also by much greater computing efficiency.

Figure 4.7 shows the plan of the unsymmetrical tube-in-tube considered for this example. The structure is under uniformly distributed lateral loading of 192 kN applied in

the Y-direction at each floor through the geometric centroid of the exterior framed tube. The asymmetry of the system is introduced by the unbalanced column arrangement in the Y-direction frame panels and by the eccentric location of the core tube. Unlike the other columns in the framed panels, the three interior columns in the left frame have the same properties as corner columns, thus resulting in total column stiffness in this panel approximately 65% that of the right panel of the framed tube. The properties of all spandrel beams in this panel are: area A = 0.390 m^2; moments of inertia $I_y = 0.533x10^{-1}$ m^4, $I_z = 0.302x10^{-2}$ m^4; and torsional constant = $0.103x10^{-1}$ m^4. The properties of all other members of the outer tube are the same as listed in Table 4.1 for the preceding example. The story height = 3.66 m and the thickness of core wall = 0.305 m. The material constants are also identical to those of the preceding example. The thickness t_1 of the equivalent continuum is 20.5 and 43.8 mm for lintels in the X and Y directions, respectively, giving an equivalent closed section. The corresponding sectorial coordinate diagram is shown in Figure 4.8, for which the sectorial moment of inertia $I_{\bar{\omega}}$ = 856.0 m^6.

In the FE model, the core tube is discretized by 45 four-noded thin-shell elements in each story with each lintel beam modeled by two thin-shell elements. In the present FSM computation, to obtain the required torsionally uncoupled nodal displacement patterns for the framed tube corresponding to floor displacement, the origin of the local coordinate system for the outer framed tube is located at x = 4.11 m in the overall coordinate system, which is the shear center of a single story in this uniform building. The total number of DOFs is 12594 in FEM compared to 210 in the overall analysis and 204 in the preliminary calculations of the present FSM. Although circumstances dictated the use of different computers, CPU savings are nevertheless evidenced by the following: the time consumed by the FEM solution is 1680 sec on a PC 486/50, while on a SUN 4/40 workstation 637 sec by FSM and only 255 sec by FSM* are required for solutions of displacements presented in Figure 4.9 and 4.10. The solution denoted by FSM* is obtained

by computing nodal displacement distribution coefficients only at the first three floor levels and applying the mean values of these to the other levels, whereas by FSM these are computed at every floor level.

The accuracy of the predicted floor lateral displacements in the Y direction and rotations about the vertical axis is examined in Figures 4.9 and 4.10, respectively. Under the given loading condition, the lateral deflections of the building comprise the primary overall deformation mode, and the results obtained from the present FSM and FEM are seen to very similar. At the top of the building, the lateral displacement is 54.3 mm by FEM, 53.1 mm by FSM and 52.5 mm by FSM*, thus differing only by 2.2% and 3.3%, respectively, from the FEM results. The coupled floor rotations depicted in Figure 4.10 display equally good correlation.

4.3.3 Dynamic properties of unsymmetric tube-in-tube structure

The dynamic properties for the preceding unsymmetric tube-in-tube structure are computed for mass density of members of 2.4×10^3 kg/m^3, which is employed in forming the consistent mass matrices for the columns, beams and core element. Additional concentrated translational mass and mass moment of inertia about the vertical axis assumed at floor levels are 1.43×10^6 kg and 2.71×10^8 kg $\cdot$ m^2, respectively.

The first five natural frequencies and corresponding modes of vibration presented in Figure 4.11 show almost similar agreement for the dynamic properties as for the preceding static results. The fundamental frequency is 0.256 Hz by FSM, 0.251 Hz by FSM* and 0.269 Hz by FEM, thus showing 4.8% and 6.7% error for this mode, respectively, with the maximum error in frequency of 10.6% which occur for mode 3. Since the asymmetry of this structure, introduced by the aforementioned unbalanced stiffness distribution and eccentrically located core, results in an eccentricity of the order of 10%, the structural responses are expected to be weakly coupled. This is confirmed by

Figure 4.12 which shows a top view of the associated modes from NISA. Evidently modes 1 and 4 are coupled, whereas modes 2 and 5 are purely translational and mode 3 is primarily torsional.

4.4 Summary

The finite story method has been applied to the analysis of tube-in-tube structures in which the core tube is modeled as a thin-walled beam element. Because the floor out-of-plane stiffness is considered negligible, the vertical displacements and rotations about the orthogonal horizontal axes in the core tube are uncoupled from those in the framed tube. Thus, the nodal displacement fields are determined only by analyzing two-story segments of only the framed tube. The element stiffness matrix of the thin-walled beam, given by equation (3.20), is reformed by condensing out the degrees-of-freedom related to the warping deformation at beam ends in order to conform to the generalized coordinates in the overall analysis by FSM.

Numerical results have shown that the present extension of the FSM is effective in providing good solutions of gross structural deformations for tube-in-tube structures under the actions of shear due to torsion, or bending coupled with torsion. The proposed method is also efficient in the estimation of the natural frequencies and modes of vibration of tube-in-tube structures.

Table 4.1 Member properties of unsymmetric 30-story tube-in-tube structure

Member	Area (m^2)	Shear Area (m^2)	Moment of Inertia (m^4)	Torsion Constant (m^4)
Interior column	0.337	0.281	$I_x=0.261\times10^{-2}$ $I_y=0.344\times10^{-1}$	0.860×10^{-2}
Corner column	0.674	0.562	$I_x=0.370\times10^{-1}$ $I_y=0.370\times10^{-1}$	0.172×10^{-1}
Spandrel beam	0.368	0.307	$I_y=0.447\times10^{-1}$ $I_z=0.285\times10^{-2}$	0.958×10^{-2}
Core tube	6.74		$I_x=37.3$ $I_y=43.8$	47.9

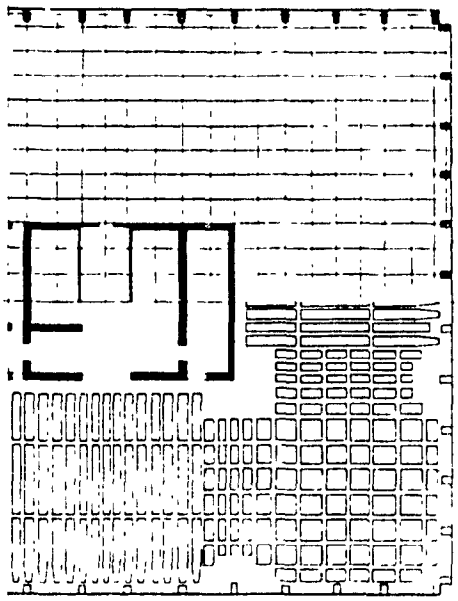

(a) Half of the typical floor of the Brunswick Office Building in Chicago

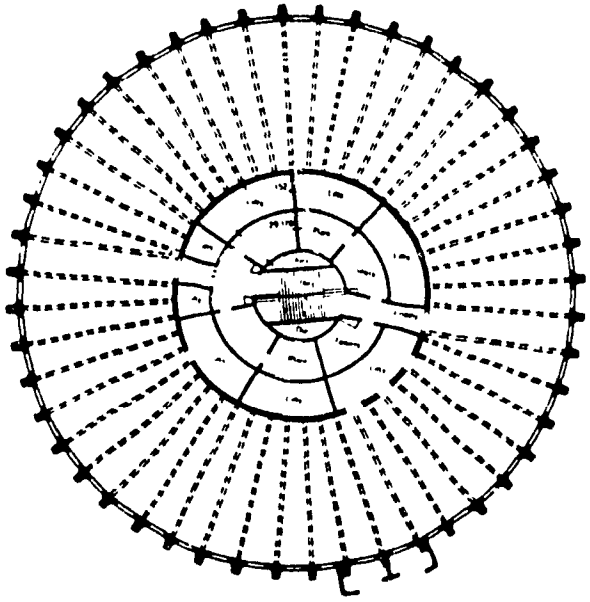

(b) Floor plan of Hope Well Tower in Hong Kong

Figure 4.1 Examples of tube-in-tube structures

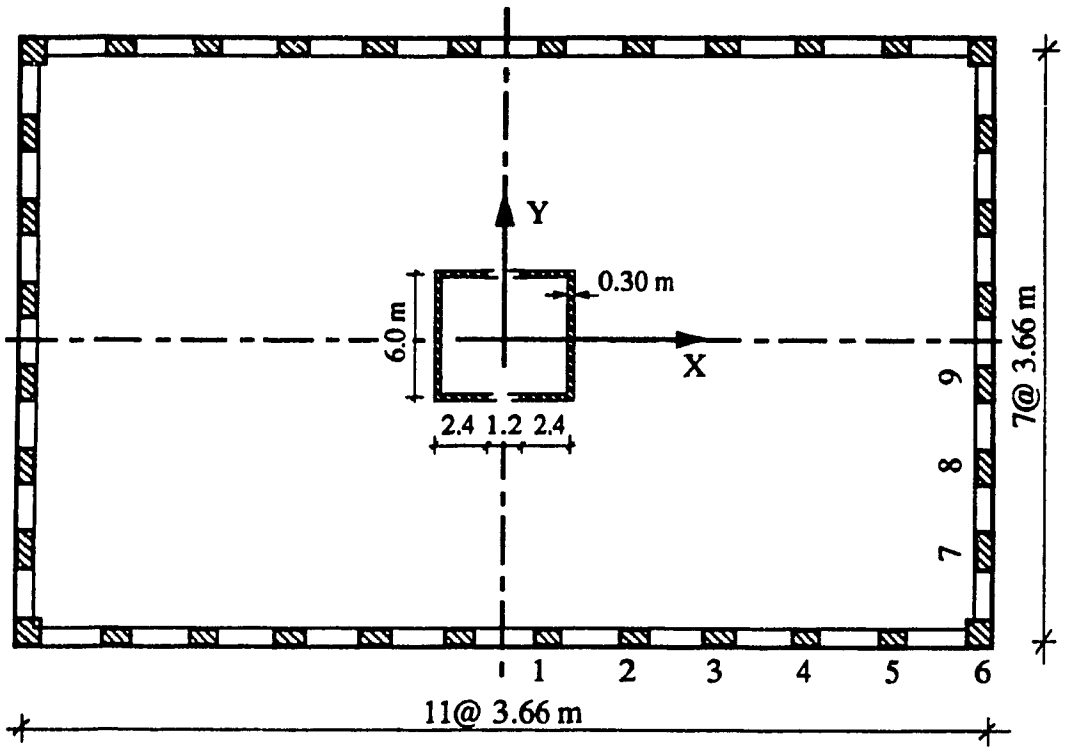

Figure 4.2 Plan of symmetric 30-story tube-in-tube structure under torsion

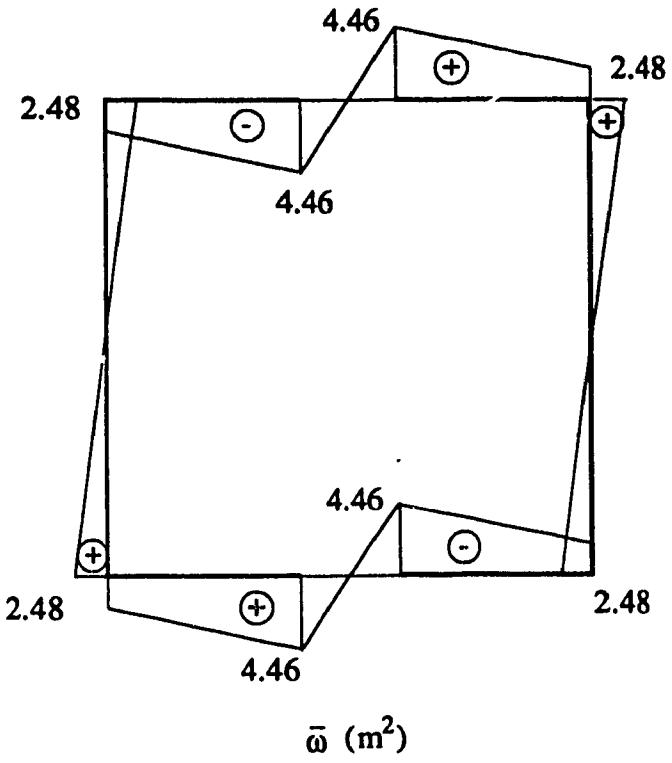

Figure 4.3 Sectorial coordinate diagram of core tube in symmetric 30-story tube-in-tube structure

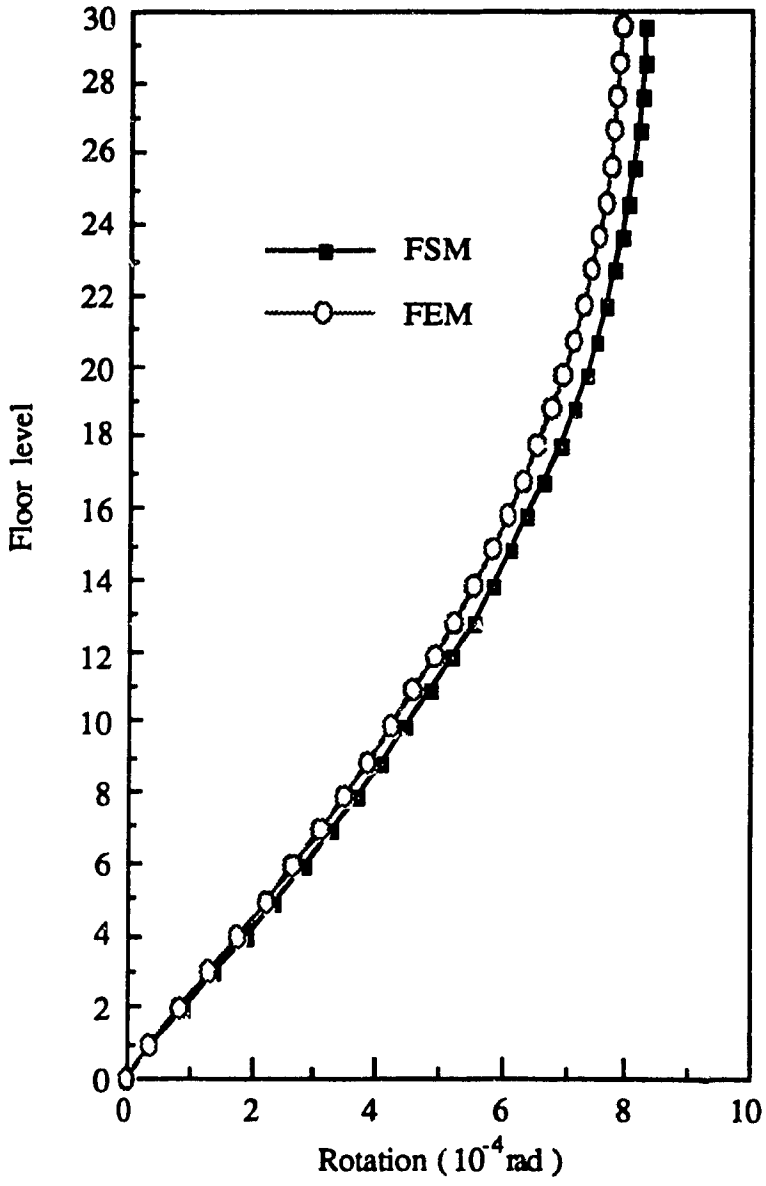

Figure 4.4 Floor rotations for symmetric 30-story tube-in-tube structure

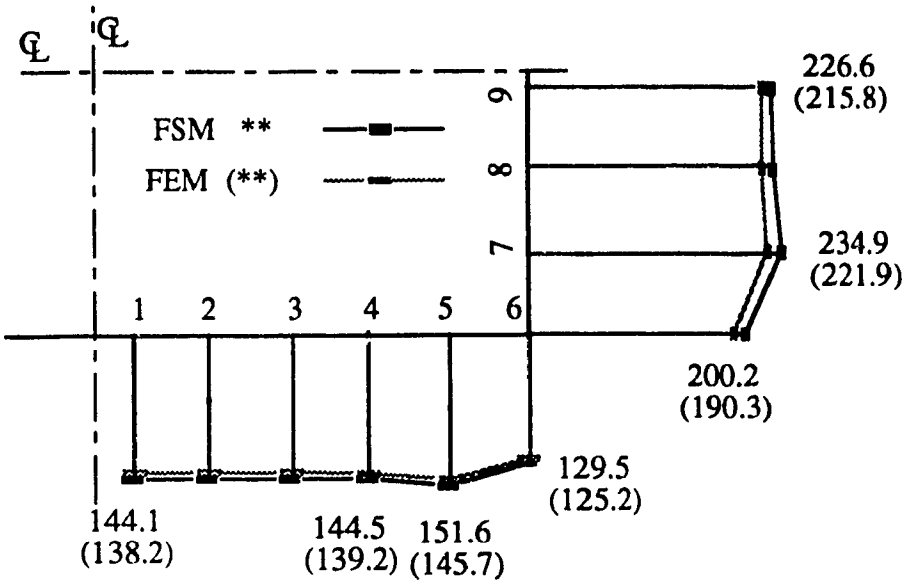

Figure 4.5 Distribution of column shear forces at ground level for symmetric 30-story tube-in-tube structure

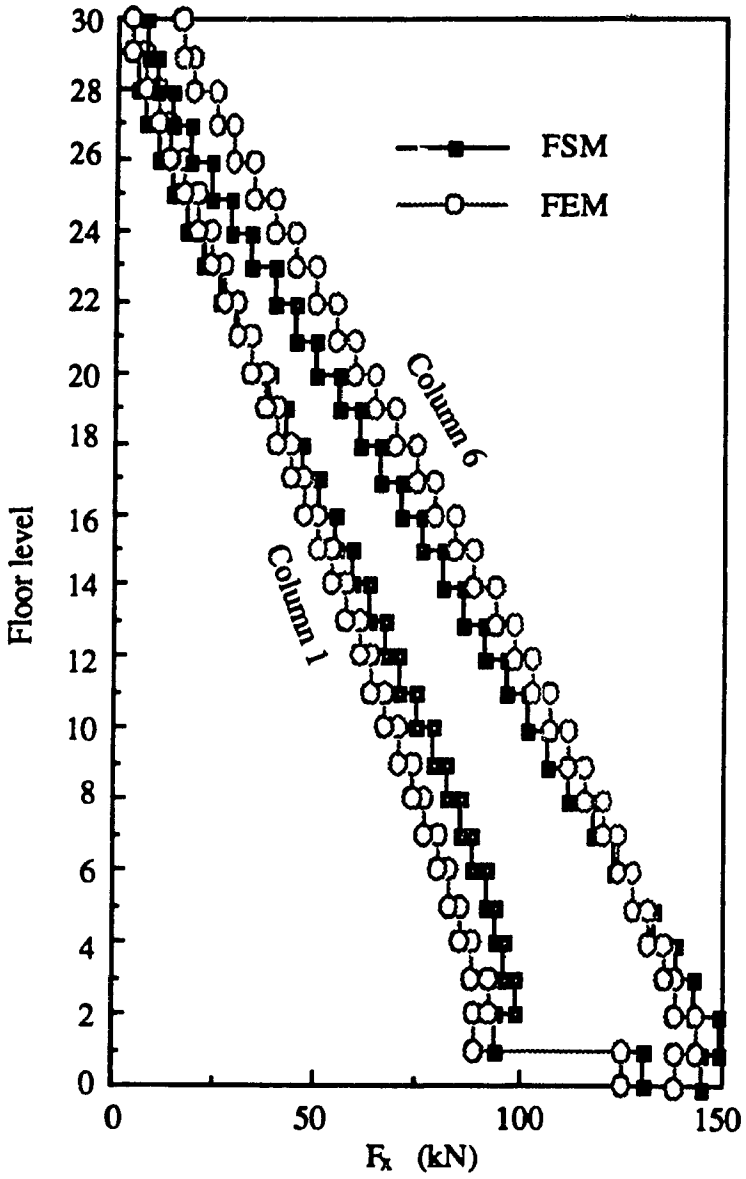

Figure 4.6 Column shears in outer frame of symmetric 30-story tube-in-tube structure

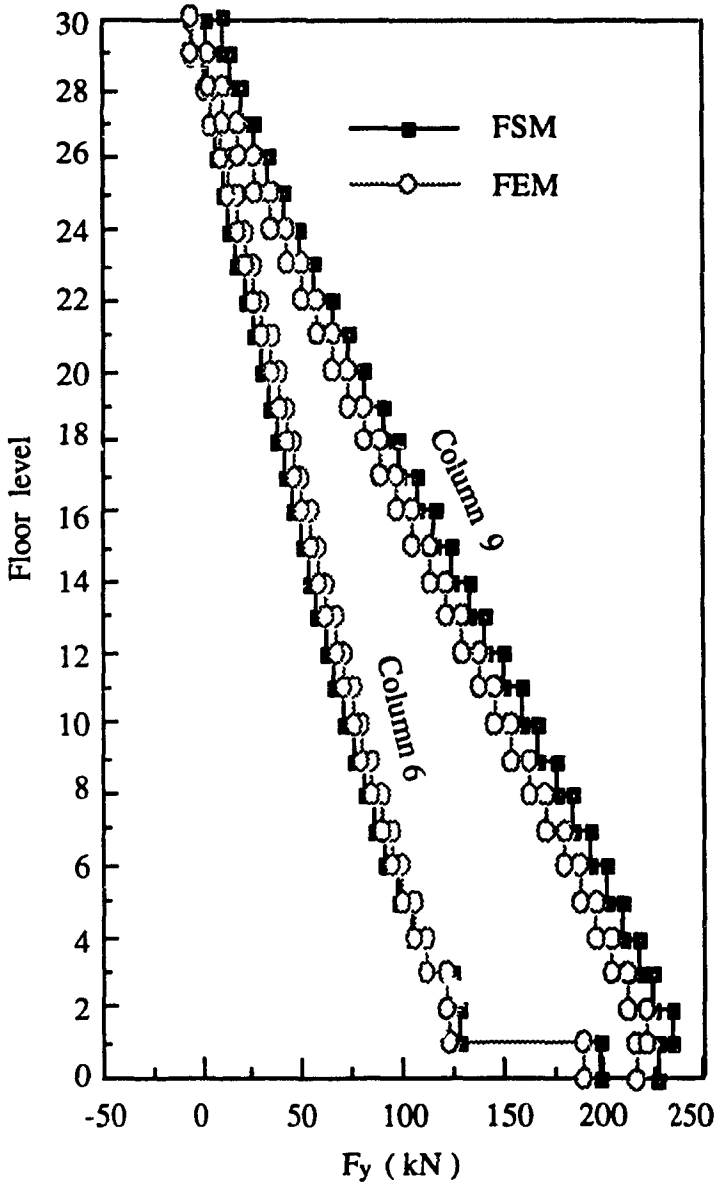

Figure 4.6 (Continued)

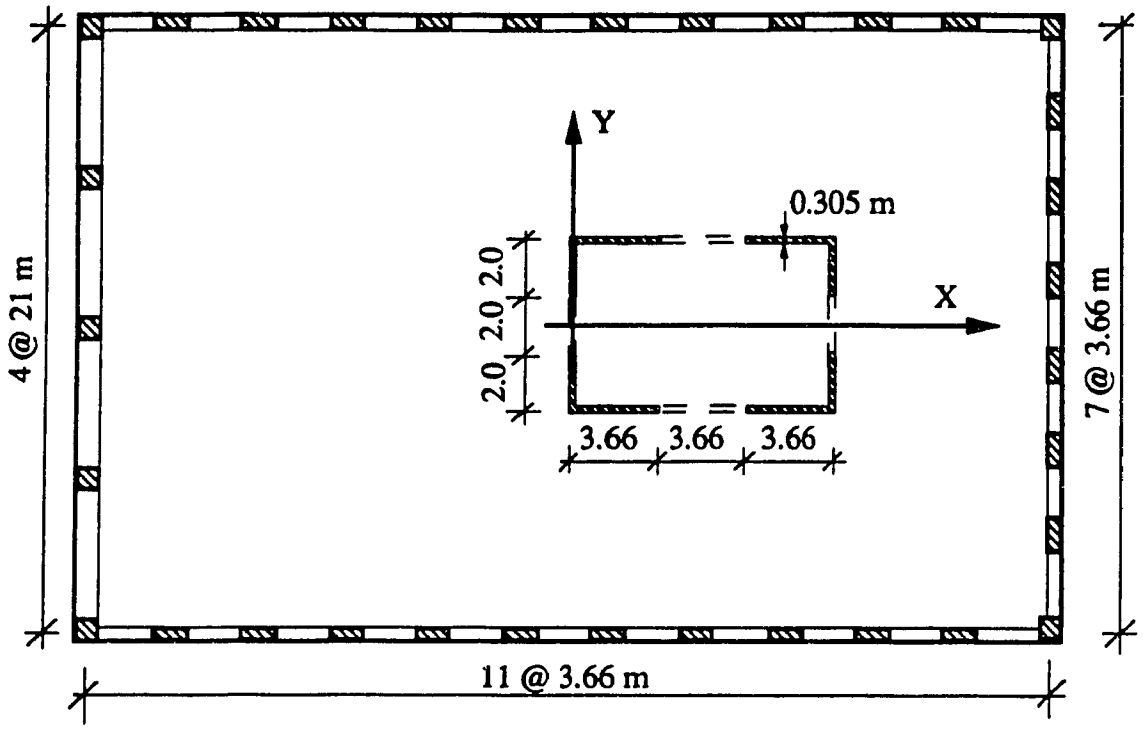

Figure 4.7 Plan of unsymmetric 30-story tube-in-tube structure under lateral load

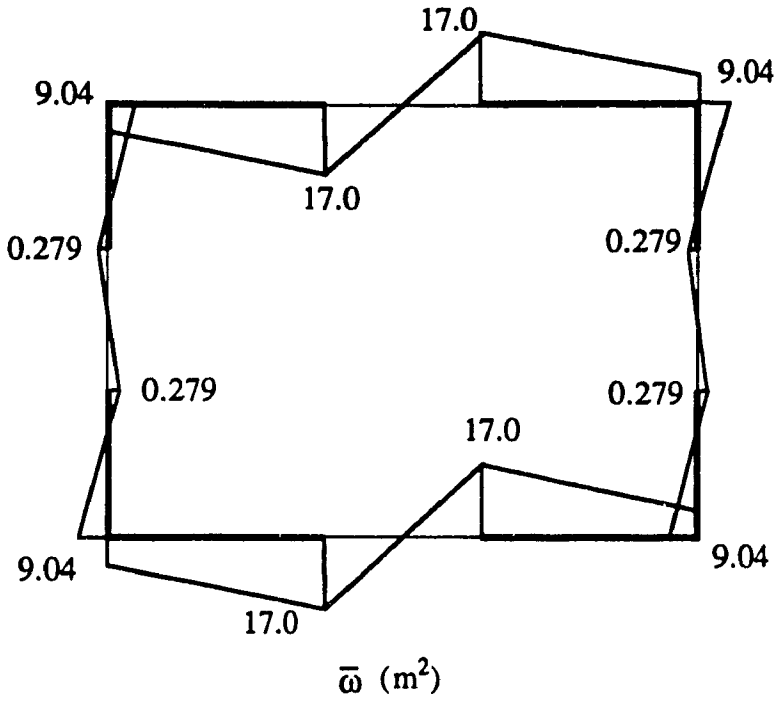

Figure 4.8 Sectorial coordinate diagram of the core tube in unsymmetric 30-story tube-in-tube

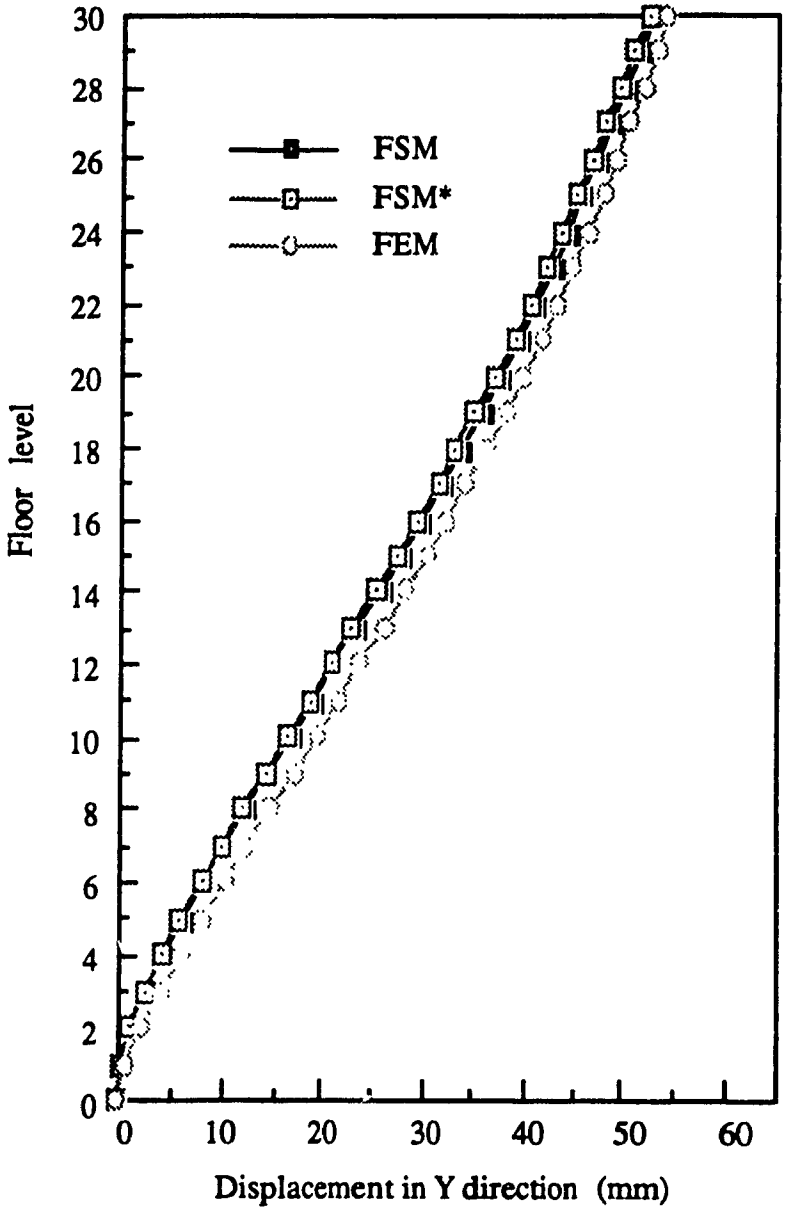

Figure 4.9 Lateral displacements for unsymmetric 30-story tube-in-tube

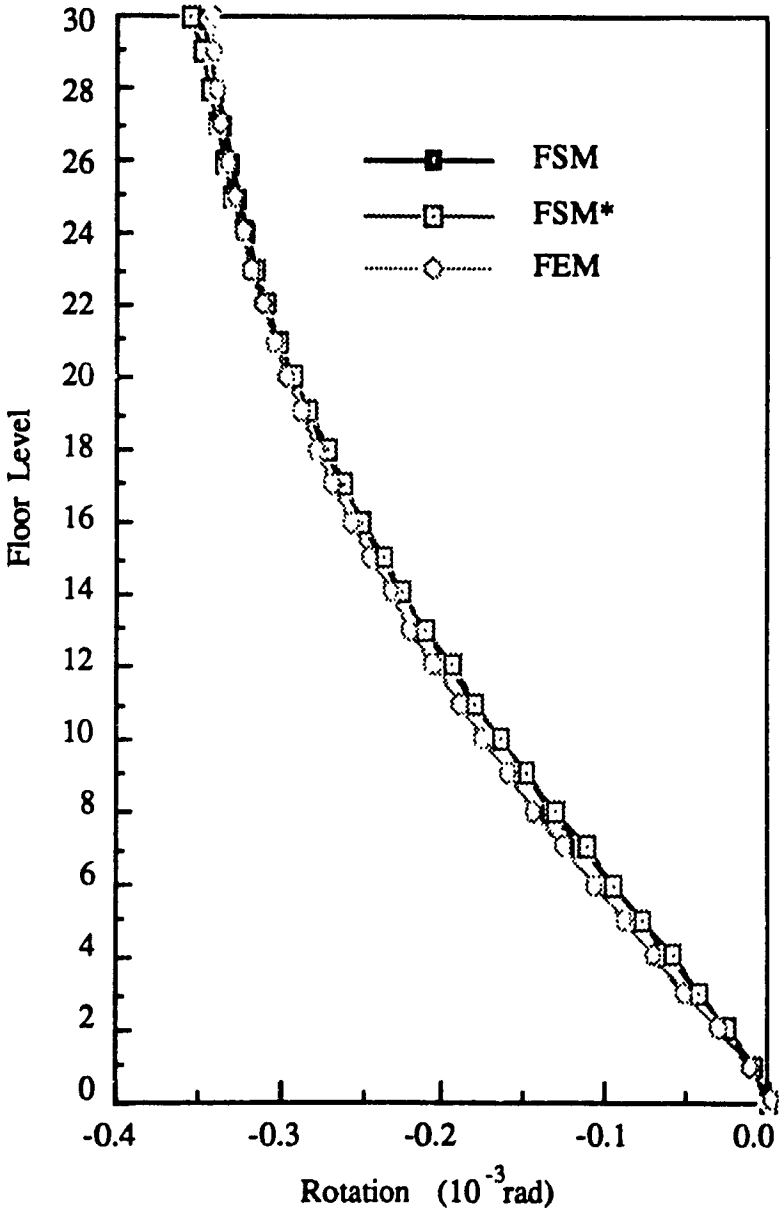

Figure 4.10 Floor rotations for unsymmetric 30-story tube-in-tube

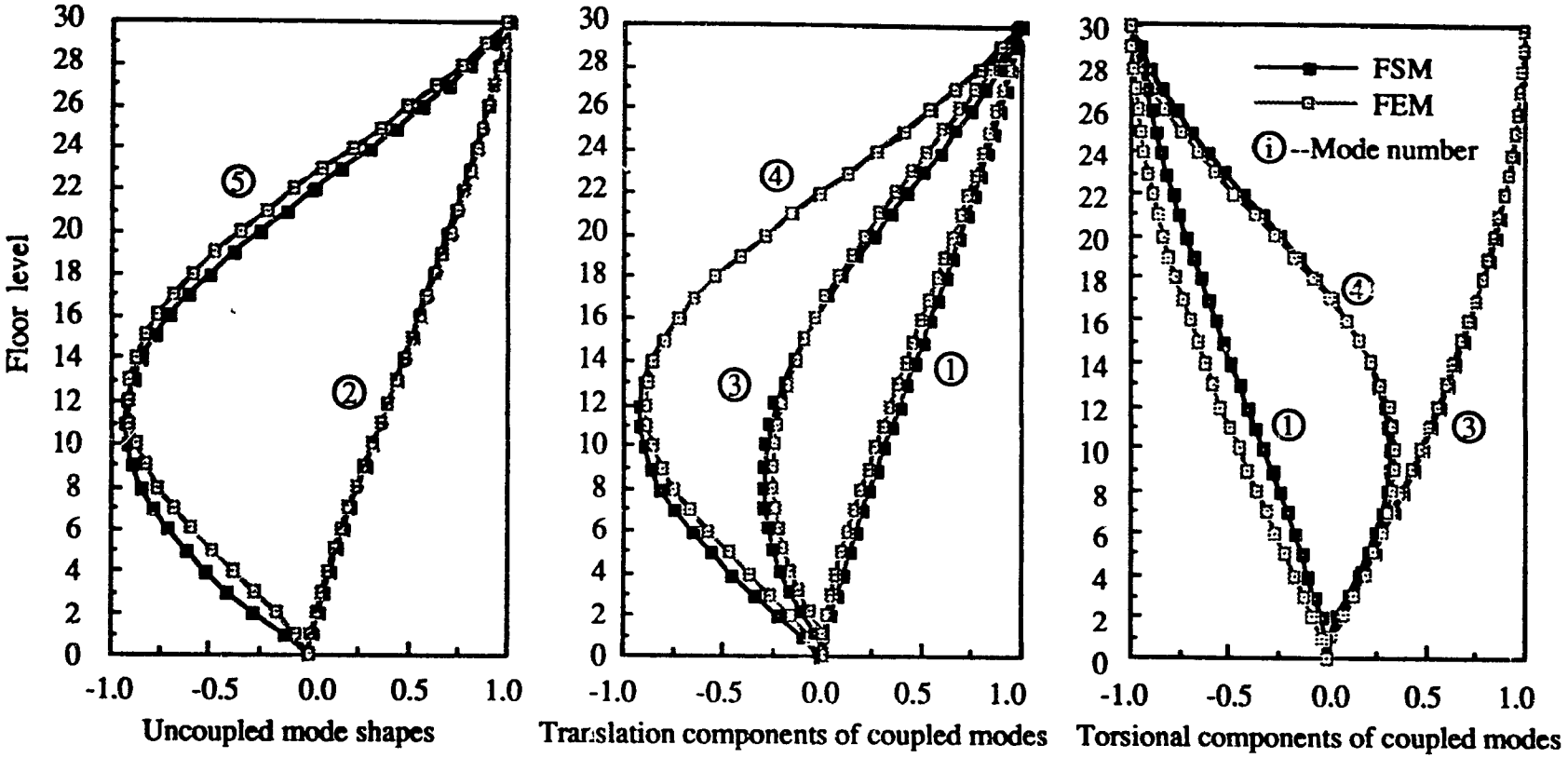

	Natural frequency (Hz)				
MODE	1	2	3	4	5
FSM	0.256	0.399	0.690	0.849	1.264
FSM*	0.251	0.394	0.691	0.834	1.238
FEM	0.269	0.412	0.625	0.909	1.286

Figure 4.11 Natural frequencies and modes of vibration for unsymmetric 30-story tube-in-tube

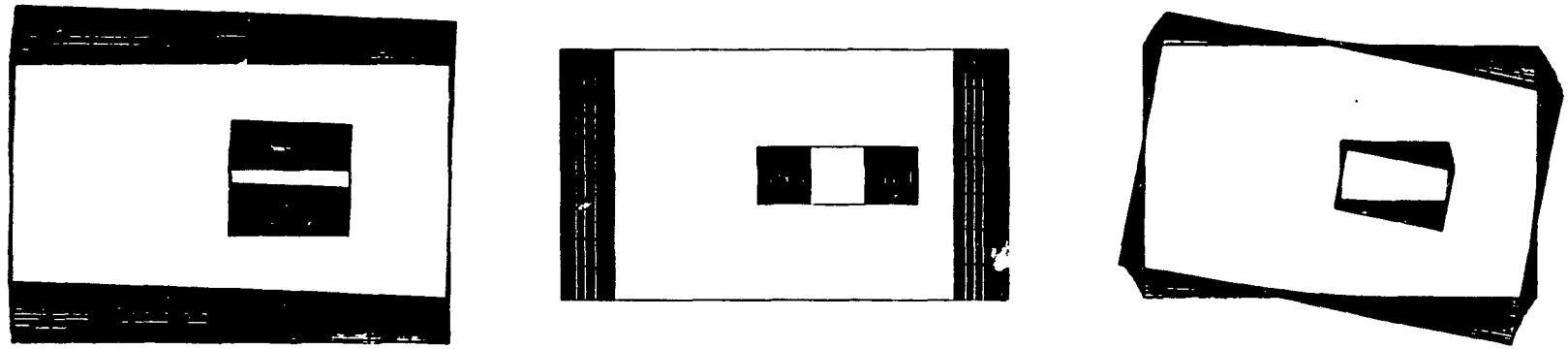

Mode 1 Mode 2 Mode 3

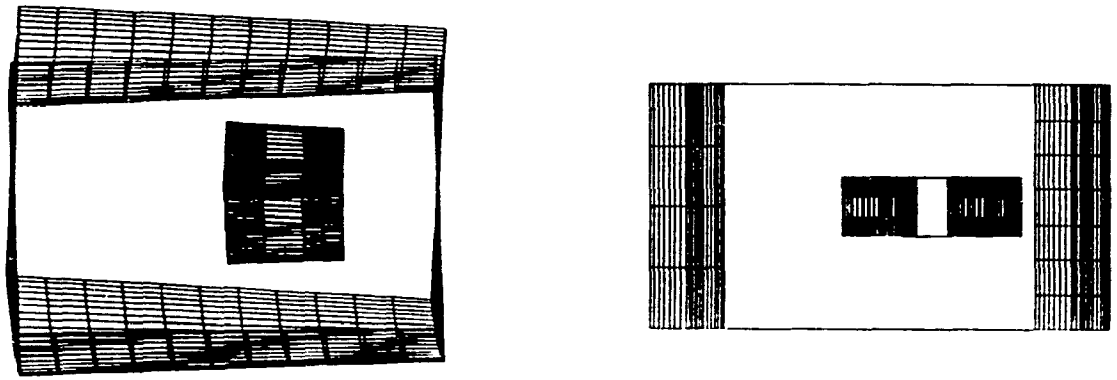

Mode 4 Mode 5

Figure 4.12 Top view of mode shapes for unsymmetric 30-story tube-in-tube

Chapter 5
Coupling Effect of Floor Systems

5.1 Introduction

Previous Chapters were devoted to the analysis of framed tube, core tube and tube-in-tube structures under lateral and torsional loads, in which floor systems were assumed to behave as in-plane rigid diaphragms with the out-of-plane stiffness of floor slabs neglected. This assumption is realistic for most buildings with an ordinary ratio of the transverse dimensions, i.e. not very long and narrow, and it effectively reduces the total number of displacement unknowns. However, for core structures with floor slabs acting as lintels and for tube-in-tube structures, the floor out-of-plane stiffness increases the overall lateral load resistance [1, 6, 7, 45], and thus deserves consideration in analysis and design.

This Chapter examines the contribution to lateral load resistance of the floors in tube-in-tube structures. The structure of interest is a combination of a relatively weak framed tube and a strong core tube. The functions of floor systems and the interaction between floor slabs and the vertical structural components are briefly discussed and existing methods of analysis taking into account the floor out-of-plane stiffness are reviewed. A structural model accounting for floor out-of-plane stiffness by the finite story method (FSM) is proposed for tall building responses under lateral loads. The numerical example is a tube-in-tube structure with two-way joist (waffle) floor slabs and subjected,

separately, to the actions of lateral load and torsion. The computations are made using the program developed based on the present FSM and the FE software NISA, with attention focused on the effect of the floor out-of-plane stiffness on the overall displacements.

5.1.1 Functions and interaction with vertical components of floor systems

The primary functions of a floor system are to collect and distribute gravity loads to the vertical structural components, and to transmit lateral loads to the various lateral load resisting systems. Floors also function as horizontal braces for the vertical structural components, thereby stiffening the entire building system.

The two mechanisms by which the out-of-plane stiffness of the floor slabs enhances a building's lateral load resistance [46] are: (1) For floors rigidly connected to columns and shear walls, out-of-plane rotations are induced in the floors as these vertical components undergo flexural deformation. Consequently, the bending stiffness of floors resists this deformation of the vertical structural components; and (2) Relative transverse (vertical) displacements are induced in the floors due to uneven axial deformations in columns or cross-section warping in shear cores. As in the preceding case, the transverse shear and bending stiffness of the floors restrain the displacements in the vertical structural components, thus introducing interaction between the slabs and the vertical components which also increases the lateral load resistance of the whole system.

Evidently, the above two kinds of interaction between slabs and vertical components depend on the connection between these components. The conditions of the connections may be simply supported, elastically clamped or fixed. For simple connections, only the relative vertical displacements in columns and/or shear walls cause out-of-plane deformations in slabs. For slabs monolithically connected with the vertical structural members, both kinds of the aforementioned interaction will take place. In this study, floor slabs are considered monolithically connected with columns and shear walls.

5.1.2 Review of literature

The initial investigation on the bending stiffness of floor slabs in symmetric cross-wall systems was carried out by Qadeer and Stafford Smith [46]. In the analysis, the slabs are replaced by equivalent beams and the structures are analyzed as 2-D coupled walls. The effective width of the equivalent beams is shown in a set of design curves corresponding to different geometric layout parameters. These curves were obtained by means of the finite difference method and verified by experiments. Similar theoretical and experimental studies [47-49] extended to various shear wall configurations including walls of box shape. Since the above investigation concerned symmetric cross-wall systems, the effective width obtained may not be suitable for 3-D problems involving buildings which do not possess symmetric layouts.

Stafford Smith and Taranath [37] included the warping stiffness contributed by floor slabs in the analysis of core tubes by the finite element method. The floor slabs were modeled by 4-noded plate elements. The floor slab warping stiffness is the bimoment generating a unit warping deformation of the core tube at the floor level. The warping stiffness coefficient thus obtained is incorporated into the stiffness matrix of the core tube, which is represented by the corresponding open section thin-walled beam. Wong and Coull [50] reported similar studies on the warping stiffness contributed by floor slabs. Different combinations of monolithic, free and simple support conditions of the floor slabs were studied.

For the 3-D analysis of wall-frame structures, a two-step procedure was proposed by Taranath [7] to take into account the out-of-plane stiffness of slabs. In this method, the out-of-plane stiffness of slabs and joists at selected joints along the girders is first computed by full finite element analysis. In the overall structural analysis, the slabs and joists are represented by the obtained stiffness coefficients, which are incorporated with associated coefficients of the girders. Thus, only vertical structural components and lateral

load resisting girders of floor systems are modeled for the overall structural behavior. This analysis procedure can be applied to various structures on the condition that the out-of-plane stiffness at each selected joint is determined individually.

It has been concluded in the above studies that effective coupling of core walls can be achieved even with a relatively flexible slab system [50]. The out-of-plane stiffness of floor slabs could considerably reduce the overall torsional rotations and warping stresses in walls [37]. Simply ignoring the restraint effects of floor slabs would be unnecessarily conservative in designs. It has also been indicated that the coupling effect between the inner core and the outer framed tube in tube-in-tube structures should be considered [1]. However, the tremendously increased number of elements and associated degrees-of-freedom in a full finite element (FE) modeling to include floor slab out-of-plane stiffness makes the standard FEM unsuitable for such an analysis in the early design stages. Apparently, a general and reliable analysis procedure for estimating the effect of floor out-of-plane stiffness in three-dimensional problems would fulfill the practical needs in preliminary designs.

5.2 Preliminary examination of coupling effect of floor slab using single-story segment of tube-in-tube structure

In the analytical model of tube-in-tube structures in which floor slabs are idealized as in-plane rigid diaphragms, both the framed tube and the core tube undergo the same in-plane rigid body displacements, while deforming individually in the out-of-plane direction. When the out-of-plane stiffness of slabs is included in the structural model, the slabs interact with open section core walls along the interior edges and with frame panels along the exterior edges. The floors couple the nodal vertical displacements and the rotations about the two horizontal axes (w, θ_x and θ_y) between core walls, and between the core tube and the framed tube.

The floor slabs surrounding the core walls increase the bending and warping stiffness of the core tubes. This constraining effect of floor slabs has been studied by several researchers as described in the preceding Section [37, 49, 50]. In these studies, attention was focused on the coupling effect of floor slabs between the core walls, while the coupling between the inner core tube and the outer framed tube has not been examined.

The interaction between the slabs and frames alone usually does not cause any apparent difference in lateral load resistance, since the deep spandrel beams in framed tube structures are strong in connecting columns. However, the out-of-plane stiffness of the slabs couples the out-of-plane deformations of the outer framed tube with those of the inner core tube. This coupling effect increases the overall structural integrity by making the two subsystems behave out-of-plane partly as a composite section.

The coupling effect of slabs between core walls as well as between the core and the framed tube are illustrated by the example of a one-story segment of the tube-in-tube structure shown in Figure 5.1. The material and structural geometry properties are given in Section 5.4.1. To show the coupling effect of floor slabs, let the floor undergo a unit horizontal displacement in the Y direction ($v = -1.0$) and a unit rotation about the vertical axis Z ($\theta_z = -1.0$), separately, and examine the nodal rotations θ_x about the horizontal axis X in the one-story segment. The bottom of the one-story segment is fixed. The analysis is performed by the finite element method, for which the element mesh of a quarter of this segment is shown in Figure 5.6.

Figures 5.2 and 5.3 display the nodal rotations θ_x in a quarter of the structure due to the aforementioned floor rigid body displacements. In Figures 5.2a and 5.3a, nodes 1-6 belong to the frame panel perpendicular to the floor displacement (flange frame); node 7 is at a corner of the framed tube; and nodes 8-11 are in the frame panel parallel to the floor displacement (web frame). Figures 5.2b and 5.3b show the corresponding nodal rotations

θ_x in a quarter of the core walls. Nodes 1-4 are in the flange of the middle wall, and the nodes 5-8 are in the flange of the channel wall on the right side. Inspection of the data indicates that, with the slab out-of-plane stiffness included, the nodal rotations θ_x in flanges, due to either floor horizontal displacement $v = -1.0$ or rotation $\theta_z = -1.0$, of both the framed tube and the core tube are considerably reduced, whereas rotations θ_x in the web frame panels show only small changes. The reduction of θ_x in the framed tube are attributed to the coupling effect of the floor slab between the core and the frame panels. Figure 5.2b shows that, under the lateral loading, including floor out-of-plane stiffness causes only small changes in the relative nodal rotations θ_x at nodes 4 and 5. This is because the opening is in the flange walls of the core. For a core tube with openings in the web walls, larger changes in the relative nodal rotations θ_x at the wall ends will occur by including floor out-of-plane stiffness. Figure 5.3b illustrates that the floor slab acting as a brace of core walls effectively restrains the relative nodal rotations θ_x at the ends of walls. With floor coupling between the walls, the relative rotation θ_x between nodes 4 and 5 is reduced from 11.9 rad to 2.35 rad for unit floor rigid body rotation about the vertical axis. However it should be noted that, in a tube-in-tube structure, the coupling between the core walls is also influenced by the connecting conditions of slabs with the peripheral frame panels and the spans of the slabs between the core walls and the frame panels.

5.3 Structural modeling including floor system

The present finite story method (FSM) is now extended to include the out-of-plane stiffness of floors in the analysis. The floor slabs are considered as one-way or two-way stiffened plates for which the element stiffness matrix of the equivalent plate can be obtained by standard finite element analysis, thus allowing the floor substructures to be discretized by the equivalent plate elements. By defining master nodes where the floor joins with vertical structural components, a condensed floor substructural stiffness matrix

corresponding to these master nodes is formed. In the overall analysis, the effect of floor out-of-plane stiffness in constraining the out-of-plane displacements of the interior core tube, and in coupling the core tube out-of-plane deformations with those of the exterior framed tube, is incorporated by nodal displacement transformation in the FSM. The procedure is explained below with reference to a tube-in-tube structure with a two-way joist floor system. It is also applicable to core supported structures or flat plate structures with other kinds of floor systems.

5.3.1 Condensed floor substructure stiffness matrix

The conventional spacing of one-way joists and waffle slabs of either 0.6 m or 0.9 m is being replaced in practice by skip joists with spacing of 1.5 m or 2.0 m [4, 7]. If each segment of the joist between joints is modeled as a beam and each area of the slab bounded by the joists as one plate element, the total number of elements of a tube-in-tube will increase tremendously. Since the interaction between the floor slabs and the shear walls, and between the floor slabs and the framed panels, occurs mainly in the surrounding regions, it is unnecessary to model the floor by a fine mesh in the large space between the exterior framed tube and the interior core tube. Thus, the floor is discretized in accordance with column lines. Each segment of the slab divided by column lines may enclose several perpendicularly connected joists and is considered to be a stiffened plate element.

As shown in Figure 5.4, the stiffened plate element is analyzed fully by FEM in which each segment of the joist between joints is a beam element, and the plate is discretized by joist lines. Considering the corner nodes and any other node connecting with vertical structural components as master nodes and the remainder as slave nodes, the element stiffness matrix corresponding to the DOFs at the master nodes is obtained by means of the condensation technique. With the order of the foregoing matrix determined by the number of master nodes chosen, the condensed kth floor substructure stiffness

matrix $[S^s]_k$ is established by a further condensation based on stiffened plate elements in which the master nodes are only those in conjunction with the core walls and the columns in the frame panels. Thus, supposing there are m_c columns in the framed tube and n_c core tube nodes at the kth floor level, the order of the condensed floor stiffness matrix $[S^s]_k$ is of the order $3(m_c+n_c)$ by $3(m_c+n_c)$.

5.3.2 Nodal displacement fields in the framed tube

Since the nodal vertical displacements and the rotations about the two horizontal axes (w, θ_x and θ_y) in the framed tube are coupled by the floor slabs with those in the core tube, the nodal displacement fields at floor levels are determined by analyzing two-story segments of the tube-in-tube structure. The aim of this substructural analysis is to obtain the approximate nodal displacement patterns in the framed tube, including the floor out-of-plane coupling effects. The core tube in this segmental analysis acts only as a support of floor slab interior edges.

With the above in mind, the open section walls of the core tube in the segmental analysis are modeled approximately as piers which are represented by a 12x12 stiffness matrix $[k_w]$, with the warping deformations at the two ends hidden by the static condensation in the element analysis. Figure 5.5 shows how the pier, which is located at the shear center of the core wall, and the interior edges of the floor are related. The node of the pier is defined as a master node and the nodes on the floor slab interior edges connecting with the core walls are defined as relevant slave nodes. The vertical displacements and rotations about the horizontal axes of the slave nodes defined by

$$\begin{aligned} w_s &= w_m + (y_s - y_m)\ \theta_{xm} - (x_s - x_m)\ \theta_{ym} \\ \theta_{xs} &= \theta_{xm} \\ \theta_{ys} &= \theta_{ym} \end{aligned} \qquad (5.1)$$

in which w_s, θ_{xs} and θ_{ys} are displacements of slave nodes; w_m, θ_{xm} and θ_{ym} represent displacement of the master node and; (x_s, y_s) and (x_m, y_m) denote coordinates of the slave and master nodes in the global coordinate system, respectively. Compared with Reference [36], the above nodal transformation does not include the warping deformation mode at the slave nodes. Because the analysis of the two-story segment is to determine the nodal displacement patterns in the peripheral framed tube, rather than the core tube structural behavior or the coupling effect of floor slabs between core walls, the warping deformation mode at the slab interior edge is not considered. By equation (5.1), the DOFs at the n_c nodes of the core walls are correspondingly transformed into DOFs at the m_w nodes of the piers. The transformed floor substructural stiffness matrix $[S^{st}]_k$ is of the order $3(m_c+m_w)$ by $3(m_c+m_w)$, where m_c = the number of columns and m_w = the number of piers in the kth story.

The structural stiffness matrix for the two story segment is established by assembling the stiffness matrices of the framed tube, core tube and the transformed floor slab as follows:

$$[S] = \sum_{k=1}^{2} \left(\left(\sum_{1}^{m_c} [k_c] + \sum_{1}^{m_b} [k_b] + \sum_{1}^{m_w} [k_w] \right)_k + [S^{st}]_k \right) \qquad (5.2)$$

where $[k_c]$, $[k_b]$ and $[k_w]$ represent stiffness matrices of the columns and beams in the framed tube, and of piers representing the core tube in the kth story, respectively. The order of $[S]$ is $6(m_w+m_c+1)$ by $6(m_w+m_c+1)$.

5.3.3 Analysis procedure

The coupling effects between the framed tube and the core tube, and between the core walls, are approached separately. First, the out-of-plane deformation coupling between the framed tube and the core tube is taken into account in determining the nodal

displacement fields of the framed tube. Therefore, in the overall analysis the kth story framed tube substructure stiffness matrix accounting for floor out-of-plane stiffness is formed by

$$[S^{f*}]_k = \sum_1^{m_c} [k_c^*]_k + \sum_1^{m_b} [k_b^*]_k \tag{5.3}$$

in which m_c and m_b are the numbers of columns and beams in the kth story, respectively; N denotes the total number of stories in the building and; $[k_c^*]$ and $[k_b^*]$ are column and beam element stiffness matrices corresponding to the generalized displacement coordinates given by equation (2.16).

Secondly, the coupling effect of floor slabs between the core walls is taken into account by adding the stiffness coefficients corresponding to the $3m_w$ DOFs of core walls in the transformed floor stiffness matrix $[S^{st}]_k$ to the associate coefficients in the stiffness matrix $[S^c]_k$ of the core tube. Thus, the modified stiffness matrix of the core tube in the kth story $[S^{c*}]_k$ is obtained. The core tube substructure stiffness matrix in the kth story is itself formed by

$$[S^c]_k = \sum_1^{m_w} [k_w]_k \tag{5.4}$$

The overall generalized displacement coordinate vector for the tube-in-tube remains the same as previously defined by equation (4.12), namely

$$\{D\} = [D_1^f \quad D_2^f \quad \dots \quad D_N^f \mid \quad d_1^c \quad d_2^c \quad \dots \quad d_N^c \quad]^T$$

where

$$[d_k^c\} = [w_1^c \ \theta_{x1}^c \ \theta_{y1}^c \ \dots \ w_{m_w}^c \ \theta_{xm_w}^c \ \theta_{ym_w}^c]^T$$

and for which the corresponding overall structural stiffness matrix is given by

$$[K^*] = \sum_{1}^{N} \{ \sum_{1}^{m_c} [k_c^*]_k + \sum_{1}^{m_b} [k_b^*]_k + [S^{c*}]_k \} \tag{5.5}$$

5.4 Numerical examples

The symmetric tube-in-tube structure of Figure 5.1 is analyzed by the present FSM and the general FEM, separately under bending and torsion actions. The results illustrate the validity and efficiency of the present modeling, and also demonstrate the contribution of floor slabs to lateral load resistance.

5.4.1 Symmetric 30-story tube-in-tube with waffle slabs under lateral load

The 30-story symmetric tube-in-tube with a waffle floor system shown in Figure 5.1 is analyzed under uniformly distributed lateral load 192 kN in the Y direction at floor levels. The floor slabs are connected monolithically with the peripheral framed and the interior core tubes. The story height is 3.66 m. Elastic modulus E = 2.39×10^4 MPa, and shear modulus G = 0.995×10^4 MPa. The slab thickness = 114 mm; the cross-section of joists in the floor system is 152x508 mm; the wall thickness = 305 mm and; and the spacing of skip joists in the two perpendicular directions = 1.83 m. The properties of members in the framed tube and joists in the floor frames are listed in Table 5.1.

In the FSM, the floor slabs are discretized by 96 equivalent plate elements, with each consisting of four 1.83x1.83 m four-node plate elements and twelve joist beam elements. In the FE model, only a quarter of the building is analyzed by taking advantage of symmetry and appropriate boundary conditions associated with the applied load conditions are imposed along the center lines of the cross-section. The core walls in the quarter structure are discretized by 42 four-node thin-shell elements per story, and the slab

is divided into 112 four-node thin-plate elements of 1.83x1.83 m in size. Figure 5.6 shows the element mesh for one-quarter of a one-story segment.

The saving in computational effort of the FSM is evident because the total number of unknowns in the overall analysis does not increase by including the floor slabs. In this example, the total number of unknowns is 264 in the two-story segment, and 420 in the overall analysis. The required CPU on a Sun Workstation 4/40 increases only by 135 sec, from 552 sec for the 30-story tube-in-tube with floors modeled as in-plane rigid diaphragms to 687 sec for the structure accounting for floor slabs. In contrast, the total number of DOFs increases about three times by the full FEM model of a quarter of the structure to include floor slabs - 9162 for the calculation in which floors are modeled as rigid diaphragms to 26712 for the calculation in which floors are modeled by beam and plate elements. The CPU for the FE calculation of a quarter of the symmetric tube-in-tube structure on a PC 486/50 computer increased from 334 sec not including floor slabs to 8427 sec including floor slabs.

Figure 5.7 shows the displacements at floor levels. In the case of the slab out-of-plane stiffness ignored, the top drift is 55.8 mm by FEM, and 55.2 mm by FSM. However, when the out-of-plane stiffness is included, it is 43.8 mm by both FEM and FSM, in which the nodal displacement patterns are calculated at every floor level, and 45.4 mm by FSM* in which the nodal displacement patterns are determined at every other floor level. The calculated decrease in top displacement by including floor slabs is 21.5% according to FEM, and 20.7% according to FSM.

5.4.2 Symmetric 30-story tube-in-tube with waffle slabs under torsion

The torsional behavior of the above structure is analyzed in this example. Torque equal to 40.7 kN · m is applied at each floor level. Figure 5.8 depicts the obtained floor rotations in comparison with the solution by FEM. The top rotation in the analysis without

considering floor slab out-of-plane stiffness is 0.137×10^{-3} rad by the FSM, and 0.140×10^{-3} by the FEM. The floor slabs contribute to warping stiffness and, hence reduce the floor rotations. The top rotation when accounting for floor slabs is 0.113×10^{-3} rad by FSM, for reduction of 17.5%; and 0.119×10^{-3} rad using the FEM, representing a reduction of 15% in displacement due to stiffness of the floor slabs.

It is interesting to note the difference between the overall deformation modes displayed in Figures 5.7 and 5.8. Under lateral loading the tube-in-tube, which comprises a relatively weak periphery framed tube and a relatively strong core tube, deforms in a mode close to bending rather than shear, whereas under the action of torsion the structure deforms in a frame racking mode rather than cantilever bending. This shows that the overall behavior of this structure is not dominated completely by the framed tube. Thus, the core tube is seen to contribute to resisting lateral loads while, on the other hand, due to its central location and small in-plane dimensions relative to the framed tube, the overall behavior under torsion depends largely on the framed tube only.

5.4.3 Discussion of floor coupling effects

As noted previously, the floor slabs in a tube-in-tube structure couple the out-of-plane deformations between the core walls, as well as between the core tube and the framed tube. In the structural modeling of the finite strip method, these two coupling effects are considered in assembling the core tube stiffness matrix and in determining nodal displacement fields in the framed tube.

To examine which one of the above floor slab coupling effects plays a more important role, three cases of treating floor slabs in the tube-in-tube structure under lateral loads and torsion action are analyzed, separately. These are: (1) the floor slab out-of-plane stiffness is ignored; (2) the floor slab out-of-plane stiffness is included and; (3) the floor

slab out-of-plane stiffness is included in assembling the core tube stiffness matrix only, i.e. the coupling effect of floor slabs between the core tube and the framed tube is ignored.

Figure 5.9 shows the solutions in terms of lateral displacements for the above three cases of coupling as obtained by FSM. The deflections at the top level are 55.2 mm, 43.8 mm and 49.7 mm, respectively. Thus, by considering both of the coupling effects of slabs, the deflection at the top is reduced by 20.0%, while it is reduced by 9.94% when considering only the coupling between the core walls. Evidently both types of coupling appear to be of equal importance in this structure under lateral loading.

Figure 5.10 presents the results for the same comparison for the structure subjected to torsion. Although the coupling of slabs between the core walls effectively increases the core tube warping and torsion stiffnesses, as analyzed in Section 5.4.2, the overall structural response nevertheless depends mainly on the framed tube. Therefore, the effect of the floor slabs observed in Figure 5.10 is due almost entirely to the torsional coupling of the core and the framed tube.

It is important to recognize that Figures 5.8 and 5.9 represent only one example structure. The effect of floor slab coupling is influenced by many factors such as: slab spans between the core walls and between the core tube and the framed tube; floor aspect ratio; wall cross-sectional dimensions and configuration and; stiffness ratios of slabs to walls and slabs to frames. Because these factors vary in different situations, so will the effect of the floor slabs. However, it can be seen from the above analysis that the coupling of floor slabs between the core tube and the framed tube may be equally important as that between the walls of the core tube. Thus the effects of both should be considered when modeling floor out-of-plane stiffness in tube-in-tube structures.

5.5 Summary

This Chapter has demonstrated that the finite story method can be applied effectively to account for floor slab out-of-plane stiffness in tube-in-tube structures. The efficiency and accuracy in predicting structural overall responses are illustrated by numerical examples in comparison with full finite element analysis. The floor slab coupling effects are explained by analyzing a one-story segment, and discussed by separating the coupling between the core walls to exhibit the coupling effect between the core tube and the framed tube in a 30-story tube-in-tube structure. This shows that coupling between the core tube and the framed tube may play a similar role as that between the core walls in increasing the overall structural lateral load resistance.

Table 5.1 Member properties of 30-story tube-in-tube with waffle floor slabs

Member	Area (m^2)	Shear Area (m^2)	Moment of Inertia (m^4)	Torsion Constant (m^4)
Interior column	0.223	0.186	$I_x=0.173\times10^{-2}$ $I_y=0.993\times10^{-2}$	0.529×10^{-2}
Corner column	0.581	0.484	$I_x=0.281\times10^{-1}$ $I_y=0.281\times10^{-1}$	0.505×10^{-1}
Spandrel beam	0.257	0.214	$I_y=0.153\times10^{-1}$ $I_z=0.199\times10^{-2}$	0.635×10^{-2}
Joist	0.774×10^{-1}	0.645×10^{-1}	$I_y=0.167\times10^{-2}$ $I_z=0.150\times10^{-3}$	0.110×10^{-1}

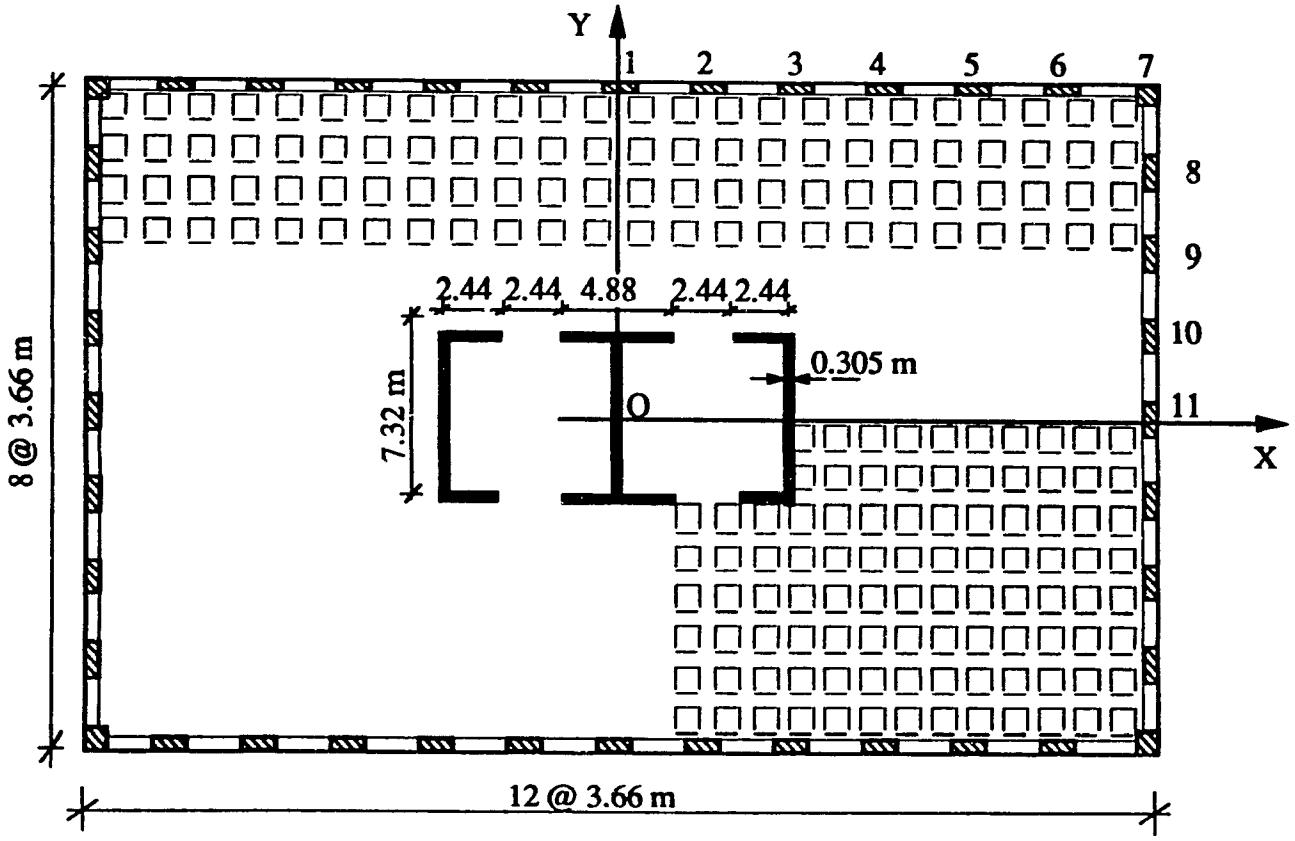

Figure 5.1 Plan of 30-story tube-in-tube with waffle floor slabs

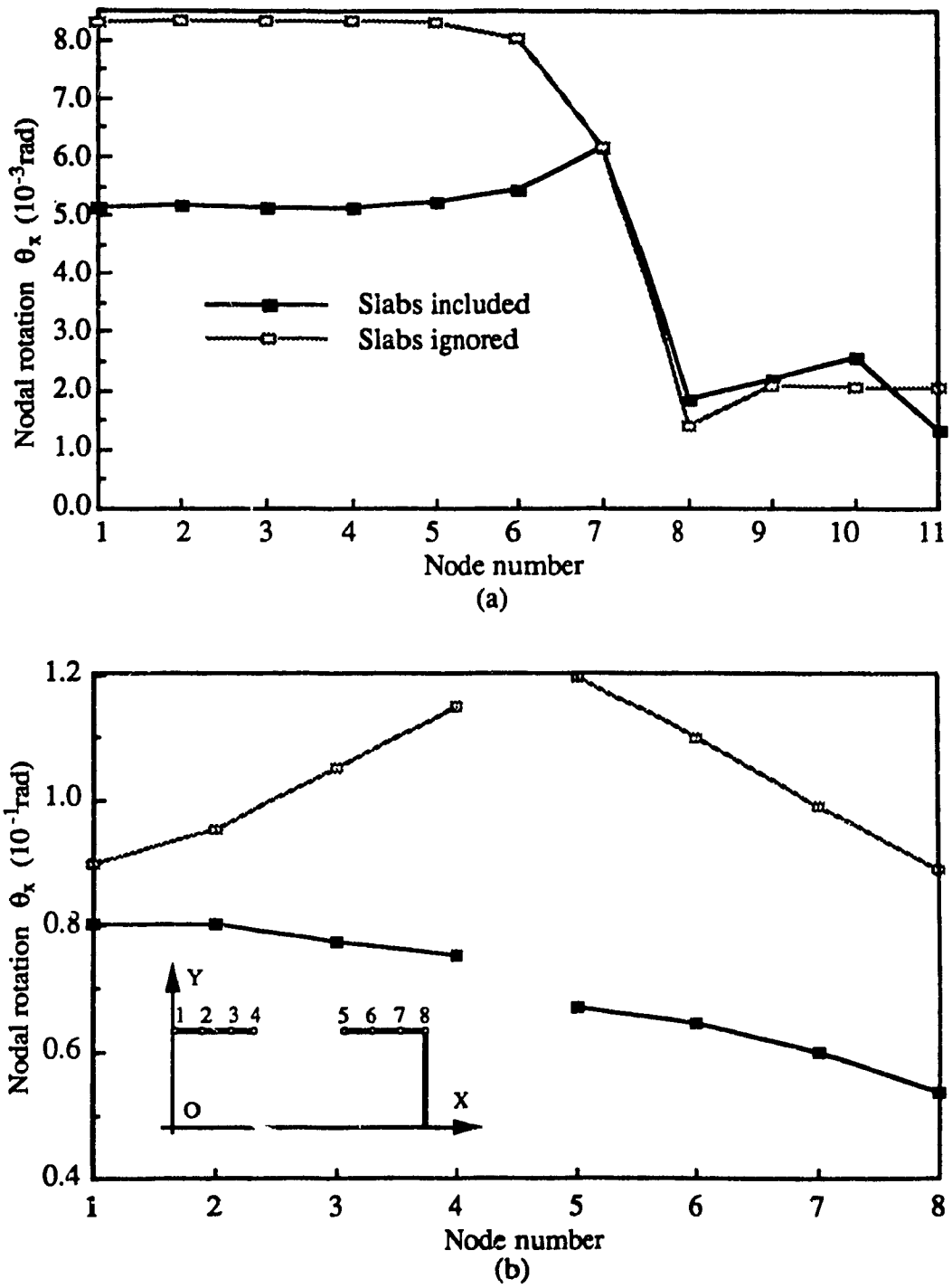

Figure 5.2 Nodal rotations in single-story segment due to the floor displacement v= -1.0: (a) quarter of the outer framed tube, (b) flanges of the inner core tube

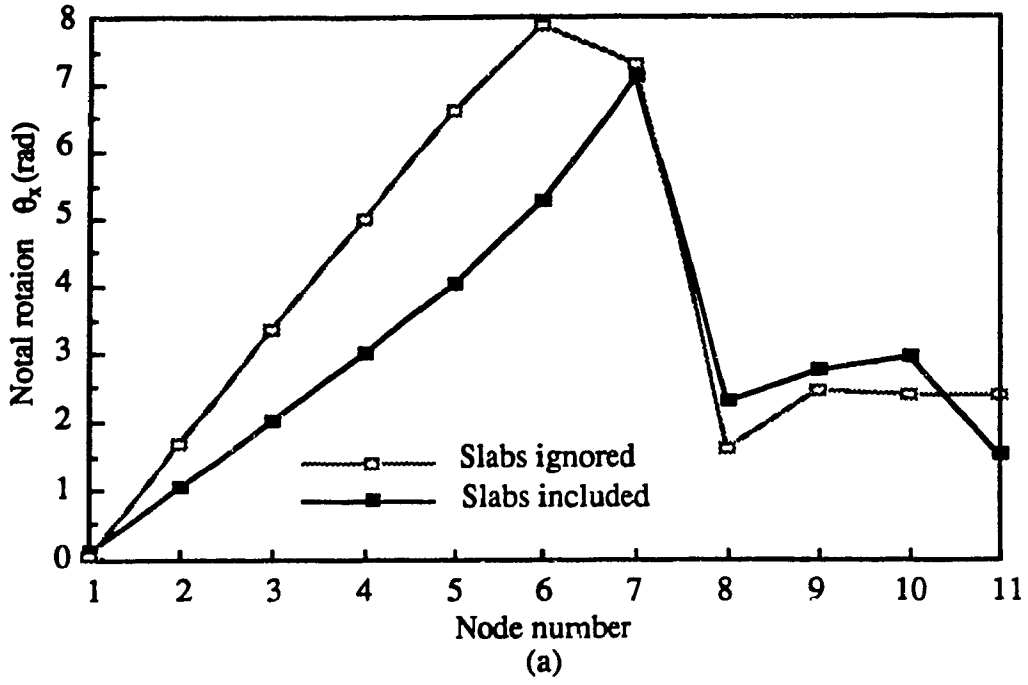

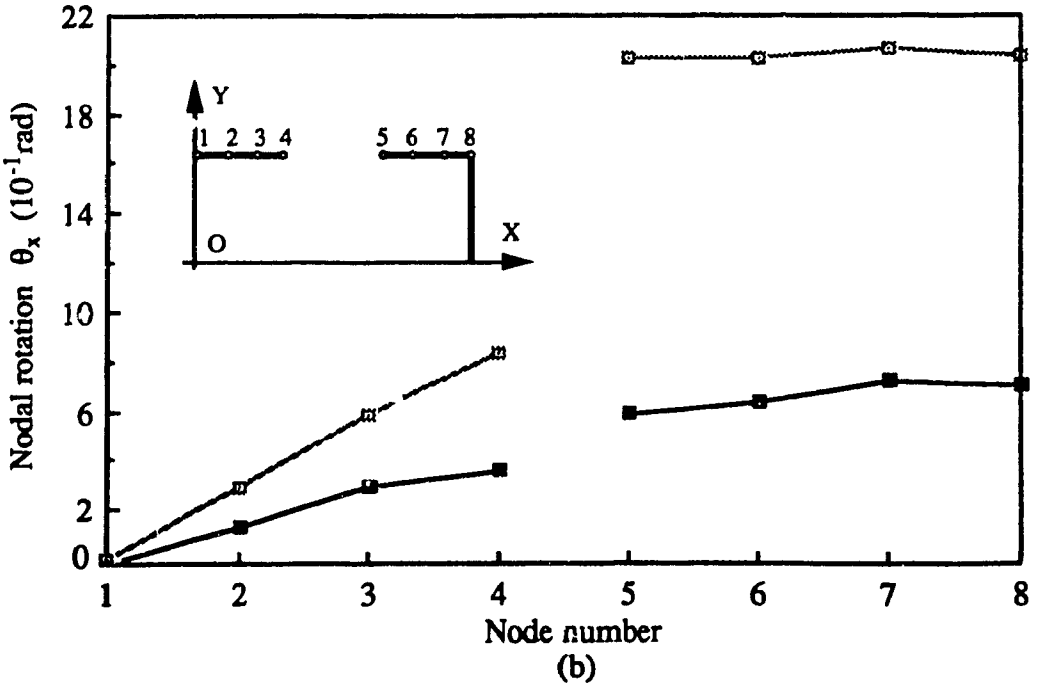

Figure 5.3 Nodal rotations in single-story segment due to the floor rotation θ_z= -1.0 : (a) quarter of the outer framed tube, (b) flanges of the inner core tube

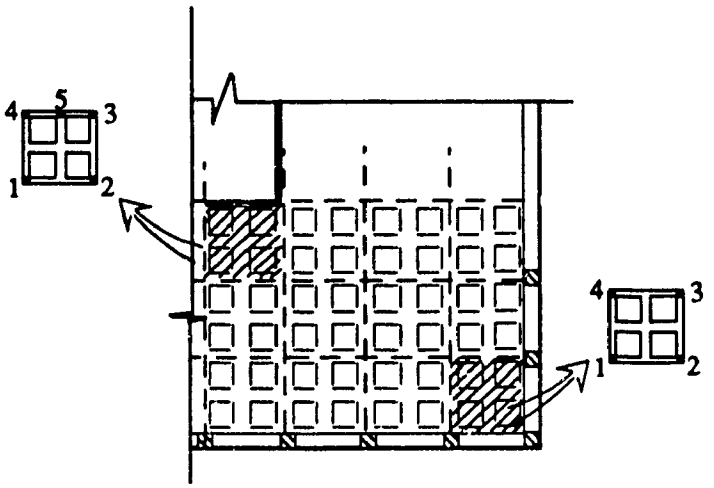

Figure 5.4 Equivalent stiffened plate for floor in finite story method

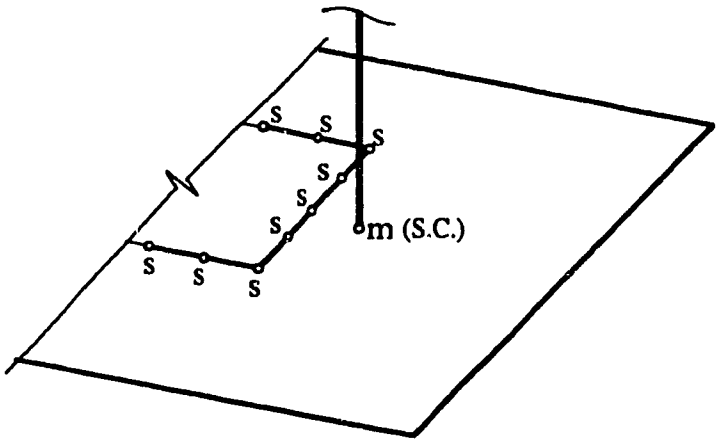

s = slave node of thin-walled pier
m = master node of thin-walled pier

Figuer 5.5 Connection between thin-walled pier and floor slab interior edge

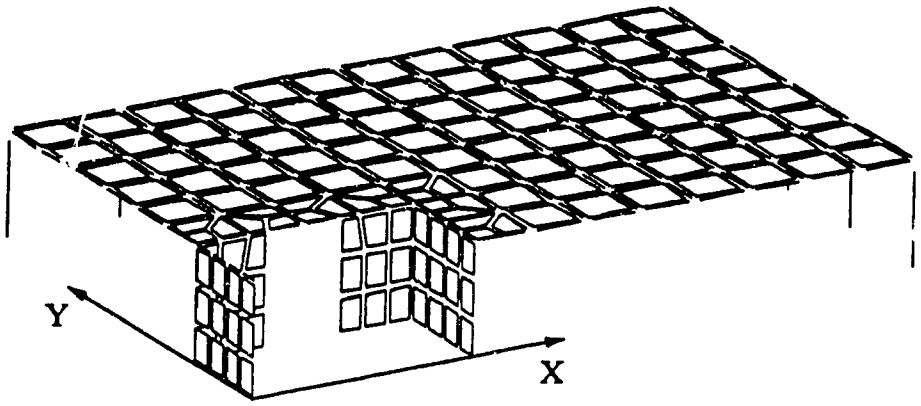

Figure 5.6 Element mesh of a quarter of 30-story tube-in-tube structure

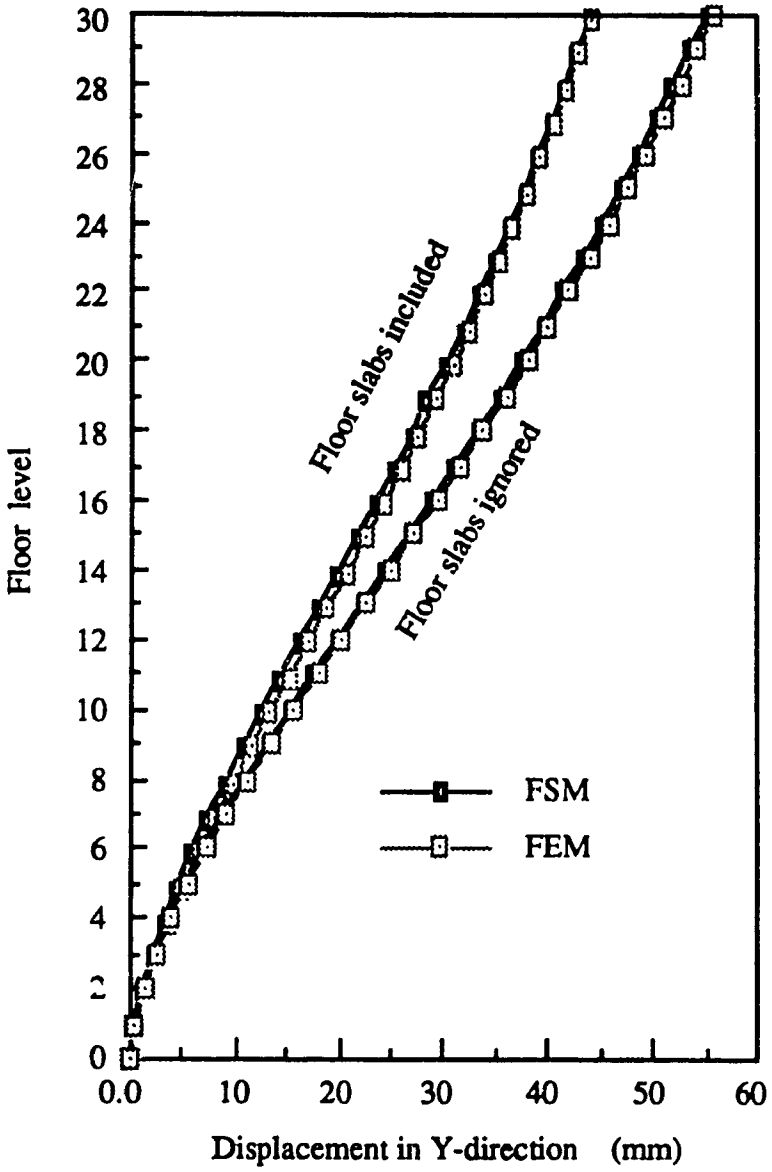

Figure 5.7 Deflections for 30-story tube-in-tube under lateral load

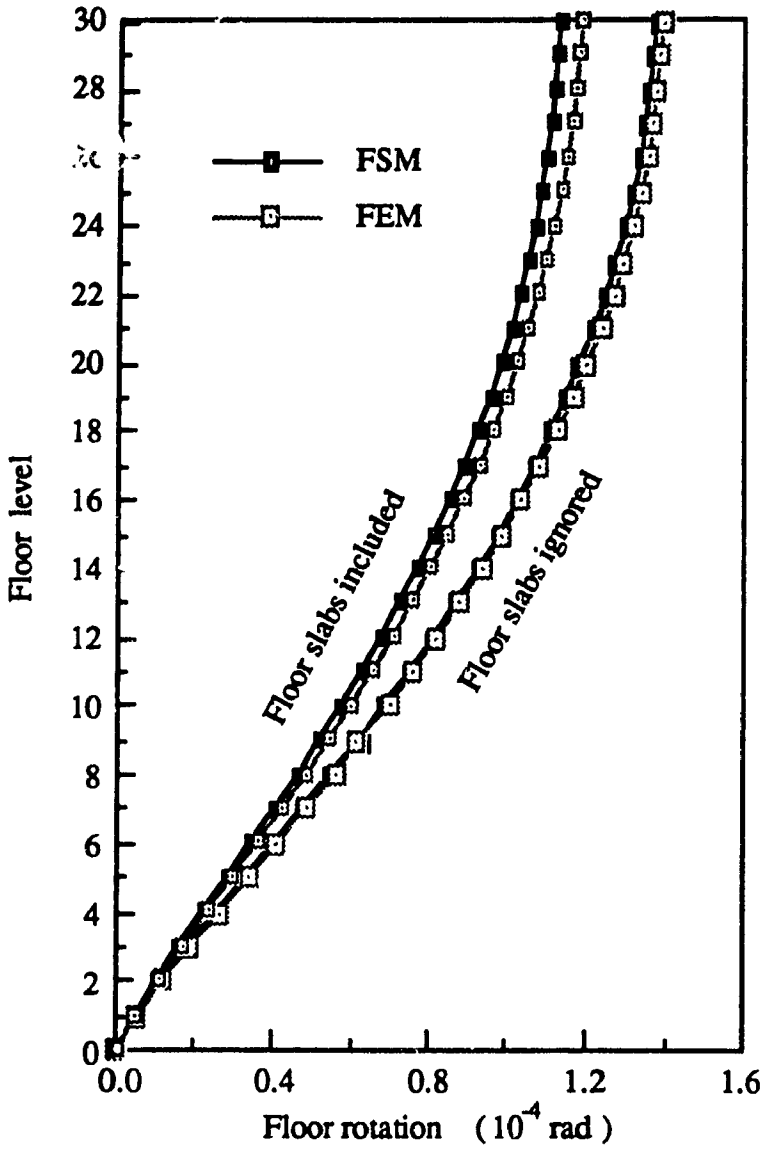

Figure 5.8 Floor rotations for 30-story tube-in-tube under torsion

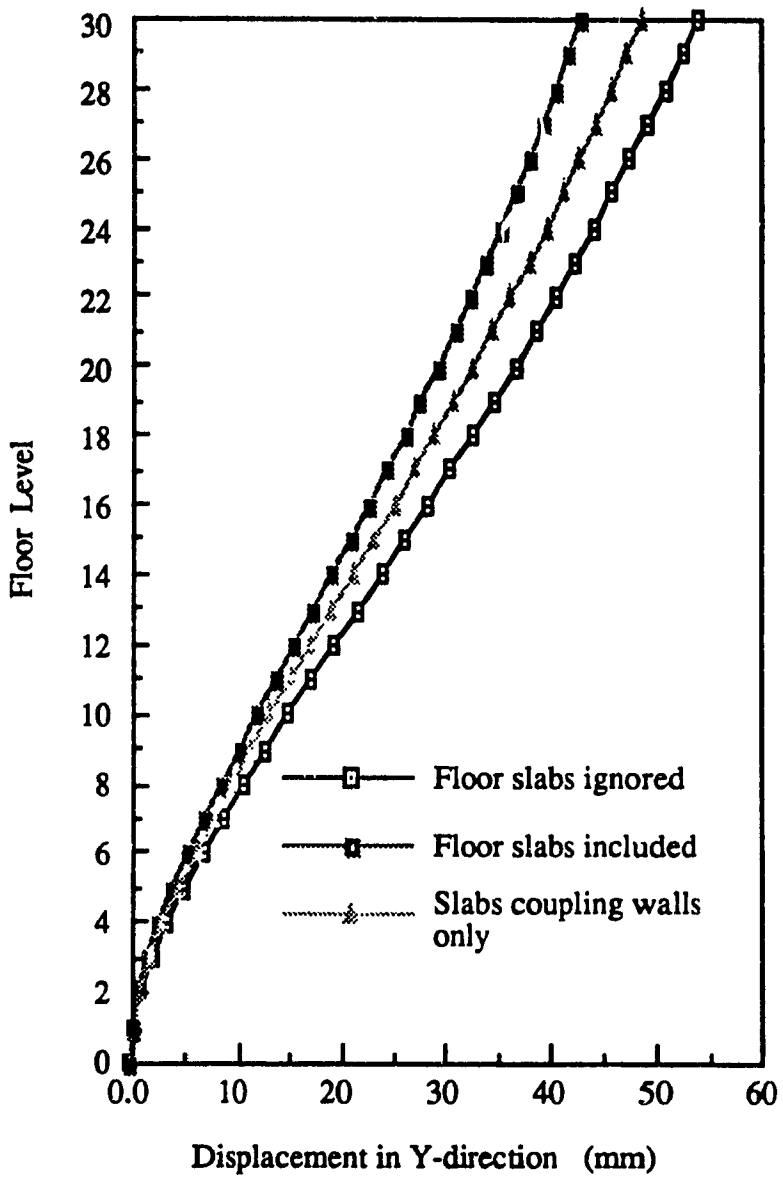

Figure 5.9 Floor coupling effects under lateral load

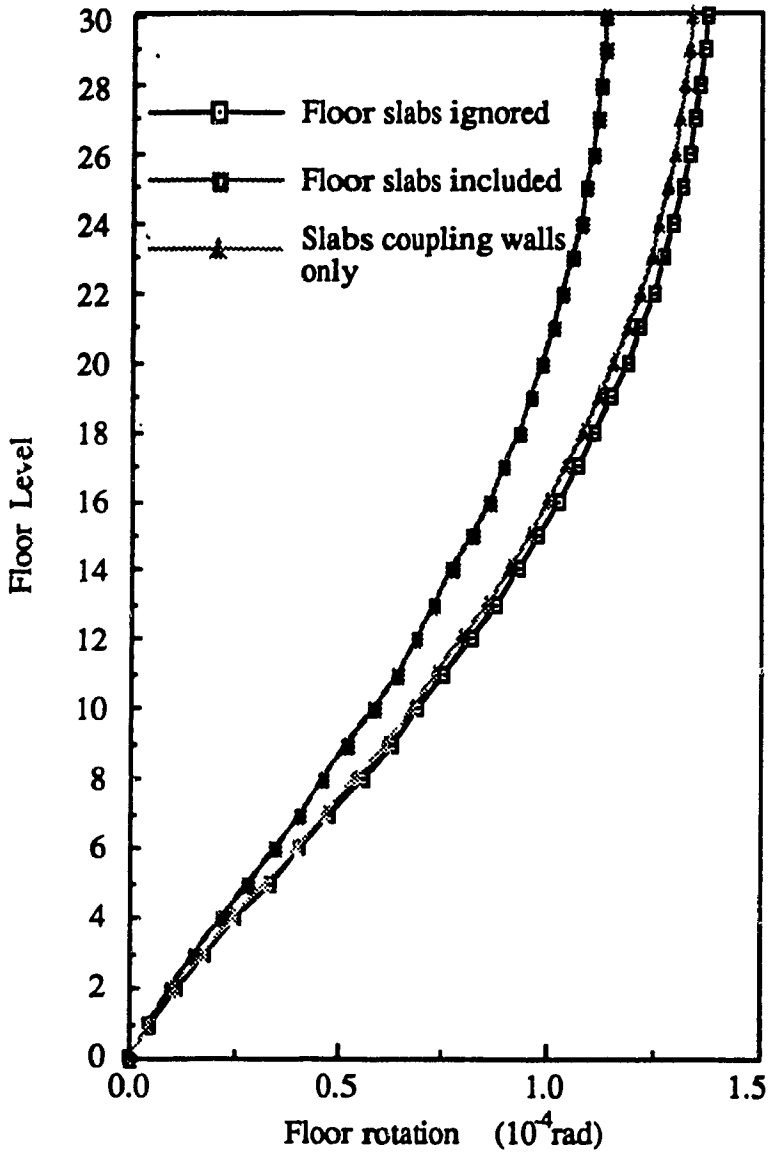

Figure 5.10 Floor coupling effects under torsion

Chapter 6
Conclusions and further work

6.1 Conclusions

Arising out of the work presented in this thesis, the following conclusions are noted:

1. The present finite story method (FSM) based on nodal displacement fields is reliable in predicting gross structural deformations of both symmetric and unsymmetric framed tube and tube-in-tube structures of tall buildings.

2. The method provides good solutions for natural frequencies and modes of vibration of either symmetric or unsymmetric framed tube and tube-in-tube structures.

3. In general, the number of times nodal displacement fields need to be computed along the height of the building is not critical for floor slab displacements and natural frequencies. In the case of buildings under pure torsion, it has no influence on nodal displacements and member forces.

4. Calculations by the proposed FSM method are inexpensive compared with full FEM, since the problem size is greatly reduced. Also greatly reduced are the computing effort and the associated data preparation task. Furthermore, since all matrices are of much smaller order, implementation on standard personal computers is feasible.

5. The prediction of accurate member forces is not included in this work. This limitation concerning consistently accurate member forces is due mainly to the omitting

the shear lag in the bending deformation modes in analyzing the two-story substructures for nodal displacement fields. The present nodal displacement fields introduce negligible differences in floor displacements and natural frequencies, but may show notable differences in member forces.

6. The stiffness matrices for the core tubes modeled as story-wise thin-walled beam elements are formed for warp-restrained torsion. The torsion related stiffness coefficients obtained from the solution of the governing differential equation are accurate and the calculation for these coefficients is simple. The obtained stiffness matrices are applicable to a wide range of core tubes including: completely open or close sections, as well as cores with openings arranged in rows for access and; core walls with changing story-wise thickness. Core tubes with story-wise changes in the location of the shear center along the height are, however, not included in the present modeling.

7. The present finite story method can be used to estimate the coupling effect of floor slabs in tube-in-tube structures. Under lateral loads, the coupling effects of slabs between the core tube and the framed-tube may be as important as that between the walls comprising the core tube, whereas under torsion loading, it may become the primary contribution of the floor slabs in the response of the overall system.

8. Although the present analysis procedure concerns mainly tubular structures, it can be readily applied to the analysis of flat plate structures.

6.2 Further work

The present work could be further developed in the following respects:

1. The coupling effect of floor slabs is influenced by various factors as described in Chapter 5. Based on the preliminary study presented in Chapter 5, a complete investigation should examine a range of each of these factors. Thus, general conclusions

indicating the variations of coupling effect in tube-in-tube structures vs. these factors can be obtained.

2. To eliminate the limitation of the represent FSM in member force calculations in framed tube structures, the shear lag in the bending deformation mode should be included in determining nodal displacement fields of the framed tube. Superposing a shear lag function, which is parabolic in the flange frames and cubic in the web frames, to the assumed linearly distributed nodal vertical displacements in the bending modes could be a solution.

3. Although the assumed flexurally rigid arms of beam and column members in framed tubes are acceptable in preliminary calculations for overall structural deformations, a refined model of member joints needs to be considered for accurate member forces.

4. The finite story method can be applied to the analysis of bundled tube structures with setbacks along the building height. At the transfer floor level which connects stories with different floor plan layouts, it is necessary to determine nodal displacement distribution coefficients.

5. The computer program developed according to the present finite story method can be optimized in developing subroutines to handle symmetric and asymmetric boundary conditions along the building height, so that symmetric systems can be analyzed by halves or quarters of the whole structures.

References

[1] Monograph on planing and design of tall buildings, CB, ASCE, 1980

[2] Developments in tall buildings, Beedle, L.S., ed., Council on tall building and urban habitat, Hutchinson ross publishing company, 1983

[3] Second century of the skyscraper, Beedle, L. S., ed., Council on tall buildings and urban habitat, Van nostrand reinhold company, 1983

[4] Khan, F. R., Current trends in concrete high-rise buildings, Handbook of concrete engineering, Fintel, M., ed., Van an nostrand reinhold company, 1985

[5] Advances in tall buildings, Council on tall buildings and urban habitat, 1986

[6] Tall building structures - design and analysis, Stafford Smith, B., and Coull, A., John wiley & sons, Inc., 1991

[7] Structural analysis & design of tall buildings, Taranath, B. S., McGraw-Hill, Inc., 1988

[8] High-rise building structures, Schueller, W., Robert E. Krieger Publishing Company, 1986

[9] Khan, F. R. and Amin, R., Analysis and design of framed tube structures for tall concrete buildings, The Structural Engineer, **51**(3), 85-92, 1973

[10] Coull A. and Subedi, N. K., Framed tube structures for high-rise buildings, J. Struct. Div. ASCE, **97**, 2097-2105, 1971

[11] Coull, A. and Subedi, N. K., Hull-core structures subjected to bending and torsion, Proc. of the 9th congress, IABSE, Amstredam, Holland, 613-621, 1972

[12] Ast, P. F. and Schwaighofer, J., Economical analysis of large framed-tube structures, Build. Sci., **9**, 73-77, 1974

[13] Rutenberg, A., Analysis of tube structures using plane frame programs, Proc. of the Regional Conf. on Tall Buildings, Bangkok, 397-413, 1974

[14] Mazzeo, A. L. and Fries, A. D., Perimetral tube for 37-story steel building, J. Struct. Div., ASCE, **98**, 1255-1272, 1972

[15] Coull, A. and Bose, B., Simplified analysis of frame-tube structures, J. Struc. Div., ASCE, **101**, 2223-2240, 1975

[16] Coull, A. and Bose, B., Torsion of frame-tube structures, J. Struct. Div., ASCE, **102**, 2366-2370, 1976

[17] Moselhi, O., Fazio, P., and Zielinski, Z., Simplified analysis of wall-frame structures, Can. J. Civ. Eng., **5**, 262-273, 1978

[18] Ha, H., and Fazio, P., and Moselhi, M., Orthotropic membrane for tall building analysis, J. Struct. Div.. ASCE, **104**, 1495-1505, 1978

[19] Khan, A. H. and Stafford Smith, B., A simple method of analysis for deflection and stresses in wall-frame structures, Build. and Environ., **11**, 69-78, 1976

[20] Han, P. S. and Lukkunaprasit, P., Finite strip analysis of framed tube structures, Proc. 3rd international conference on tall buildings, HongKong GuangZhou, 236-242, 1984

[21] Ha, K. H. and Desbois, Finite elements for tall building analysis, Comput. Struct., **33**, 249-255, 1989

[22] Kwan, A. K. H., Simplified method for approximate analysis of framed tube structures, J. Struct. Div., ASCE, **120**, 1221-1239, 1994

[23] Takabatak, H., Mukai, H. and Hirano, T., Doubly symmetric tube structures, I: static analysis, J. Struct. Div., ASCE, **119**, 1981-2001, 1993

[24] Rosman, R., Torsion of perforated concrete shafts, J. Struct. Div., ASCE., **95**, 991-1010, 1969

[25] Michael, D., Torsional coupling of core walls in tall buildings, The Structural Engineer, **47**, 67-71, 1969

[26] Gluck, J., Lateral-load analysis of asymmetric multistory structures, J. Struct. Div., ASCE, **96**, 317-333, 1970

[27] Heidebrecht, A. C. and Stafford Smith, B., Approximate analysis of open-section shear walls subject to torsional loading, ASCE, **99**, 2355-2373, 1973

[28] Khan, M. A. H. and Stafford Smith, B., Restraining action of bracing in thin-walled open section beams, Proc. Instn Civ. Engrs., Part 2, **59**, 67-78, 1975

[29] Rutenberg, A. and Tso, W. K., Torsional analysis of perforated core structure, J. Struct. Div. ASCE, **101**, 539-550, 1975

[30] Rutenberg, A., Shtarkman M. and Eisenberger M., Torsional analysis methods for perforated cores, J. Struct. Div. ASCE, 1986, **112**, 1207-1227, 1986

[31] Tso, W. K. and Biswas J. K., General analysis of nonplanar coupled shear walls, J. Struct. Div. ASCE, **99**, 365-380, 1973

[32] Tso, W. K. and Biswas, J. K., Analysis of core wall structure subject to applied torque, Build. Sci., **8**, 251-257, 1973

[33] Khan, A. H., Tottenham, H. and Stafford Smith, B., The general theory of torsion of thin-walled structures with undeformed cross-sections, Research Report, Department of Civil Engineering and Applied Mechanics, McGill University, Montreal, 1979

[34] Hoenderkamp, J. C. D. and Stafford Smith, B., Simplified torsion analysis of high-rise structures, Build. Environ., **23**, 153-158, 1988

[35] Robert, T. M. and Achour, B., Torsion and bending of braced thin-walls, J. Struct. Div., ASCE, **116**, 1-12, 1990

[36] Heidebrecht, A. C. and Swift, R. D., Analysis of asymmetrical coupled shear walls, ACE, **97**, 1407-1422, 1971

[37] Stafford Smith, B. and Taranath, B. S., The analysis of tall core-supported structures subject to torsion, Proc. Instn Civ. Engrs., Part 2, **53**, 173-187, 1972

[38] Liauw, T. C. and Leung, K. W., Torsion analysis of core wall structures by transfer matrix method, The Struct. Engin., **53**, 187-194, 1975

[39] Liauw, T. C., Torsion of multi-story spacial core walls, Proc. Instn Civ. Engrs, Part 2, **65**, 601-609, 1978

[40] Chen, C. J., Liu, W. and Chern, S. M., Torsional analysis of shear core structures with openings, Comput. Struct. **41**, 99-104, 1991

[41] Macleod, I. A., New rectangular finite element for shear wall analysis, J. Struct. Div., ASCE, **95**, 399-409, 1969

[42] Goodno, B. J. and Gere, J. M., Analysis of shear cores using superelements, J. Struct. Div., ASCE, **102**, 267-283, 1976

[43] Gendy, A. S., Saleeb, A. F. and Chang, T. Y. P., Generalized thin-walled beam models for Flexural-torsional analysis, Comput. Struct, **42**, 531-550, 1992

[44] Kwan, A. K. H., Mixed finite element method for analysis of coupled shear/core walls, J. Struct. Div., ASCE, **119**, 1388-1401, 1993

[45] Cast-in-place concrete in tall building design and construction, Council on tall buildings and urban habitat, 123-131, 1991

[46] Qadeer, A. and Stafford smith, B., The bending stiffness of slabs connecting shear walls, ACI J., **66**, 464-473, 1969

[47] Coull, A. and El Hag, A. A., Effective coupling of shear walls by floor slabs, ACI J., **72**, 429-431, 1975

[48] Tso, W. K. and Mahmoud, A. A., Effective width of coupling slabs in shear wall buildings, J. Struct. Div., ASCE, **107**, 573-586, 1977

[49] Coull, A. and Wong, Y. C., Bending stiffness of floor slabs, Proc. Instn. Civ. Engrs, **71**, Part.2, 17-35, 1984

[50] Wong, Y. C. and Coull, A., Torsional stiffness of structural cores by surrounding floor slabs, Proc. 3rd International Conference on Tall Buildings, 229-235, HongKong and GuongZhou. 1984

[51] Ward, H. S., Dynamic characteristics of a multi-story concrete building, J. Struct. Div., ASCE, **95**, 553-3571, 1969

[52] Rutenberg, A., Tso, W. K. and Heidebrecht, A. C., Dynamic properties of asymmetric wali-frame structures, Earth. Eng. Struct. Dyn., **5**, 41-51, 1977

[53] Cheung, Y. K. and Swaddiwudhipong, S., Free vibration of frame shear wall structures on flexible foundations, Earth. Eng. Struct. Dyn., **7**, 355-367, 1979

[54] Ellis, B. R., An assessment of the accuracy of predicting the fundamental natural frequencies of buildings and the implications concerning the dynamic analysis of structures, Pro. Instn. Civ. Engrs, Part 2, **69**, 763-776, 1980

[55] Stafford Smith, B. and Crowe, E., Estimating periods of vibration of tall buildings, J. Struct. Div., ASCE, **112**, 1005-1019, 1986

[56] Takabatak, H., Mukai, H. and Hirano, T., Doubly symmetric tube structures, II: dynamic analysis, J. Struc. Div., ASCE, **119**, 2002-2016, 1993

[57] Leung, A. T. Y., Low cost analysis of building frames for lateral loads, Comput. Struct., **17**, 475-483, 1983

[58] Leung, A. T. Y., Micro-computer analysis of three dimensional tall buildings, Comput. Struct., **21**, 639-661, 1985

[59] Leung, A. T. Y. and Wong, S. C., Local-global distribution factor method for tall building frames, Comput. Struct., **29**, 497-502, 1988

[60] Wong, C. W. and Lau, S. L., Simplified finite element analysis for three - dimensional tall building structures, Comput. Struct., **33**, 821-830, 1989

[61] Ha, K. H., Tall frame analysis by reduced generalized coordinates, J. Struc. Div., ASCE, **104**, 527-536, 1978

[62] Pocanschi, A. and Olariu, L., Response of a medium-rise frame-tube model under static and dynamic actions, ACI J., **79**, 154-159, 1982

[63] Vlasov, V. S., Thin-walled Elastic Beams, English translation by Israel Program for Scientific Translation, Jerusalem, 1961

[64] Benscoter, S. U., A theory of torsion bending for multicell beams, J. Appl. Mech., **21**, 25-34, 1954

[65] Modern Multi-story concrete buildings, CPCA publication, 1989

[66] Cook, R. D., Malkus, D. and Plesha, M. E., Concepts and applications of finite element method, 1989

Appendix I Stiffness matrices of elements

For column and beam elements, bending, shearing, axial and torsional deformations are considered. The stiffness matrices of columns, beams and plates used in the FSM computer program are listed herein, in which I_x, I_y and I_z are moments of inertia; A = cross-section area; A_s = A/1.2 and; l = length of the element.

(1) Stiffness matrix of column

$$b_y = \frac{12EI_x}{GA_s l^2}, \qquad b_x = \frac{12EI_y}{GA_s l^2},$$

$$d_y = \frac{EI_x}{(1+b_y)\,l^3}, \qquad d_x = \frac{EI_y}{(1+b_x)\,l^3},$$

$$C_1 = 12d_y, \qquad C_2 = 12d_x,$$

$$C_3 = 0.5C_2 l, \qquad C_4 = 0.5C_1 l,$$

$$C_5 = (4+b_y)\,d_y, \qquad C_6 = (4+b_x)\,d_x,$$

$$C_7 = (2-b_y)\,d_y, \qquad C_8 = (2-b_x)\,d_x,$$

$$C_9 = \frac{EA}{l}, \qquad C_{10} = \frac{GJ}{l}$$

$$[\bar{k}_c] = \left[\begin{array}{cccccc:cccccc}
C_1 & & & & & & & & & & & \\
. & C_2 & & & & & & & & & & \\
. & . & C_9 & & & & & Symm & & & & \\
. & -C_3 & . & C_5 & & & & & & & & \\
C_4 & . & . & . & C_6 & & & & & & & \\
. & . & . & . & . & C_{10} & & & & & & \\
\hdashline
-C_1 & . & . & . & C_4 & . & C_1 & & & & & \\
. & -C_2 & . & -C_3 & . & . & . & C_2 & & & & \\
. & . & -C_9 & . & . & . & . & . & C_9 & & & \\
. & -C_3 & . & C_7 & . & . & . & C_3 & . & C_5 & & \\
C_4 & . & . & . & C_8 & . & -C_4 & . & . & . & C_6 & \\
. & . & . & . & . & -C_{10} & . & . & . & . & . & C_{10}
\end{array}\right]$$

(2) Stiffness matrix of beam

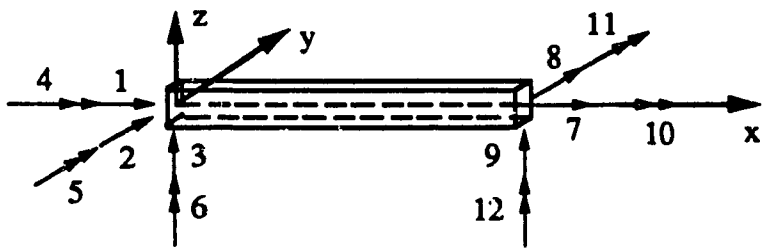

$$b_z = \frac{12EI_y}{GA_s l^2}, \qquad b_y = \frac{12EI_z}{GA_s l^2}, \qquad d_z = \frac{EI_y}{(1+b_z)\,l^3}, \qquad d_y = \frac{EI_z}{(1+b_y)\,l^3},$$

$$C_1 = 12d_z, \qquad C_2 = 12d_y, \qquad C_3 = 0.5C_1 l, \qquad C_4 = 0.5C_2 l,$$

$$C_5 = (4+b_z)\,d_z \qquad C_6 = (4+b_y)\,d_y, \qquad C_7 = (2-b_z)\,d_z, \qquad C_8 = (2-b_y)\,d_y,$$

$$C_9 = \frac{EA}{l}, \qquad C_{10} = \frac{GJ}{l}$$

$$[\bar{k}_b] = \left[\begin{array}{cccccc:cccccc}
C_9 & & & & & & & & & & & \\
. & C_2 & & & & & & & & & & \\
. & . & C_1 & & & & & Symm & & & & \\
. & . & . & C_{10} & & & & & & & & \\
. & . & -C_3 & . & C_5 & & & & & & & \\
. & C_4 & . & . & . & C_6 & & & & & & \\
\hdashline
-C_9 & . & . & . & . & . & C_9 & & & & & \\
. & -C_2 & . & . & . & -C_4 & . & C_2 & & & & \\
. & . & -C_1 & . & C_3 & . & . & . & C_1 & & & \\
. & . & . & -C_{10} & . & . & . & . & . & C_{10} & & \\
. & . & -C_3 & . & C_7 & . & . & . & C_3 & . & C_5 & \\
. & C_4 & . & . & . & C_8 & . & -C_4 & . & . & . & C_6
\end{array}\right]$$

(3) Stiffness matrix of four-noded plate element

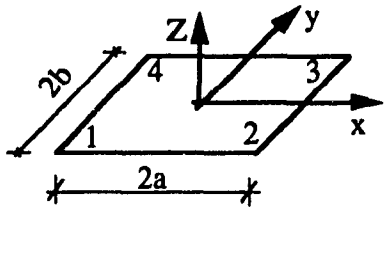

$$\{\delta_i\} = [w_i \;\; \theta_{xi} \;\; \theta_{yi}]^T$$
$$i = 1, 2, 3, 4$$

$$[\bar{k}_p] = \begin{bmatrix} k_{11} & k_{12} & k_{13} & k_{14} \\ k_{21} & k_{22} & k_{23} & k_{24} \\ k_{31} & k_{32} & k_{33} & k_{34} \\ k_{41} & k_{42} & k_{43} & k_{44} \end{bmatrix},$$

$$[k_{ij}] = \begin{bmatrix} a_{11} & a_{12} & a_{13} \\ a_{21} & a_{22} & a_{23} \\ a_{31} & a_{32} & a_{33} \end{bmatrix}, \qquad \begin{matrix} i = 1, 2, 3, 4 \\ j = 1, 2, 3, 4 \end{matrix}$$

in which,

$$a_{11} = 3D_1 [15 (\bar{\xi}_0 p^{-1} + \bar{\eta}_0 p) + (14 - 4\upsilon + 5p^{-1} + 5p) \bar{\xi}_0 \bar{\eta}_0]$$

$$a_{21} = -3D_1 b [(2 + 3\upsilon + 5p) \bar{\xi}_0 \eta_j + 15p\eta_j + 5\upsilon \bar{\xi}_0 \eta_i]$$

$$a_{22} = D_1 b^2 [2 (1 - \upsilon) \bar{\xi}_0 (3 + 5\bar{\eta}_0) + 5p (3 + \bar{\xi}_0) (3 + \bar{\eta}_0)]$$

$$a_{31} = 3D_1 a [(2 + 3\upsilon + 5p^{-1}) \xi_j \bar{\eta}_0 + 15p^{-1} \xi_j + 5\upsilon \xi_i \bar{\eta}_0]$$

$$a_{32} = -15D_1 \upsilon ab (\xi_i + \xi_j) (\eta_i + \eta_j)$$

$$a_{33} = D_1 a^2 [2 (1 - \upsilon) \bar{\eta}_0 (3 + 5\bar{\xi}_0) + 5p^{-1} (3 + \bar{\xi}_0) (3 + \bar{\eta}_0)]$$

$$D = \frac{12Et^3}{1 - \upsilon^2}, \quad (t = \text{thickness}), \quad D_1 = \frac{D}{60ab}, \qquad p = \frac{a^2}{b^2}$$

$$\bar{\xi}_o = \xi_i \xi_j, \qquad \bar{\eta}_0 = \eta_i \eta_j, \qquad \xi_i = \frac{x_i}{a}, \qquad \eta_i = \frac{y_i}{b}$$

Appendix II Consistent mass matrices of elements

In estimating dynamic properties, the mass of the framed tube is approached by consistent mass matrices of structural elements. The mass matrices of columns and beams of Appendix I are listed herein, in which $\bar{m} = \rho A l$, and ρ=mass density.

(1) Mass matrix of beam

$$[\bar{m}_b] = \left[\begin{array}{cccccc:cccccc}
\frac{\bar{m}}{3} & & & & & & & & & & & \\
. & \frac{156\bar{m}}{420} & & & & & & & & & & \\
. & . & \frac{156\bar{m}}{420} & & & & & & & & & \\
. & . & . & \frac{\rho Jl}{3} & & & & & Symm & & & \\
. & . & -\frac{22\bar{m}l}{420} & . & \frac{4.\bar{n}l^2}{420} & & & & & & & \\
. & \frac{22\bar{m}l}{420} & . & . & . & \frac{4\bar{m}l^2}{420} & & & & & & \\
\hdashline
\frac{\bar{m}}{6} & . & . & . & . & . & \frac{\bar{m}}{3} & & & & & \\
. & \frac{54\bar{m}}{420} & . & . & . & \frac{13\bar{m}l}{420} & . & \frac{156\bar{m}}{420} & & & & \\
. & . & \frac{54\bar{m}}{420} & . & -\frac{13\bar{m}l}{420} & . & . & . & \frac{156\bar{m}}{420} & & & \\
. & . & . & \frac{\rho Jl}{6} & . & . & . & . & . & \frac{\rho Jl}{3} & & \\
. & . & \frac{13\bar{m}}{420} & . & -\frac{3\bar{m}l^2}{420} & . & . & . & \frac{22\bar{m}l}{420} & . & \frac{4\bar{m}l^2}{420} & \\
. & -\frac{13\bar{m}}{420} & . & . & . & -\frac{3\bar{m}l^2}{420} & . & -\frac{22\bar{m}l}{420} & . & . & . & \frac{4\bar{m}l^2}{420}
\end{array}\right]$$

Appendix II (continued)

(2) Mass matrix of column

$$
[\bar{m}_c] = \left[\begin{array}{cccccc:cccccc}
\frac{156\bar{m}}{420} & & & & & & & & & & & \\
. & \frac{156\bar{m}}{420} & & & & & & & & & & \\
. & . & \frac{\bar{m}}{3} & & & & & & & & & \\
. & -\frac{22\bar{m}l}{420} & . & \frac{4\bar{m}l^2}{420} & & & & & Symm & & & \\
\frac{22\bar{m}l}{420} & . & . & . & \frac{4\bar{m}l^2}{420} & & & & & & & \\
. & . & . & . & . & \frac{\rho Jl}{3} & & & & & & \\
\hdashline
\frac{54\bar{m}}{420} & . & . & . & \frac{13\bar{m}}{420} & . & \frac{156\bar{m}}{420} & & & & & \\
. & \frac{54\bar{m}}{420} & . & -\frac{13\bar{m}l}{420} & . & . & . & \frac{156\bar{m}}{420} & & & & \\
. & . & \frac{\bar{m}}{6} & . & . & . & . & . & \frac{\bar{m}}{3} & & & \\
. & \frac{13\bar{m}}{420} & . & -\frac{3\bar{m}l^2}{420} & . & . & . & \frac{22\bar{m}l}{420} & & \frac{4\bar{m}l^2}{420} & & \\
-\frac{13\bar{m}}{420} & . & . & . & -\frac{3\bar{m}l^2}{420} & . & -\frac{22\bar{m}l}{420} & . & . & . & \frac{4\bar{m}l^2}{420} & \\
. & . & . & . & . & \frac{\rho Jl}{6} & . & . & . & . & . & \frac{\rho Jl}{3}
\end{array}\right]
$$

Appendix III Transformation matrices for elements

(1) Rigid end transformation matrix

The line elements in modeling the framed tubes are measured from center to center of joints, with the ends within the finite size of joints considered flexurally undeformable. Thus, elements are with flexurally rigid arms at ends (r_i, r_j) which are half of the sizes of corresponding joints. The rigid end transformation matrices of columns and beams shown in Appendix I are given by

$$[R_c] = \begin{bmatrix} 1.0 & & & r_i & & & & & & & & \\ & 1.0 & & -r_i & & & & & & & & \\ & & 1.0 & & & & & & & & & \\ & & & 1.0 & & & & & & & & \\ & & & & 1.0 & & & & & & & \\ & & & & & 1.0 & & & & & & \\ & & & & & & 1.0 & & & & & \\ & & & & & & & 1.0 & & & & -r_j \\ & & & & & & & & 1.0 & & r_j & \\ & & & & & & & & & 1.0 & & \\ & & & & & & & & & & 1.0 & \\ & & & & & & & & & & & 1.0 \end{bmatrix}$$

$$[R_b] = \begin{bmatrix} 1.0 & & & & & & & & & & & \\ & 1.0 & & & r_i & & & & & & & \\ & & 1.0 & & -r_i & & & & & & & \\ & & & 1.0 & & & & & & & & \\ & & & & 1.0 & & & & & & & \\ & & & & & 1.0 & & & & & & \\ & & & & & & 1.0 & & & & & \\ & & & & & & & 1.0 & & & & -r_j \\ & & & & & & & & 1.0 & & r_j & \\ & & & & & & & & & 1.0 & & \\ & & & & & & & & & & 1.0 & \\ & & & & & & & & & & & 1.0 \end{bmatrix}$$

(2) Coordinate transformation matrix

In assembling the overall stiffness matrices of framed tubes and floor frame systems, the element stiffness matrices in their local systems are transferred into the global coordinate system. $[T_i]$ is the transformation matrix at the node i, in which x_i, y_i are global coordinates of node i. The element transformation matrix is formed by

$$[T] = \begin{bmatrix} T_i & 0 \\ 0 & T_j \end{bmatrix}$$

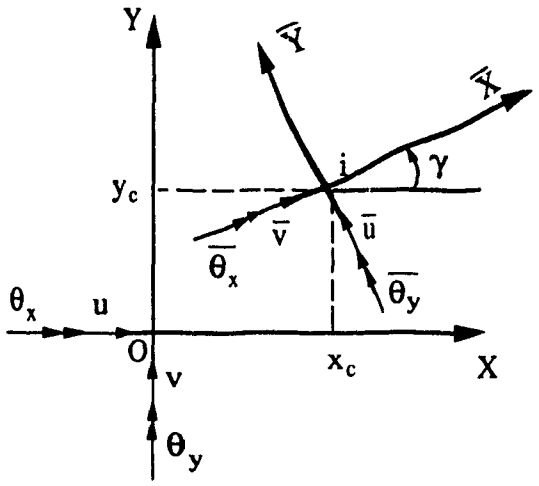

$$\{\bar{d}_i\} = [T_i]\{d_i\}$$

$$\{d_i\} = [u_i \; v_i \; w_i \; \theta_{xi} \; \theta_{yi} \; \theta_{zi}]^T$$

$$\{\bar{d}_i\} = [\bar{u}_i \; \bar{v}_i \; \bar{w}_i \; \bar{\theta}_{xi} \; \bar{\theta}_{yi} \; \bar{\theta}_{zi}]^T$$

$$[T_i] = \begin{bmatrix} \cos\gamma & \sin\gamma & . & . & . & x_i\sin\gamma - y_i\cos\gamma \\ -\sin\gamma & \cos\gamma & . & . & . & x_i\cos\gamma + y_i\sin\gamma \\ . & . & 1.0 & . & . & . \\ . & . & . & \cos\gamma & \sin\gamma & . \\ . & . & . & -\sin\gamma & \cos\gamma & . \\ . & . & . & . & . & 1.0 \end{bmatrix}$$

Appendix IV: Nodal displacement transformation matrices for columns and beams

In the FSM, the nodal displacement fields at the kth floor are represented by nodal displacement distribution coefficients β_i^l, α_{xi}^l and α_{yi}^l, (l=1,2,...,5) corresponding to five relative floor rigid body displacements with magnitude of unity. These coefficients are determined by analyzing two-story segments of the structure as detailed in Chapter 2. The nodal displacements themselves are obtained by interpolating the foregoing floor rigid body displacements, which leads to the nodal displacement transformation matrices $[g_c]$ and $[g_b]$ for columns and beams, respectively, given by

$$[g_c] = \left[\begin{array}{ccccc:ccccc}
. & . & . & . & . & 1.0 & . & . & . & . \\
. & . & . & . & . & . & 1.0 & . & . & . \\
-\beta_i^1 & -\beta_i^2 & -\beta_i^3 & -\beta_i^4 & -\beta_i^5 & \beta_i^1 & \beta_i^2 & \beta_i^3 & \beta_i^4 & \beta_i^5 \\
-\alpha_{xi}^1 & -\alpha_{xi}^2 & -\alpha_{xi}^3 & -\alpha_{xi}^4 & -\alpha_{xi}^5 & \alpha_{xi}^1 & \alpha_{xi}^2 & \alpha_{xi}^3 & \alpha_{xi}^4 & \alpha_{xi}^5 \\
-\alpha_{yi}^1 & -\alpha_{yi}^2 & -\alpha_{yi}^3 & -\alpha_{yi}^4 & -\alpha_{yi}^5 & \alpha_{yi}^1 & \alpha_{yi}^2 & \alpha_{yi}^3 & \alpha_{yi}^4 & \alpha_{yi}^5 \\
. & . & . & . & . & . & . & 1.0 & . & . \\
\hdashline
. & . & . & . & . & 1.0 & . & . & . & . \\
. & . & . & . & . & . & 1.0 & . & . & . \\
-\beta_j^1 & -\beta_j^2 & -\beta_j^3 & -\beta_j^4 & -\beta_j^5 & \beta_j^1 & \beta_j^2 & \beta_j^3 & \beta_j^4 & \beta_j^5 \\
-\alpha_{xj}^1 & -\alpha_{xj}^2 & -\alpha_{xj}^3 & -\alpha_{xj}^4 & -\alpha_{xj}^5 & \alpha_{xj}^1 & \alpha_{xj}^2 & \alpha_{xj}^3 & \alpha_{xj}^4 & \alpha_{xj}^5 \\
-\alpha_{yj}^1 & -\alpha_{yj}^2 & -\alpha_{yj}^3 & -\alpha_{yj}^4 & -\alpha_{yj}^5 & \alpha_{yj}^1 & \alpha_{yj}^2 & \alpha_{yj}^3 & \alpha_{yj}^4 & \alpha_{yj}^5 \\
. & . & . & . & . & . & . & 1.0 & . & .
\end{array}\right]$$

$$[g_b] = \left[\begin{array}{ccccc|ccccc|ccccc}
. & . & . & . & . & 1.0 & . & . & . & . & & & & & \\
. & . & . & . & . & . & 1.0 & . & . & . & & & & & \\
-\beta_i^1 & -\beta_i^2 & -\beta_i^3 & -\beta_i^4 & -\beta_i^5 & \beta_i^1 & \beta_i^2 & \beta_i^3 & \beta_i^4 & \beta_i^5 & & & & & \\
-\alpha_{xi}^1 & -\alpha_{xi}^2 & -\alpha_{xi}^3 & -\alpha_{xi}^4 & -\alpha_{xi}^5 & \alpha_{xi}^1 & \alpha_{xi}^2 & \alpha_{xi}^3 & \alpha_{xi}^4 & \alpha_{xi}^5 & & & & & \\
-\alpha_{yi}^1 & -\alpha_{yi}^2 & -\alpha_{yi}^3 & -\alpha_{yi}^4 & -\alpha_{yi}^5 & \alpha_{yi}^1 & \alpha_{yi}^2 & \alpha_{yi}^3 & \alpha_{yi}^4 & \alpha_{yi}^5 & & & & & \\
. & . & . & . & . & . & . & 1.0 & . & . & & & & & \\
\hline
 & & & & & . & . & . & . & . & 1.0 & . & . & . & . \\
 & & & & & . & . & . & . & . & . & 1.0 & . & . & . \\
 & & & & & -\beta_j^1 & -\beta_j^2 & -\beta_j^3 & -\beta_j^4 & -\beta_j^5 & \beta_j^1 & \beta_j^2 & \beta_j^3 & \beta_j^4 & \beta_j^5 \\
 & & & & & -\alpha_{xj}^1 & -\alpha_{xj}^2 & -\alpha_{xj}^3 & -\alpha_{xj}^4 & -\alpha_{xj}^5 & \alpha_{xj}^1 & \alpha_{xj}^2 & \alpha_{xj}^3 & \alpha_{xj}^4 & \alpha_{xj}^5 \\
 & & & & & -\alpha_{yj}^1 & -\alpha_{yj}^2 & -\alpha_{yj}^3 & -\alpha_{yj}^4 & -\alpha_{yj}^5 & \alpha_{yj}^1 & \alpha_{yj}^2 & \alpha_{yj}^3 & \alpha_{yj}^4 & \alpha_{yj}^5 \\
 & & & & & . & . & . & . & . & . & . & 1.0 & . & .
\end{array}\right]$$

The above transformation matrices are then employed in equations (2.16 and 2.17) to establish the column and beam matrices corresponding to the generalized displacements of the framed tube.

Appendix V Principal sectorial moment of inertia

The sectorial coordinate of thin-walled beams with closed circular or regular polygon cross-sections is zero. For any other type of cross-sections, the procedure for calculating the principal sectorial moment of inertia [63, 33] is as follows:

(1) Choose an arbitrary pole O_1 and origin M_1 in the coordinate system CXY, and calculate sectorial coordinate $\bar{\omega}_{o1}^{M1}$ based on O_1 and M_1;

(2) Determine the principal pole (shear center) according to

$$O_x = \frac{\oint_s \bar{\omega}_{o1}^{M1} y t ds}{I_x}, \qquad O_y = \frac{\oint_s \bar{\omega}^{M1}_{o1} x t ds}{I_y} \tag{V.1}$$

where O_x and O_y are distances from O_1 to the principal pole O in the X and Y directions, respectively;

(3) Calculate sectorial coordinate $\bar{\omega}_1$ based on O and M_1;

(4) Determine the principal sectorial coordinate

$$\bar{\omega} = \bar{\omega}_1 - \frac{\int_0^s \bar{\omega}_1 t ds}{A} ; \tag{V.2}$$

(5) Calculate sectorial moment of inertia $I_{\bar{\omega}}$

$$I_{\bar{\omega}} = \oint_s \bar{\omega}^2 t ds . \tag{V.3}$$